NUMERICAL ANALYSIS
OF
[illegible]

DEPARTMENT OF THE AIR FORCE

AIR UNIVERSITY

AIR FORCE INSTITUTE OF TECHNOLOGY

Wright-Patterson Air Force Base, Ohio

AFIT/GA/ENY/90D-8

NUMERICAL ANALYSIS OF CRITICAL INCLINATIONS ABOUT THE PLANET MARS

THESIS

Kenneth J. Hyatt, Captain, USAF

AFIT/GA/ENY/90D-8

AFIT/GA/ENY/90D-8

NUMERICAL ANALYSIS OF CRITICAL INCLINATIONS ABOUT THE PLANET MARS

THESIS

Presented to the Faculty of the School of Engineering
of the Air Force Institute of Technology

Air University

In Partial Fulfillment of the

Requirements for the Degree of

Master of Science in Astronautical Engineering

Kenneth J. Hyatt, B.S.
Captain, USAF

1 Nov 1990

Acknowledgments

I would like to thank my advisor, Capt. Rodney Bain, for his guidance, encouragement, and most of all his patience throughout this effort. Special thanks to the Elsa's crowd for their constant attitude checks.

Kenneth J. Hyatt

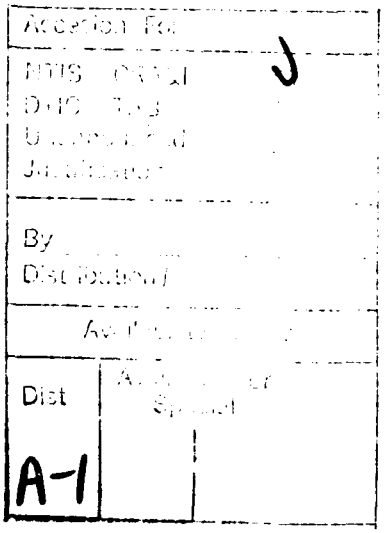

Table of Contents

List of Figures

List of Tables

List of Symbols

Symbol	
a	semi-major axis
b	semi-minor axis
e	eccentricity
i	inclination
ω	argument of periapse
Ω	argument of ascending node
f	true anomaly
M	mean anomaly
μ_m	Mars gravity constant
μ_s	Sun gravity constant
δ	satellite declination
$\bar{r}$	satellite position vector
$\bar{r}_s$	Sun position vector
I	inclination of pseudo Sun orbit
L	Mars centered latitude of Sun
Λ	right ascension of Sun
θ	satellite central angle
θ_s	Sun central angle

Abstract

Averaged equations of motion were numerically integrated over a time span of ten Earth years for various inclinations, eccentricities, and perigee heights. Each orbit (i.e. set of initial conditions) produced a standard deviation of the variations in eccentricity (SDE) and inclination (SDI). These were calculated using a polynomial approximation to the variations. Surface plots of SDI & SDE vs the initial conditions are then examined to ascertain the critical inclinations.

NUMERICAL ANALYSIS OF CRITICAL INCLINATIONS ABOUT THE PLANET MARS

I. Introduction

Satellites are placed in a variety of orbits, usually determined by the mission requirements of the satellite payload. For instance, typical planetary mapping missions require low, altitude, high inclination, and nearly circular orbits. Conversely, communication relay satellites usually occupy extremely high altitude and near zero inclination orbits. One such satellite is the commercial Intelsat satellite in Earth geosynchronous orbit. The basic Keplerian two body equations are used to find an orbit that meets the general requirements such as coverage, refresh rate, etc. However, various gravitational, atmospheric, and other effects tend to perturb the orbit from its initial conditions. These effects can be relatively large and primarily affect the inclination and eccentricity of an orbit.

The amplitudes of these variations are primarily dependent on the orbit's initial eccentricity and inclination. Higher initial eccentricities show a direct correlation to larger variations. The effect of initial inclination on the variations is more complex. Those initial inclinations that are determined to cause large

variations in eccentricity and inclination are termed critical inclinations. Figures 1 & 2 illustrate the variations in eccentricity and inclination for an example orbit.

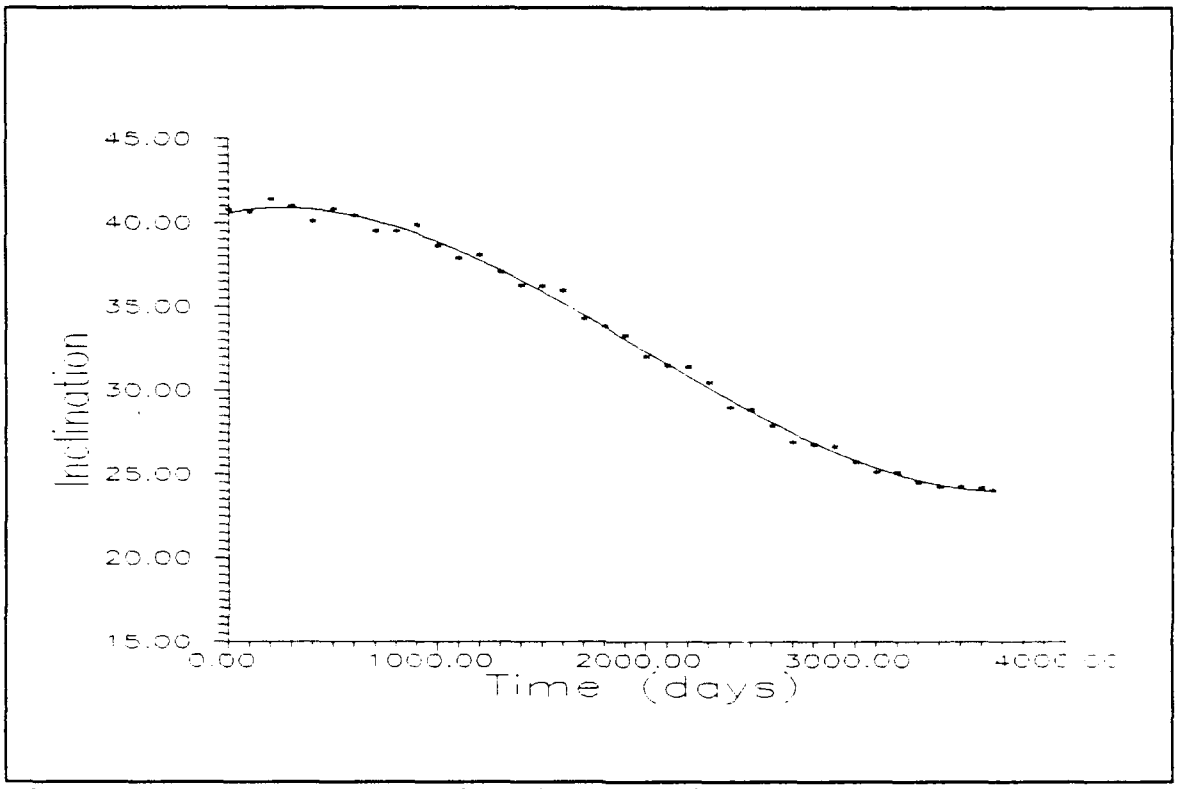

Figure 1. Example Inclination vs Time Plot: R_p = 6500 km

For the majority of satellite missions, such as Earth communication satellites, it is desirable to minimize the perturbations. The initial orbits are selected to meet mission requirements and the satellites are station kept in those orbits by thrusters. These thrusters require fuel, which is often the limiting factor of satellite lifetime.

An alternate approach seeks to select orbit initial

conditions to maximize the perturbations. Such an orbit could be used as a transfer orbit to save maneuvering fuel. However, such a transfer often takes much longer than mission constraints allow.

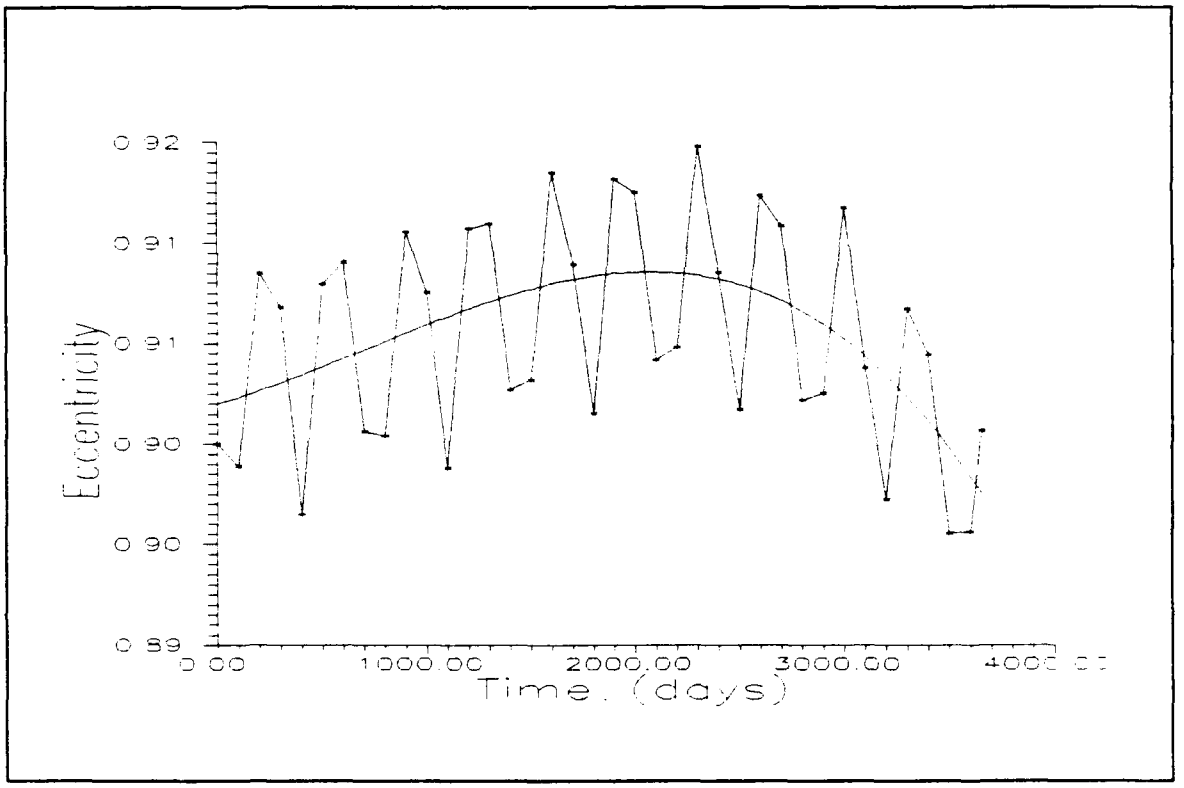

Figure 2. Example Eccentricity vs Time Plot: R_p = 6500 km

Whether the designer seeks to minimize or maximize the perturbations, the locations of the critical inclinations are required. Therefore, the evolution of the selected orbit over the lifetime of the satellite must be examined. Both an analytic and numerical approach were applied in finding the critical inclinations.

Both approaches start with the same governing equations

of motion, the Lagrange Planetary Equations in their disturbing function form. The disturbing function accounted for only the predominate gravitational perturbations of the Mar's equatorial bulge (J2) and solar third body perturbations. The Mars J_2 zonal harmonic is two orders of magnitude larger than the other harmonics and is twice as large as the Earths. This simplified the equations of motion to permit an analytical analysis and reduced the integration time for the numeric approach. The analytic analysis represents the limiting case of variations over an infinite time span. Therefore, a full numerical analysis was required to find intermediate critical inclinations.

The numerical approach integrated orbits for six different perigee heights, over a full range of initial eccentricities and inclinations. This involved the integration of over 56,000 orbits for a ten Earth year time span. The integration of such a large number of orbits was necessary to provide sufficient information for the determination of the critical inclinations. However, the shear amount of data precludes analysis of each individual orbit. Therefore, an approach involving the determination of a figure of merit for each orbit was used to reduce the amount of data to a manageable size. The standard deviations in eccentricity and inclination were selected as the figures of merit and calculated for each orbit. Three-

dimensional surface plots of these deviations vs the initial eccentricities and inclinations were then used to determine the critical inclinations. The affect of using linear, quadratic, and cubic data fits in calculating the standard deviations was also examined. Figures 1 & 2 show a cubic fit to the data.

II. Analytical Development

Reference Frame

A Mars centered reference frame and classical elements were used describe the motion of the satellite.

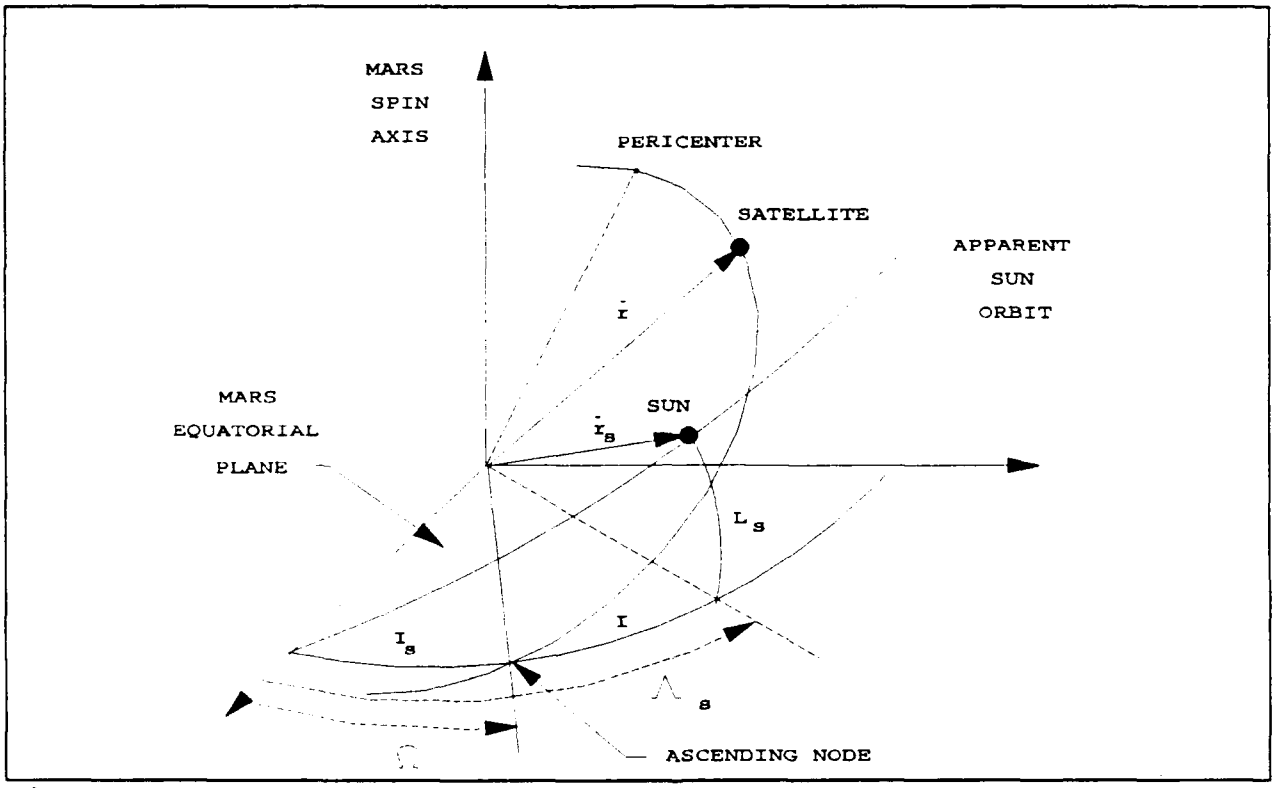

Figure 3. Planet (Mars) Centered Reference Frame

Satellite orbital elements are defined as follows:

r = satellite radius vector

i = inclination of satellite orbit

Ω = argument of ascending node for satellite orbit

ω = argument of periapsis for satellite orbit

θ = satellite central angle

By referencing everything to a Mars centered coordinate frame, the Sun appears to orbit Mars in this reference frame.

Therefore, the motion of the Sun with respect to Mars can be described by a set of orbital elements as if the Sun was orbiting Mars. The Sun's pseudo orbital elements are defined as follows:

r_s = Sun radius vector

θ_s = Sun central angle

I_s = inclination of Sun orbit

Λ = right ascension of the Sun

L = Planet centered latitude of the Sun

Equations of Motion

For a basic two body problem of a satellite orbiting Mars, the motion can be described by the six classical orbital elements that are constant in the inertial frame. Once these are known for some epoch time, the position and velocity of the satellite can be determined for any other time using the two body equations. In reality, the two body elements are not constant. They change with time due to the perturbative effects of drag, Mars geopotential, Sun third body effects, etc. Since these changes are relatively slow, the Keplerian elements can be used to describe the satellite motion when combined with equations of variation. The equations of variation describe the change of the keplerian elements with time, based upon the perturbations. This method is known as variation of parameters. The Lagrange disturbing function approach was used for the equations of variation.

In the Lagrange approach, the acceleration of the satellite is written as the gradient of the gravitational potentials.

Note, this is only valid for conservative forces such as gravity.

$$\frac{d^2\bar{r}}{dt^2} = \nabla(R_M + R_S) \qquad (1)$$

∇ = gradient operator

R_M = Mars gravity potential

R_S = Sun gravity potential

Through Canonical transformations, the two body motion may be eliminated and the Lagrange equations for the perturbing motion formed. The Lagrange Planetary Equations in their disturbing function form (4,476-483):

e = eccentricity of satellite orbit

i = inclination of satellite orbit

b = semi-minor axis of satellite orbit

M = Mean Anomaly of satellite orbit

n = mean motion of satellite

μ = gravitational parameter

(4.2828287E04 Kg^3/sec^2 for Mars)

(1.3271544E11 Kg^3/sec^2 for Sun)

R = the disturbing function

$$\frac{de}{dt} = \frac{b^2}{na^4e}\frac{\partial R}{\partial M} - \frac{b}{na^3e}\frac{\partial R}{\partial \omega}$$

$$\frac{di}{dt} = -\frac{1}{nab\sin i}\frac{\partial R}{\partial \Omega} + \frac{\cos i}{nab\sin i}\frac{\partial R}{\partial \omega}$$

$$\frac{da}{dt} = \frac{2}{na}\frac{\partial R}{\partial M}$$

$$\frac{d\Omega}{dt} = \frac{1}{nab\sin i}\frac{\partial R}{\partial i} \qquad (2)$$

$$\frac{d\omega}{dt} = -\frac{\cos i}{nab\sin i}\frac{\partial R}{\partial i} + \frac{b}{na^3e}\frac{\partial R}{\partial e}$$

$$\frac{dM}{dt} = n - \frac{2}{na}\frac{\partial R}{\partial a} - \frac{b^2}{na^4e}\frac{\partial R}{\partial e}$$

$$\text{where} \quad b = a\sqrt{1-e^2} \quad \& \quad n = \sqrt{\frac{\mu}{a^3}}$$

Only the Mars J_2 and Sun third body disturbing potentials were considered. Their development followed that of Breakwell's Investigation of High Eccentricity Orbits About Mars (5) and Durand's June 1989 MS Thesis (7).

Mars Disturbing Function

The first non-zero zonal harmonic is the J_2 term that accounts for the equatorial bulge. This is the predominate geopotential term for most planets and the only harmonic examined in both the analytic and numerical developments. The J_2 disturbing function has been shown to be

$$R_m = \frac{\mu_m J_2 R_e^2}{2r^3} (1 - 3 \sin^2 \delta) \tag{3}$$

where R_e is the Mars equatorial radius and δ is the declination. A transformation of the declination to a form containing the true anomaly and the argument of periapsis was accomplished using spherical geometry. From the spherical geometry

$$\begin{aligned} \sin\delta &= \sin i \sin\alpha \\ &= \sin i \sin(\pi - (f + \omega)) \\ &= \sin i \sin(f + \omega) \end{aligned} \tag{4}$$

Squaring this equation yields

$$\begin{aligned} \sin^2\delta &= \sin^2 i \sin^2(f + \omega) \\ &= \frac{1}{2} \sin^2 i [1 - \cos 2(f + \omega)] \end{aligned} \tag{5}$$

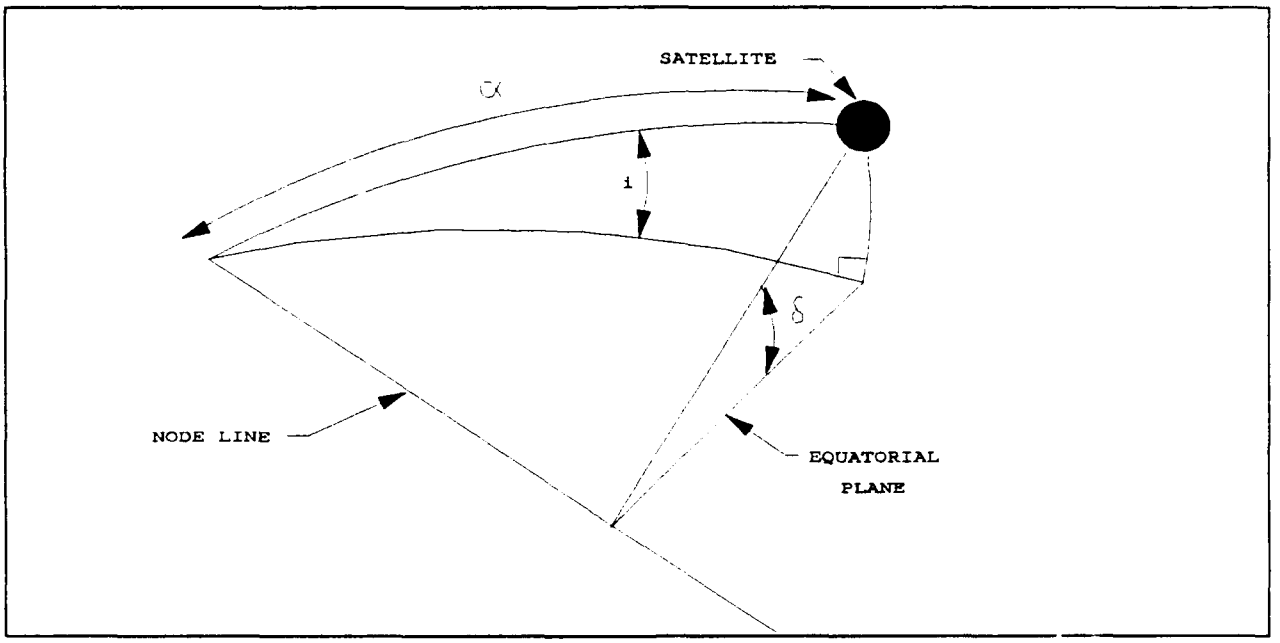

Figure 4. Spherical Trigonometry of an Orbit

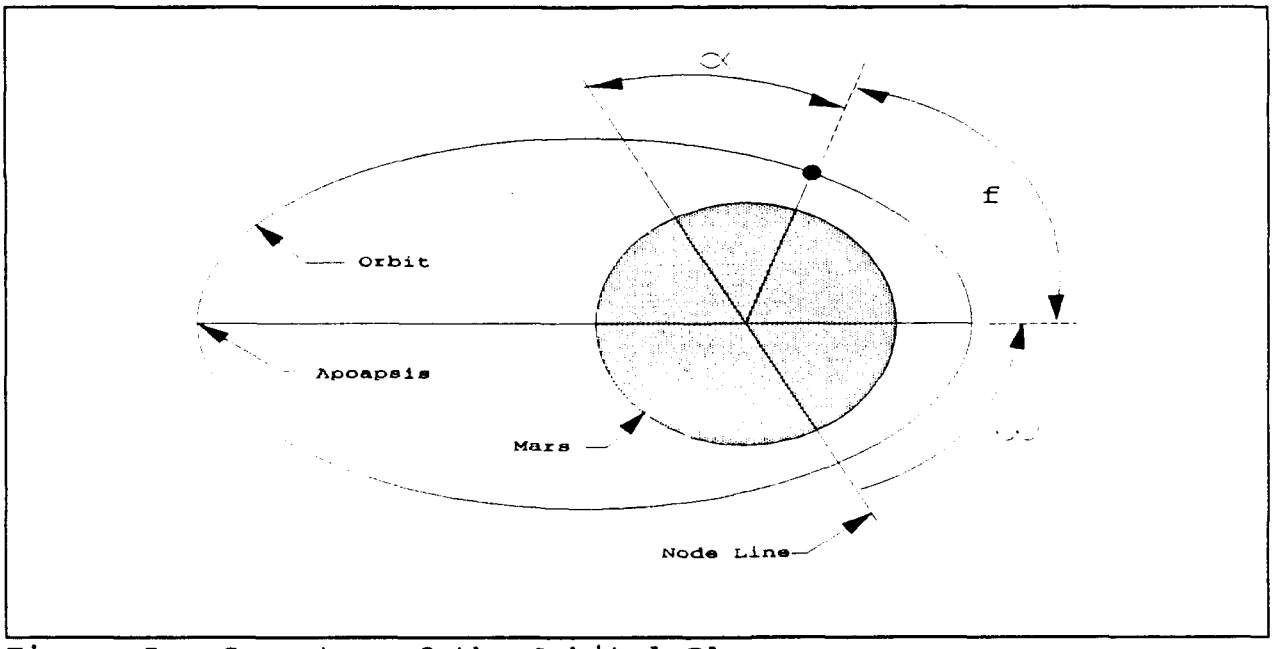

Figure 5. Geometry of the Orbital Plane

The transformed disturbing function is thus

$$R_m = \frac{\mu_m J_2 R_e^2}{2r^3}\left[1 - \frac{3}{2}\sin^2 i + \frac{3}{2}\sin^2 i \cos 2(f+\omega)\right] \qquad (6)$$

Averaging of the Mars Disturbing Function

The mean anomaly was averaged out of the Mars disturbing function by integrating the function over one orbit and dividing by the change in mean anomaly (2π).

$$\bar{R}_m = \frac{1}{2\pi}\int_0^{2\pi} R_m \, dM \qquad (7)$$

The integration was accomplished using Hansen's Coefficients (2). A brief description and derivation of this is included in Appendix A. Substituting in the disturbing function yields

$$\bar{R}_m = \frac{1}{2\pi}\int_0^{2\pi} \frac{\mu_m J_2 R_e^2}{2r^3}\left(1 - \frac{3}{2}\sin^2 i\right) dM + \frac{1}{2\pi}\int_0^{2\pi} \frac{3\mu_m J_2 R_e^2}{4r^3}\sin^2 i \cos 2(f+\omega)\, dM \qquad (8)$$

Let

$$A = \frac{\mu_m J_2 R_e^2}{2a^3}\left(1 - \frac{3}{2}\sin^2 i\right)\frac{1}{2\pi}\int_0^{2\pi}\left(\frac{r}{a}\right)^{-3} dM$$

$$B = \frac{3\mu_m J_2 R_e^2}{4a^3}\sin^2 i \left\{\frac{1}{2\pi}\int_0^{2\pi}\left(\frac{r}{a}\right)^{-3}\cos 2(f+\omega)\, dM\right\} \qquad (9)$$

Using trigonometry, B was transformed to

$$B = \frac{3\mu_m J_2 R_e^2}{4a^3} \sin^2 i \left\{ \frac{1}{2\pi} \int_0^{2\pi} \left(\frac{r}{a}\right)^{-3} (\cos 2f \cos 2\omega - \sin 2f \sin 2\omega)\, dM \right\}$$

$$B = \frac{3\mu_m J_2 R_e^2}{4a^3} \sin^2 i \left\{ (\cos 2\omega) \frac{1}{2\pi} \int_0^{2\pi} \left(\frac{r}{a}\right)^{-3} \cos 2f\, dM + \right.$$

$$\left. - \sin 2\omega \, \frac{1}{2\pi} \int_0^{2\pi} \left(\frac{r}{a}\right)^{-3} \sin 2f\, dM \right\}$$

(10)

By employing Hansen's coefficients from Appendix A

$$\frac{1}{2\pi} \int_0^{2\pi} \left(\frac{r}{a}\right)^{-3} dM = X_0^{-3,0} = (1-e^2)^{-3/2}$$

$$\frac{1}{2\pi} \int_0^{2\pi} \left(\frac{r}{a}\right)^{-3} \sin 2f\, dM = 0 \qquad \textbf{(11)}$$

$$\frac{1}{2\pi} \int_0^{2\pi} \left(\frac{r}{a}\right)^{-3} \cos 2f\, dM = X_0^{-3,2} = 0$$

From this "B" is found to equal zero. Therefore the averaged disturbing function is equal to the "A" equation.

$$\bar{R}_m = \frac{\mu_m J_2 R_e^2}{2a^3 (1-e^2)^{3/2}} \left(1 - \frac{3}{2} \sin^2 i\right) \qquad \textbf{(12)}$$

Solar Disturbing Function

The third body effects of the Sun on the satellite motion may be derived from Newton's basic Law of Universal Gravitation.

$$\bar{F}_1 = -Gm_1\left[\frac{m_2}{r_{21}^3}\bar{r}_{21} + \frac{m_3}{r_{31}^3}\bar{r}_{31}\right]$$
$$\bar{F}_2 = -Gm_2\left[\frac{m_1}{r_{12}^3}\bar{r}_{12} + \frac{m_3}{r_{32}^3}\bar{r}_{32}\right] \qquad (13)$$

$$\frac{d^2\bar{r}_1}{dt^2} = \frac{\bar{F}_1}{m_1} = -G\left[\frac{m_2}{r_{21}^3}\bar{r}_{21} + \frac{m_3}{r_{31}^3}\bar{r}_{31}\right]$$
$$\frac{d^2\bar{r}_2}{dt^2} = \frac{\bar{F}_2}{m_2} = -G\left[\frac{m_2}{r_{12}^3}\bar{r}_{12} + \frac{m_3}{r_{32}^3}\bar{r}_{32}\right] \qquad (14)$$

$$\bar{r}_{21} = \bar{r}_1 - \bar{r}_2 \quad \& \quad \frac{d^2\bar{r}_{21}}{dt^2} = \frac{d^2\bar{r}_1}{dt^2} - \frac{d^2\bar{r}_2}{dt^2}$$
$$\frac{d^2\bar{r}_{21}}{dt^2} = -G\left[\frac{m_2}{r_{21}^3}\bar{r}_{21} + \frac{m_3}{r_{31}^3}\bar{r}_{31}\right] + G\left[\frac{m_1}{r_{12}^3}\bar{r}_{12} + \frac{m_3}{r_{32}^3}\bar{r}_{32}\right] \qquad (15)$$
$$\frac{d^2\bar{r}_{21}}{dt^2} = -G\frac{(m_2 + m_1)}{r_{21}^3}\bar{r}_{21} + Gm_3\left[\frac{\bar{r}_{32}}{r_{32}^3} - \frac{\bar{r}_{31}}{r_{31}^3}\right]$$

Since m2 >> m1, let m2 + m1 = m2

$$\frac{d^2\bar{r}_{21}}{dt^2} = -\frac{\mu_m}{r_{21}^3}\bar{r}_{21} - \mu_s\left[\frac{\bar{r}_{31}}{r_{31}^3} - \frac{\bar{r}_{32}}{r_{32}^3}\right] \tag{16}$$

With a change of variables to the notation of figure 3.

$$\begin{aligned} \bar{r}_{21} &= \bar{r} \\ \bar{r}_{23} &= -\bar{r}_{32} = \bar{r}_s \\ \bar{r}_{31} &= \bar{r} - \bar{r}_s \end{aligned} \tag{17}$$

The acceleration of the satellite is

$$\frac{d^2\bar{r}}{dt^2} = -\frac{\mu_m}{r^3}\bar{r} - \mu_s\left[\frac{\bar{r} - \bar{r}_s}{|\bar{r}_s - \bar{r}|^3} + \frac{\bar{r}_s}{r_s^3}\right] = \nabla(R_M + R_S) \tag{18}$$

The first term of the above equation is the Mars and satellite two body problem. The second term is the acceleration due to the Sun third body effects. As shown above, the acceleration of the satellite can be expressed as the gradient of the gravitational potentials of the Sun and Mars. Therefore, the gradient of the Sun's potential is

$$\nabla R_S = \mu_s\left[\frac{\bar{r}_s - \bar{r}}{|\bar{r}_s - \bar{r}|^3} - \frac{\bar{r}_s}{r_s^3}\right] \tag{19}$$

By finding the equation that satisfies this condition, the Sun's gravitational potential is found to be

$$R_S = \mu_s \left[\frac{1}{|\bar{r}_s - \bar{r}|} - \frac{\bar{r}\cdot\bar{r}_s}{r_s^3} \right] \tag{20}$$

Now this must be put in the form of a disturbing function to the Mars-satellite two body problem.

$$\begin{aligned} \bar{\rho} &= \bar{r}_s - \bar{r} \\ \rho^2 &= |\bar{r}_s - \bar{r}|^2 = (\bar{r}_s - \bar{r})\cdot(\bar{r}_s - \bar{r}) \\ \rho^2 &= \bar{r}_s\cdot\bar{r}_s - 2\bar{r}\cdot\bar{r}_s + \bar{r}\cdot\bar{r} \\ \rho^2 &= r_s^2 - 2rr_s\cos B + r^2 \\ \text{where} \quad B &= \frac{\bar{r}\cdot\bar{r}_s}{rr_s} \end{aligned} \tag{21}$$

By factoring out r_s^2 and taking the square root

$$\rho = r_s\left[1 + \frac{r^2}{r_s^2} - \frac{2r}{r_s}\cos B\right]^{1/2} = |\bar{r}_s - \bar{r}| \tag{22}$$

Substituting in, the Mars gravitational potential becomes

$$R_S = \frac{\mu_s}{r_s}\left[\left(1 + \frac{r^2}{r_s^2} - \frac{2r}{r_s}\cos B\right)^{-1/2} - \frac{r\cos B}{r_s}\right] \tag{23}$$

Using the binomial expansion

$$\left[1+\left(\frac{r^2}{r_s^2}-\frac{2r}{r_s}\cos B\right)\right]^{-1/2} = \sum_{n=0}^{\infty}\binom{-\frac{1}{2}}{n}\left(\frac{r^2}{r_s^2}-\frac{2r}{r_s}\cos B\right)^n \qquad (24)$$

$$= 1 - \frac{1}{2}\left(\frac{r^2}{r_s^2}-\frac{2r}{r_s}\cos B\right) + \frac{3}{8}\left(\frac{r^2}{r_s^2}-\frac{2r}{r_s}\cos B\right)^2 + \ldots$$

The higher order terms above $(r/r_s)^2$ can be neglected since $r_s >>> r$. The above series is approximated as

$$\left[1+\left(\frac{r^2}{r_s^2}-\frac{2r}{r_s}\cos B\right)\right]^{-1/2} = 1 - \frac{1}{2}\left(\frac{r^2}{r_s^2}-\frac{2r}{r_s}\cos B\right) + \frac{3}{8}\left(\frac{4r^2}{r_s^2}\cos^2 B\right) \qquad (25)$$

The Sun gravitational potential becomes

$$R_S = \frac{\mu_s}{r_s}\left[1 - \frac{r^2}{2r_s^2} + \frac{3r^2}{2r_s^2}\cos^2 B\right] \qquad (26)$$

$$= \frac{\mu_s}{r_s}\left[1 + \frac{r^2}{2r_s^2}(3\cos^2 B - 1)\right]$$

The Suns gravitational potential at Mars is equal to the two body term plus the disturbing function.

$$R_S = \frac{\mu_s}{r_s} + R_s \qquad (27)$$

Therefore, the solar disturbing function is

$$R_s = \frac{\mu_s r^2}{2r_s^3}\left[3\cos^2 B - 1\right] = \frac{\mu_s r^2}{2r_s^3}\left[3\left(\frac{\bar{r}\cdot\bar{r}_s}{r r_s}\right)^2 - 1\right] \tag{28}$$

The radial vectors are now transformed to the orbital elements of the satellite and Sun, defined in figure (1). For ease of notation, the sin and cos functions will be abbreviated using S = sin and C = cos. From the physical geometry, the unit vectors in the radial satellite and Sun directions are

$$\hat{e}_r = \frac{\bar{r}}{r} = \begin{bmatrix} C_\Omega C_\theta - S_\Omega C_i S_\theta \\ S_\Omega C_\theta + C_\Omega C_i S_\theta \\ S_i S_\theta \end{bmatrix}$$

$$\hat{e}_s = \frac{\bar{r}_s}{r_s} = \begin{bmatrix} C_\Lambda C_L \\ C_L S_\Lambda \\ S_L \end{bmatrix} \tag{29}$$

The dot product of these unit vectors is

$$\hat{e}_r\cdot\hat{e}_s = \frac{\bar{r}\cdot\bar{r}_s}{r r_s}$$

$$= C_\Omega C_\theta C_\Lambda C_L - S_\Omega C_i S_\theta C_\Lambda C_L + S_\Omega C_\theta C_L S_\Lambda + C_\Omega C_i S_\theta C_L S_\Lambda + S_i S_\theta S_L \tag{30}$$

$$= C_\theta C_L(C_\Omega C_\Lambda + S_\Omega S_\Lambda) + C_i S_\theta C_L(C_\Omega S_\Lambda - S_\Omega C_\Lambda) + S_i S_\theta S_L$$

$$= C_\theta C_L C_{(\Omega-\Lambda)} + C_i S_\theta C_L S_{(\Omega-\Lambda)} + S_i S_\theta S_L$$

Substituting into the solar disturbing function results in

$$R_s = \frac{\mu_s r^2}{2 r_s^3} \left\{ 3 \left[C_\theta C_L C_{(\Omega - \Lambda)} + C_i S_\theta C_L S_{(\Omega - \Lambda)} + S_i S_\theta S_L \right]^2 - 1 \right\} \qquad (31)$$

Expanding squared term yields

$$R_s = \frac{\mu_s r^2}{2 r_s^3} \left\{ 3 \left[K_1 C_\theta^2 + 2 K_2 C_\theta S_\theta + K_3 S_\theta^2 \right] - 1 \right\} \qquad (32)$$

Where

$$\begin{aligned} K_1 &= \left(C_L C_{(\Omega - \Lambda)} \right)^2 \\ K_2 &= S_L C_L S_i C_{(\Omega - \Lambda)} - C_L^2 C_i S_{(\Omega - \Lambda)} C_{(\Omega - \Lambda)} \\ K_3 &= \left(C_i C_L S_{(\Omega - \Lambda)} - S_L S_i \right)^2 \end{aligned} \qquad (33)$$

The disturbing function is now written in terms of the satellites true anomaly using

$$\begin{aligned} \theta &= f + \omega \\ C_\theta^2 &= \frac{1}{2} \left(1 + C_{2\theta} \right) \\ S_\theta^2 &= \frac{1}{2} \left(1 - C_{2\theta} \right) \\ 2 S_\theta C_\theta &= S_{2\theta} \end{aligned} \qquad (34)$$

The final form of the solar disturbing function is

$$R_s = \frac{\mu_s r^2}{2 r_s^3} \left\{ \frac{3}{2} A_1 C_{2(f+\omega)} + 3 A_2 S_{2(f+\omega)} + \frac{3}{2} A_3 - 1 \right\} \qquad (35)$$

Where

$$A_1 = K_1 - K_3$$
$$A_2 = K_2 \qquad (36)$$
$$A_3 = K_1 + K_3$$

Averaging the Solar Disturbing Function

Just as with the Mars gravitational disturbing function, the fast periodic mean anomaly can be averaged out of the solar disturbing function. This is accomplished by integrating the disturbing function with respect to the mean anomaly over one orbit and dividing by the total change in mean anomaly (2π). Thus the average solar disturbing function is

$$\bar{R}_s = \frac{1}{2\pi} \int_0^{2\pi} R_s \, dM \tag{37}$$

Before integrating, the true anomaly must be separated from the argument of periapsis ω. Using the trigonometric relations

$$\begin{aligned} C_{2(f+\omega)} &= C_{2f} C_{2\omega} - S_{2f} S_{2\omega} \\ S_{2(f+\omega)} &= S_{2f} C_{2\omega} + C_{2f} S_{2\omega} \end{aligned} \tag{38}$$

The solar disturbing function may now be written as

$$\begin{aligned} R_s = \frac{\mu_s r^2}{2 r_s^3} \Big\{ & \frac{3}{2} A_1 C_{2f} C_{2\omega} - \frac{3}{2} A_1 S_{2f} S_{2\omega} + 3 A_2 S_{2f} C_{2\omega} + \\ & + 3 A_2 C_{2f} S_{2\omega} + \frac{3}{2} A_3 - 1 \Big\} \\ R_s = \frac{\mu_s r^2}{2 r_s^3} \Big\{ & \Big(\frac{3}{2} A_1 C_{2\omega} + 3 A_2 S_{2\omega} \Big) C_{2f} + \Big(3 A_2 C_{2\omega} - \frac{3}{2} A_1 S_{2\omega} \Big) S_{2f} + \\ & + \frac{3}{2} A_3 - 1 \Big\} \end{aligned} \tag{39}$$

Upon rearranging to a form useful for employing Hansen's Coefficients

$$R_s = \frac{\mu_s a^2}{2 r_s^3}\left\{\left(\frac{3}{2}A_1 C_{2\omega} + 3A_2 S_{2\omega}\right)\left(\frac{r}{a}\right)^2 C_{2f} + \left(3A_2 C_{2\omega} - \frac{3}{2}A_1 S_{2\omega}\right)\left(\frac{r}{a}\right)^2 S_{2\omega} + \left(\frac{3}{2}A_3 - 1\right)\left(\frac{r}{a}\right)^2\right\} \tag{40}$$

Employing Hansen's coefficients (Appendix A) to average out the Mean Anomaly using

$$\frac{1}{2\pi}\int_0^{2\pi}\left(\frac{r}{a}\right)^2 C_{2f}\, dM = X_0^{2,2} = \frac{5e^2}{2}$$

$$\frac{1}{2\pi}\int_0^{2\pi}\left(\frac{r}{a}\right)^2 S_{2f}\, dM = 0 \tag{41}$$

$$\frac{1}{2\pi}\int_0^{2\pi}\left(\frac{r}{a}\right)^2 dM = X_0^{2,0} = 1 + \frac{3}{2}e^2$$

After substitution, the averaged solar disturbing function becomes

$$\bar{R}_s = \frac{\mu_s a^2}{2 r_s^3}\left\{\left(\frac{3}{2}A_1 C_{2\omega} + 3A_2 S_{2\omega}\right)\frac{5e^2}{2} + \left(\frac{3}{2}A_3 - 1\right)\left(1 + \frac{3}{2}e^2\right)\right\}$$

$$= \frac{\mu_s a^2}{4 r_s^3}\left\{\frac{15}{2}e^2 A_1 C_{2\omega} + 15e^2 A_2 S_{2\omega} + (2 + 3e^2)\left(\frac{3}{2}A_3 - 1\right)\right\} \tag{42}$$

Substituting in the "A" variables results in

$$\begin{aligned}\bar{R}_s = \frac{\mu_s a^2}{4 r_s^3}\Bigg\{ & \frac{15}{2} e^2 \left[C_L^2 C_{(\Omega-\Lambda)}^2 - (C_i C_L S_{(\Omega-\Lambda)} - S_L S_i)^2 \right] C_{2\omega} \\ & + 15 e^2 \left\{ C_L S_L S_i C_{(\Omega-\Lambda)} - C_L^2 C_i C_{(\Omega-\Lambda)} S_{(\Omega-\Lambda)} \right\} S_{2\omega} + \\ & + (2 + 3e^2) \left[\frac{3}{2} \left[C_L^2 C_{(\Omega-\Lambda)}^2 + (C_i C_L S_{(\Omega-\Lambda)} - S_L S_i)^2 \right] - 1 \right] \Bigg\}\end{aligned} \tag{43}$$

However, this form still contains periodic effects due to the motion of the Sun. These may be averaged out when the mean motion of the Sun is greater than the rate of change of either ω or Ω. To find the condition under which this holds, use the Lagrange Planetary Equations to get the changes in ω and Ω. Use only the J2 portion of the disturbing function (R_m) to simplify the comparison. This is valid since, the affect of the J2 disturbing function is much greater than the solar effects. The necessary partial of the Mars disturbing function are

$$\begin{aligned}\frac{\partial \bar{R}_m}{\partial i} &= - \frac{3 n^2 J_2 R_e^2}{2 (1-e^2)^{3/2}} \sin i \cos i \\ \frac{\partial \bar{R}_m}{\partial e} &= \frac{3 n^2 J_2 R_e^2 e}{2 (1-e^2)^{5/2}} \left(1 - \frac{3}{2} \sin^2 i \right)\end{aligned} \tag{44}$$

The rates of change of Ω and ω are then

$$\frac{d\Omega}{dt} = -\frac{3nJ_2R_e^2}{2a^2(1-e^2)^2}\cos i$$
$$\frac{d\omega}{dt} = \frac{3nJ_2R_e^2}{2a^2(1-e^2)^2}\left(1 - \frac{3}{2}\sin^2 i + \cos^2 i\right) \quad (45)$$

By comparing the magnitudes of these rates of change

$$\frac{d\Omega}{dt} \sim \frac{d\omega}{dt} \sim \frac{J_2R_e^2\mu_m^{1/2}}{a^{7/2}(1-e^2)^2} \quad (46)$$

Therefore, the averaging of the solar motion is valid when

$$n_s > \frac{J_2R_e^2\mu_m^{1/2}}{a^{7/2}(1-e^2)^2} \quad (47)$$

This occurs for high eccentricity orbits with the lower bound of eccentricity decreasing with increasing periapsis radius. The majority of the orbits analyzed in the numerical section fall into this category.

After several change of variables and assuming the Sun's pseudo orbit to be circular, the time varying solar terms can be removed. The slowly varying solar disturbing function becomes

$$\bar{R}_s = \frac{n_s^2\, a^2}{4} \left\{ [2+3e^2] \left[\frac{3}{8} C_{2\Omega} S_{I_s}^2 S_I^2 + \frac{3}{2} C_I S_I S_{I_s} C_{I_s} C_\Omega \right.\right.$$
$$+ \frac{1}{4}\left(1 - \frac{3}{2} S_{I_s}^2\right)\left(3\, C_I^2 - 1\right) \Big\} + \frac{15}{4} e^2 \left\{ \frac{1}{4} S_{I_s}^2 (1+C_I^2)\, (C_{2\Omega+2\omega} + C_{2\Omega-2\omega}) \right. \quad (48)$$
$$\left. - C_I S_I C_{I_s} S_{I_s}\, (C_{\Omega+2\omega} + C_{\Omega-2\omega}) + S_I^2 \left(1 - \frac{3}{2} S_{I_s}^2\right) C_{2\omega} \right]$$
$$\left. - \frac{15}{2} e^2 \left[\frac{1}{4} C_I S_{I_s}^2 (C_{2\Omega-2\omega} - C_{2\Omega+2\omega}) - \frac{1}{2} S_{I_s} S_I C_{I_s} (C_{\Omega-2\omega} - C_{\Omega+2\omega}) \right] \right\}$$

where the mean motion of the Sun is

$$n_s = \sqrt{\frac{\mu_s}{a_s^3}} \quad (49)$$

The Combined Mars and Solar Disturbing Function

The mean anomaly and the periodic effects of the Sun's motion have been successfully averaged out of the disturbing functions, resulting in

$$R = \bar{R}_m + \bar{R}_s \tag{50}$$

$$\begin{aligned}\bar{R} = {} & \frac{\mu_m J_2 R_e^2}{2a^3 (1-e^2)^{3/2}}\left(1 - \frac{3}{2}\sin^2 i\right) \\ & + \frac{n_s^2 a^2}{4}\left\{ [2+3e^2]\left[\frac{3}{8} C_{2\Omega} S_{I_s}^2 S_I^2 + \frac{3}{2} C_I S_I S_{I_s} C_{I_s} C_\Omega \right.\right. \\ & \left. + \frac{1}{4}\left(1 - \frac{3}{2} S_{I_s}^2\right)(3C_I^2 - 1)\right\} + \frac{15}{4} e^2 \left\{\frac{1}{4} S_{I_s}^2 (1+C_I^2)\,(C_{2\Omega+2\omega} + C_{2\Omega-2\omega}) \right. \\ & \left. - C_I S_I C_{I_s} S_{I_s}\,(C_{\Omega+2\omega} + C_{\Omega-2\omega}) + S_I^2\left(1 - \frac{3}{2} S_{I_s}^2\right) C_{2\omega}\right] \\ & \left. - \frac{15}{2} e^2 \left[\frac{1}{4} C_I S_{I_s}^2 (C_{2\Omega-2\omega} - C_{2\Omega+2\omega}) - \frac{1}{2} S_{I_s} S_I C_{I_s} (C_{\Omega-2\omega} - C_{\Omega+2\omega})\right]\right\}\end{aligned} \tag{51}$$

Determination of Critical Inclinations by Analytic Methods

The long period variations in eccentricity and inclination may now be obtained through use of Hamiltonian mechanics and canonical transformations. Detailed explanitions are in ref (5).

The transformation of the disturbing function results in an equation with six divisors. Eleven critical inclinations result when these are equated to zero.

Table 1. Critical Inclinations

63.4 deg	116.6 deg
46.4 deg	106.8 deg
73.2 deg	133.6 deg
56.1 deg	111.0 deg
69.0 deg	123.9 deg
90.0 deg	

These inclinations represent the limiting case for critical inclinations and were derived with the simplification of solar averaging. Due to the complexity of the problem, a systematic numerical approach is necessary to ascertain the true nature of the critical inclinations without the above simplifications. However, the results in table (1) should roughly correspond to any numeric results.

III. Numerical Development and Results

The analytical development produced eleven critical inclinations resulting from resonant situations. This occurred when terms in the denominator of the equations of motion went to zero, thus indicating large amplitude motion. However, in reality these amplitudes are not infinite. They build up over time due to the additive effect of the resonance condition. The equations of motion are still valid and can be numerically integrated as long as the integration time is small enough that the amplitude does not exceed the limitations of the computer (overflow condition). The effect of the resonance will still be visible even with the limited integration time. The amplitude of the motion will not go to infinity, but will be large compared to non-resonance conditions. Therefore, a numerical approach may be used to find the critical inclinations.

This involves integrating a sufficient number of orbits over a range of eccentricities, inclinations, and periapsis altitudes (initial conditions) to permit the determination of critical inclinations.

Equations of Motion

The numerical analysis used a transformed set of the Lagrange Planetary Equations used in the analytic analysis. The change of variables was used to simplify the implementation of the equations on the computer. The same

disturbing function used in the analytic approach was used for the numerical integration. As discussed previously, the mean anomaly is averaged out of the disturbing function while still preserving the effects of the resonance conditions. This averaging out of the mean anomaly eases the numerical integration by simplifying the equations of motion. The integration time is also greatly reduced. A step size of days instead of minutes can be used.

Since the mean anomaly was averaged out and the primary interest was the slow variable changes, such as inclination and eccentricity, the dM/dt equation was not needed. Furthermore, the semi-major axis remains constant (da/dt=0) since the mean anomaly was averaged out of the disturbing function ($\partial R/\partial M=0$). This reduced the number of relevant Lagrange Equations to the following four:

$$\begin{aligned}
\frac{de}{dt} &= \frac{b^2}{na^4e}\frac{\partial R}{\partial M} - \frac{b}{na^3e}\frac{\partial R}{\partial \omega} \\
\frac{di}{dt} &= -\frac{1}{nab\sin i}\frac{\partial R}{\partial \Omega} + \frac{\cos i}{nab\sin i}\frac{\partial R}{\partial \omega} \\
\frac{d\Omega}{dt} &= \frac{1}{nab\sin i}\frac{\partial R}{\partial i} \\
\frac{d\omega}{dt} &= -\frac{\cos i}{nab\sin i}\frac{\partial R}{\partial i} + \frac{b}{na^3e}\frac{\partial R}{\partial e}
\end{aligned} \qquad (52)$$

$$\text{where} \quad b = a\sqrt{1-e^2} \quad \& \quad n = \sqrt{\frac{\mu}{a^3}}$$

A change of variables from the classical (a,e,i,Ω,ω,M) to the new variables (a,h,k,Ω,λ^N,i) was then used to facilitate the integration.

$$h = e \sin\omega$$
$$k = e \cos\omega \tag{53}$$
$$\lambda_N = \frac{M+\omega}{S_0} + (\Omega - \phi)$$

The transformation to the h and k variables avoids the singularities due to the classical variable set (a,e,i,Ω,M). The transformed equations are non-singular for zero eccentricity, but singular for zero inclination. The stroboscopic mean node (λ_N) transformation permits the averaging of the motion due to the fast mean anomaly variable, while maintaining the longer term resonance effects as discussed in the analytic section. The following derivatives are required in the transformation:

$$\frac{\partial R}{\partial \omega} = \frac{\partial R}{\partial h}\frac{\partial h}{\partial \omega} + \frac{\partial R}{\partial k}\frac{\partial k}{\partial \omega} = k\frac{\partial R}{\partial h} - h\frac{\partial R}{\partial k}$$
$$\frac{\partial R}{\partial e} = \frac{\partial R}{\partial h}\frac{\partial h}{\partial e} + \frac{\partial R}{\partial k}\frac{\partial k}{\partial e} = \frac{h}{e}\frac{\partial R}{\partial h} + \frac{k}{e}\frac{\partial R}{\partial k} \tag{54}$$

$$\frac{dh}{dt} = \frac{\partial h}{\partial e}\frac{de}{dt} + \frac{\partial h}{\partial \omega}\frac{d\omega}{dt} = \frac{h}{e}\frac{de}{dt} + k\frac{d\omega}{dt}$$

$$\frac{dh}{dt} = \frac{h}{e}\left(-\frac{b}{na^3e}\right)\left(k\frac{\partial R}{\partial h} - h\frac{\partial R}{\partial k}\right)$$

$$+ k\left[-\frac{\cos i}{nab\sin i}\frac{\partial R}{\partial i} + \frac{b}{na^3e}\left(\frac{h}{e}\frac{\partial R}{\partial h} + \frac{k}{e}\frac{\partial R}{\partial k}\right)\right] \qquad (55)$$

$$\frac{dh}{dt} = \frac{b}{na^3}\frac{\partial R}{\partial k} - \frac{k\cos i}{nab\sin i}\frac{\partial R}{\partial i}$$

$$\frac{dk}{dt} = \frac{\partial k}{\partial e}\frac{de}{dt} + \frac{\partial k}{\partial \omega}\frac{d\omega}{dt} = \frac{k}{e}\frac{de}{dt} - h\frac{d\omega}{dt}$$

$$\frac{dk}{dt} = \frac{k}{e}\left(-\frac{b}{na^3e}\right)\left(k\frac{\partial R}{\partial h} - h\frac{\partial R}{\partial k}\right)$$

$$- h\left[-\frac{\cos i}{nab\sin i}\frac{\partial R}{\partial i} + \frac{b}{na^3e}\left(\frac{h}{e}\frac{\partial R}{\partial h} + \frac{k}{e}\frac{\partial R}{\partial k}\right)\right] \qquad (56)$$

$$\frac{dk}{dt} = -\frac{b}{na^3}\frac{\partial R}{\partial h} + \frac{\cos i}{nab\sin i}\frac{\partial R}{\partial i}$$

The four relevant Lagrange Planetary Equations are then transformed to the new elements.

$$\frac{dh}{dt} = \frac{b}{na^3}\frac{\partial R}{\partial k} - \frac{k\cot i}{nab}\frac{\partial R}{\partial i}$$

$$\frac{di}{dt} = \frac{\cot i}{nab}\left(k\frac{\partial R}{\partial h} - h\frac{\partial R}{\partial k}\right) - \frac{1}{nab\sin i}\frac{\partial R}{\partial \Omega}$$

$$\frac{dk}{dt} = -\frac{b}{na^3}\frac{\partial R}{\partial h} + \frac{h\cot i}{nab}\frac{\partial R}{\partial i} \qquad (57)$$

$$\frac{d\Omega}{dt} = \frac{1}{nab\sin i}\frac{\partial R}{\partial i}$$

where $b = a\sqrt{1-e^2}$ & $e = \sqrt{h^2 + k^2}$

Now the disturbing function must also be transformed to the new variables $(a,h,k,\Omega,\lambda^N,i)$.

$$
\begin{aligned}
R = {} & \frac{\mu_m J_2 R_e^2}{2a^3(1-h^2-k^2)^{3/2}}\left(1 - \frac{3}{2}\sin^2 i\right) \\
& + \frac{\mu_s a^2}{4r_s^3}\left\{\frac{15}{2}\left[C_L^2 C_{(\Omega-\Lambda)}^2 - (C_i C_L S_{(\Omega-\Lambda)} - S_L S_i)^2\right](k^2 - h^2)\right. \\
& + 30\left[C_L S_L S_i C_{(\Omega-\Lambda)} - C_L^2 C_i C_{(\Omega-\Lambda)} S_{(\Omega-\Lambda)}\right]hk \\
& \left. + (2 + 3h^2 + 3k^2)\left[\frac{3}{2}\left[C_L^2 C_{(\Omega-\Lambda)}^2 + (C_i C_L S_{(\Omega-\Lambda)} - S_L S_i)^2\right] - 1\right]\right\}
\end{aligned}
\tag{58}
$$

The following four partial derivatives of this disturbing function were then used in the transformed Lagrange Planetary equations.

$$
\begin{aligned}
\frac{\partial R}{\partial k} = {} & \frac{3\mu_m J_2 R_e^2 k}{2a^3(1-h^2-k^2)^{5/2}}\left(1 - \frac{3}{2}\sin^2 i\right) \\
& + \frac{\mu_s a^2 k}{4r_s^3}\left\{15\left[C_L^2 C_{(\Omega-\Lambda)}^2 - (C_i C_L S_{(\Omega-\Lambda)} - S_L S_i)^2\right]\right. \\
& + 30\left[C_L S_L S_i C_{(\Omega-\Lambda)} - C_L^2 C_i C_{(\Omega-\Lambda)} S_{(\Omega-\Lambda)}\right]h \\
& \left. + 6k\left[\frac{3}{2}\left[C_L^2 C_{(\Omega-\Lambda)}^2 + (C_i C_L S_{(\Omega-\Lambda)} - S_L S_i)^2\right] - 1\right]\right\}
\end{aligned}
\tag{59}
$$

$$\frac{\partial R}{\partial h} = \frac{3\mu_m J_2 R_e^2 h}{2a^3(1-h^2-k^2)^{5/2}}\left(1 - \frac{3}{2}\sin^2 i\right)$$

$$+ \frac{\mu_s a^2 h}{4r_s^3}\Big\{ - 15\left[C_L^2 C_{(\Omega-\Lambda)}^2 - (C_i C_L S_{(\Omega-\Lambda)} - S_L S_i)^2\right] \qquad (60)$$

$$+ 30\left[C_L S_L S_i C_{(\Omega-\Lambda)} - C_L^2 C_i C_{(\Omega-\Lambda)} S_{(\Omega-\Lambda)}\right] k$$

$$+ 6h\left[\frac{3}{2}\left[C_L^2 C_{(\Omega-\Lambda)}^2 + (C_i C_L S_{(\Omega-\Lambda)} - S_L S_i)^2\right] - 1\right]\Big\}$$

$$\frac{\partial R}{\partial i} = \frac{-3\mu_m J_2 R_e^2}{4a^3(1-h^2-k^2)^{3/2}} \sin 2i$$

$$+ \frac{\mu_s a^2}{4r_s^3}\{15\,(C_i C_L S_{(\Omega-\Lambda)} - S_L S_i)\,(S_i C_L S_{(\Omega-\Lambda)} + S_L C_i)\,(k^2 - h^2)$$

$$+ 30\left[C_L S_L C_i C_{(\Omega-\Lambda)} + C_L^2 S_i C_{(\Omega-\Lambda)} S_{(\Omega-\Lambda)}\right] hk$$

$$- 3\,(2+3h^2+3k^2)\,(C_i C_L S_{(\Omega-\Lambda)} - S_L S_i)\,(S_i C_L S_{(\Omega-\Lambda)} + S_L C_i)\,\}$$

(61)

$$\frac{\partial R}{\partial \Omega} = \frac{\mu_s a^2}{4r_s^3}\Big\{-\frac{15}{2}\left[C_L^2 S_{2(\Omega-\Lambda)} + 2\,(C_i C_L S_{(\Omega-\Lambda)} - S_L S_i)\,C_i C_L C_{(\Omega-\Lambda)}\right](k^2-h^2)$$

$$- 30\left[C_L S_L S_i S_{(\Omega-\Lambda)} + C_L^2 C_i C_{2(\Omega-\Lambda)}\right] hk$$

$$- \frac{3}{2}\,(2+3h^2+3k^2)\left[C_L^2 S_{2(\Omega-\Lambda)} - 2\,(C_i C_L S_{(\Omega-\Lambda)} - S_L S_i)\,C_i C_L C_{(\Omega-\Lambda)}\right]\Big\}$$

(62)

These partial derivatives of the disturbing function combined with the modified Lagrange Planetary Equations were then integrated for each set of initial orbital elements.

The full set of transformed Lagrange Planetary equations, without the simplifications made previously, are as follows (17,3-3):

$$\frac{da}{dt} = \frac{2}{na}\,\frac{1}{S_0}\,\frac{\partial R}{\partial \lambda_N}$$

$$\frac{dh}{dt} = \frac{\sqrt{1-e^2}}{na^2}\,\frac{\partial R}{\partial k} - \frac{k\cot i}{na^2\sqrt{1-e^2}}\,\frac{\partial R}{\partial i} - \frac{h\sqrt{1-e^2}}{na^2 S_0}\,\beta'\,\frac{\partial R}{\partial \lambda_N}$$

$$\frac{di}{dt} = \frac{\cot i}{na^2\sqrt{1-e^2}}\left(k\,\frac{\partial R}{\partial h} - h\,\frac{\partial R}{\partial k} + \frac{1}{S_0}\,\frac{\partial R}{\partial \lambda_N}\right) - \frac{1}{na^2\sqrt{1-e^2}\,\sin i}\left(\frac{\partial R}{\partial \Omega} + \frac{\partial R}{\partial \lambda_N}\right)$$

$$\frac{dk}{dt} = -\frac{\sqrt{1-e^2}}{na^2}\,\frac{\partial R}{\partial h} + \frac{h\cot i}{na^2\sqrt{1-e^2}}\,\frac{\partial R}{\partial i} - \frac{k\sqrt{1-e^2}}{na\,S_0}\,\beta'\,\frac{\partial R}{\partial \lambda_N}$$

$$\frac{d\Omega}{dt} = \frac{1}{na^2\sqrt{1-e^2}\,\sin i}\,\frac{\partial R}{\partial i}$$

$$\frac{d\lambda_N}{dt} = \frac{n}{S_0} - \frac{d\theta}{dt} + \frac{1}{na^2 S_0}\left\{\sqrt{1-e^2}\,\beta'\left(h\,\frac{\partial R}{\partial h} + k\,\frac{\partial R}{\partial k}\right) - 2a\,\frac{\partial R}{\partial a} + \frac{S_0 - \cos i}{\sqrt{1-e^2}\,\sin i}\,\frac{\partial R}{\partial i}\right\}$$

where $\quad n = \sqrt{\frac{\mu}{a^3}} \quad e = \sqrt{h^2 + k^2} \quad \beta' = \frac{1}{1+\sqrt{1-e^2}}$

(63)

λ^N = stroboscopic mean node — e = eccentricity

θ = Greenwich hour angle — a = semi-major axis

Ω = longitude of ascending node — M = mean anomaly

ω = argument of periapsis — i = inclination

S_0 = ratio that approximates the number of orbits per planet revolution

Determination of Critical Inclinations

Critical inclinations were defined as those inclinations that produce large variations in one of the orbital elements. This numerical approach was looking for critical inclinations in both eccentricity and inclination.

Search Method

The search was accomplished by giving each orbit two figures of merit. These were the standard deviation in eccentricity and inclination. While using the standard deviation as a search criteria for critical inclinations was not an ideal approach, it proved to be a satisfactory method to handle the huge quantities of data that required processing.

Procedure

The averaged equations of motion for a satellite were numerically integrated over a 10 Earth year period for a given set of initial conditions. The variable initial conditions were systematically incremented to cover the entire spectrum of possible orbits about Mars. Initial conditions included the following:

r_p = variable	periapsis radius (5000 km, 5500 km, 6000 km, 6500 km, 7000 km, 7500 km)
e = variable	eccentricity (0.4 to 0.9, Δ = 0.02)
i = variable	inclination (0.25 to 90., Δ = 0.25)
Ω = 0	longitude of the ascending node

$\omega = 0$ argument of periapsis

$M = 0$ mean anomaly

For each orbit (set of initial conditions), the standard deviation of the variations in eccentricity and inclination were calculated using a linear, quadratic, and cubic polynomial approximation to the variations.

Two dimensional plots of the standard deviation in eccentricity (SDE) and standard deviation in inclination (SDI) vs inclination were generated for each initial eccentricity value. All the SDE vs inclination and SDI vs inclination plots were combined into three dimensional surface plots. These surface plots were then used to identify the critical inclinations in both eccentricity and inclination.

Surface Plots

A total of six sets of three dimensional surface plots were generated. Each set contains six plots of the standard deviation in eccentricity or inclination, for a given data fit, versus initial insertion orbit eccentricity and inclination. Linear, quadratic, and cubic data fits were used in determining the standard deviations.

Only the 5000 km and 7500 km periapsis radius cases include the linear, quadratic, and cubic data fits for SDE and SDI. These demonstrate the effect of using higher order polynomials in computing the standard deviations. Note the

smoothing of the features and reduction in magnitudes. The remaining surface plots are for a cubic data fit. The other linear and quadratic data fit plots are in Appendix B and C.

Standard Deviation in Eccentricity (SDE) Surface Plots

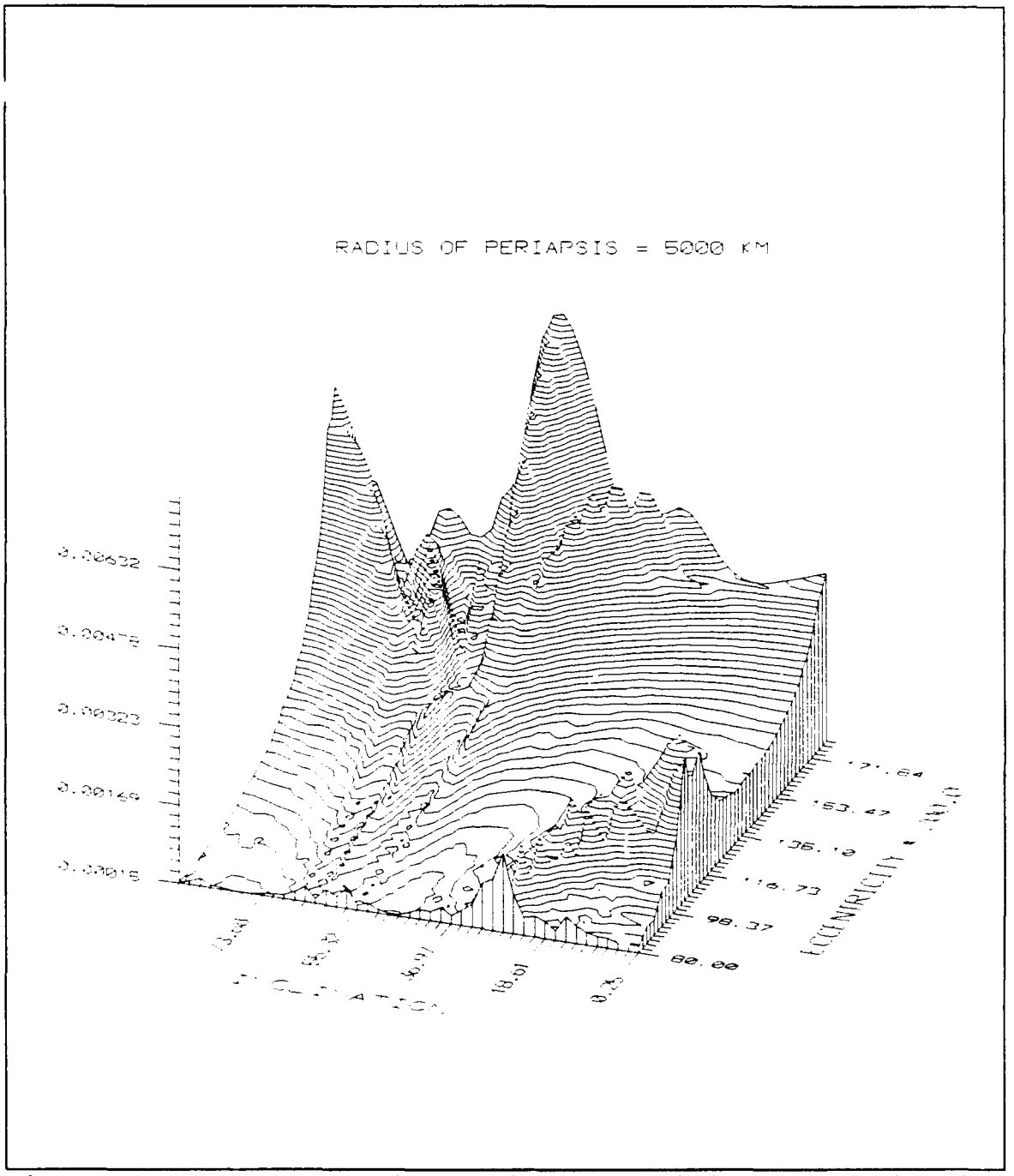

Figure 6. Standard Deviation in Eccentricity vs Inclination and Eccentricity: Periapse Radius = 5000 Km, Linear Data Fit

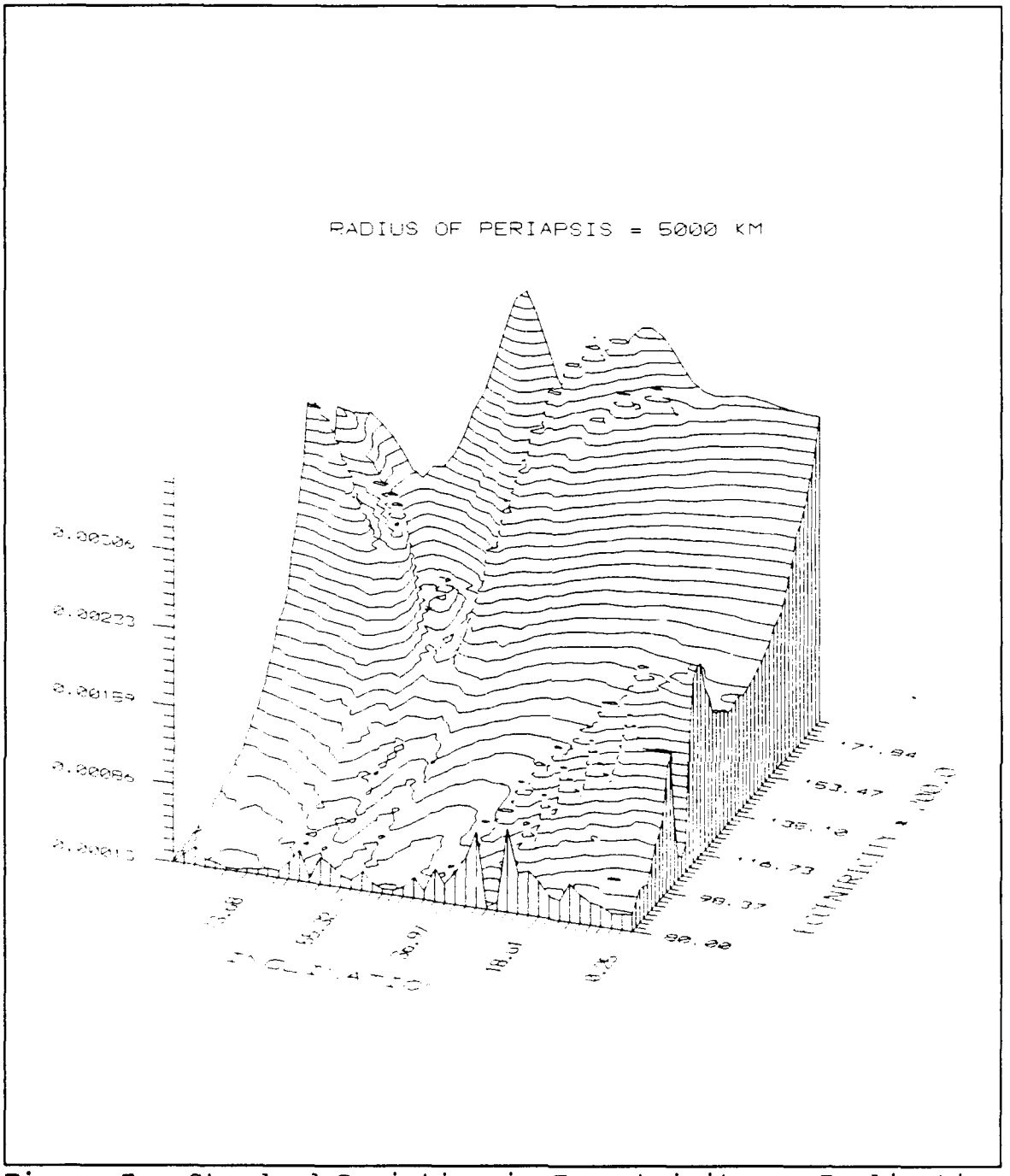

Figure 7. Standard Deviation in Eccentricity vs Inclination and Eccentricity: Periapse Radius = 5000 Km, Quadratic Data Fit

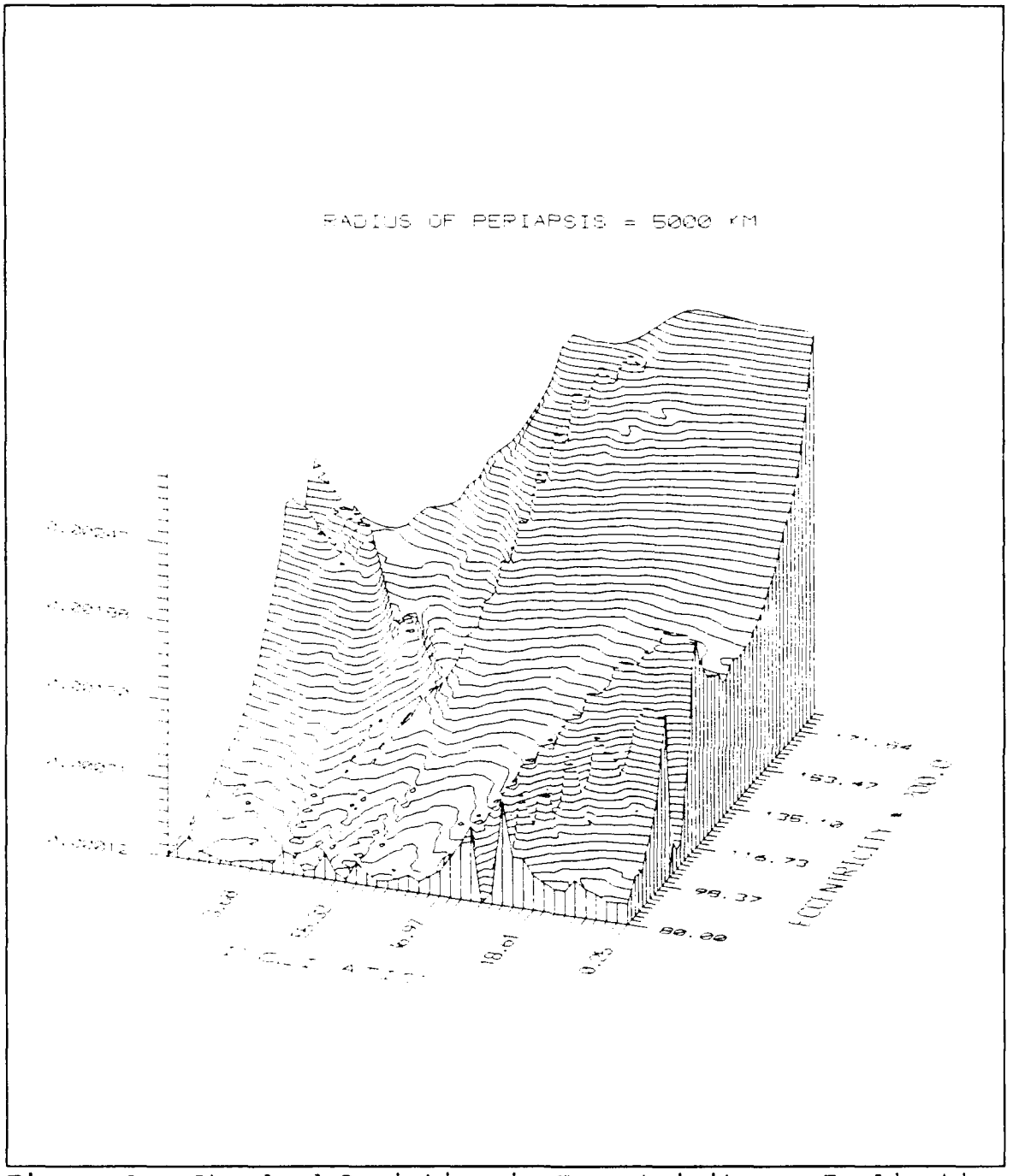

Figure 8. Standard Deviation in Eccentricity vs Inclination and Eccentricity: Periapse Radius = 5000 Km, Cubic Data Fit

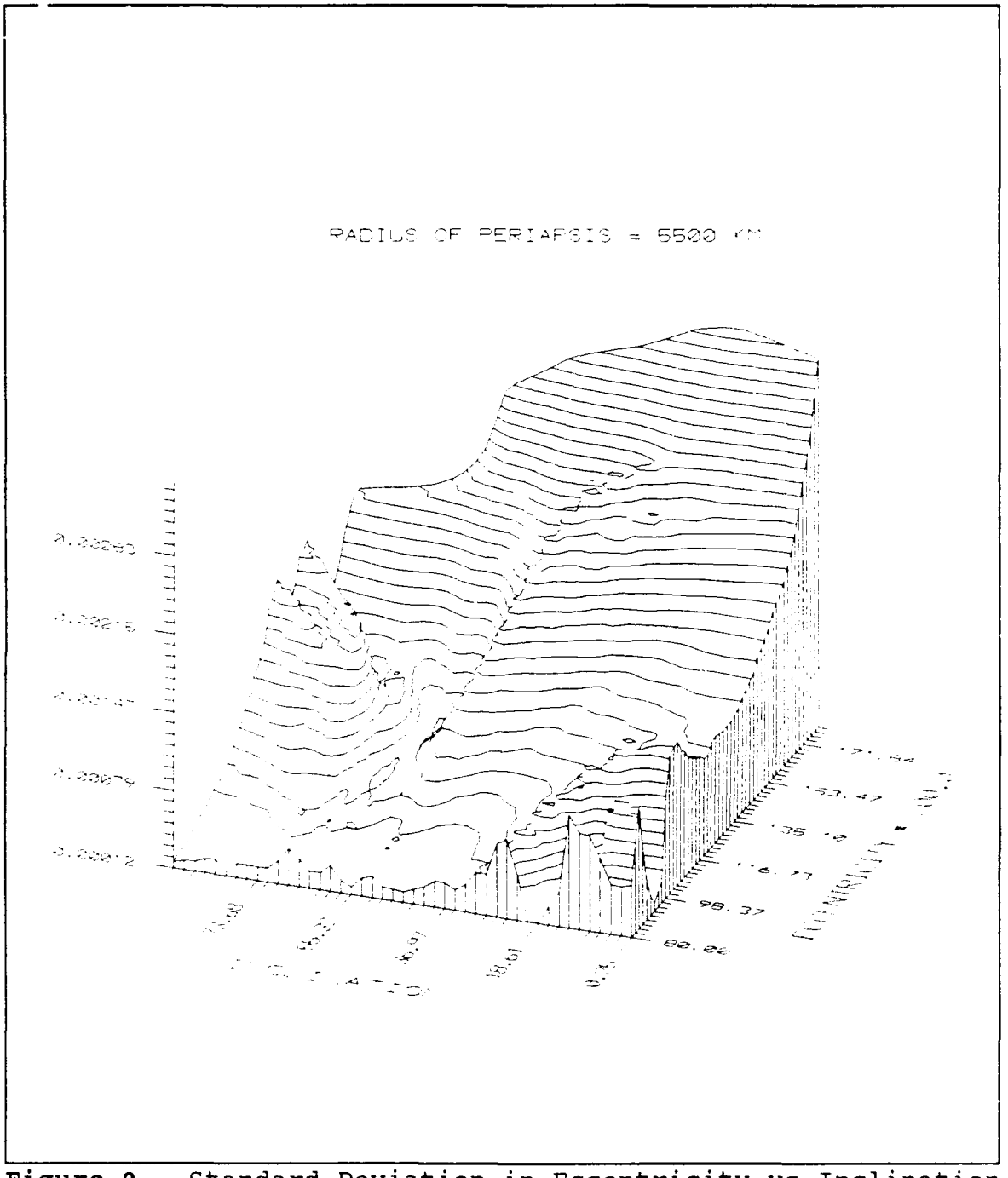

Figure 9. Standard Deviation in Eccentricity vs Inclination and Eccentricity: Periapse Radius = 5500 Km, Cubic Data Fit

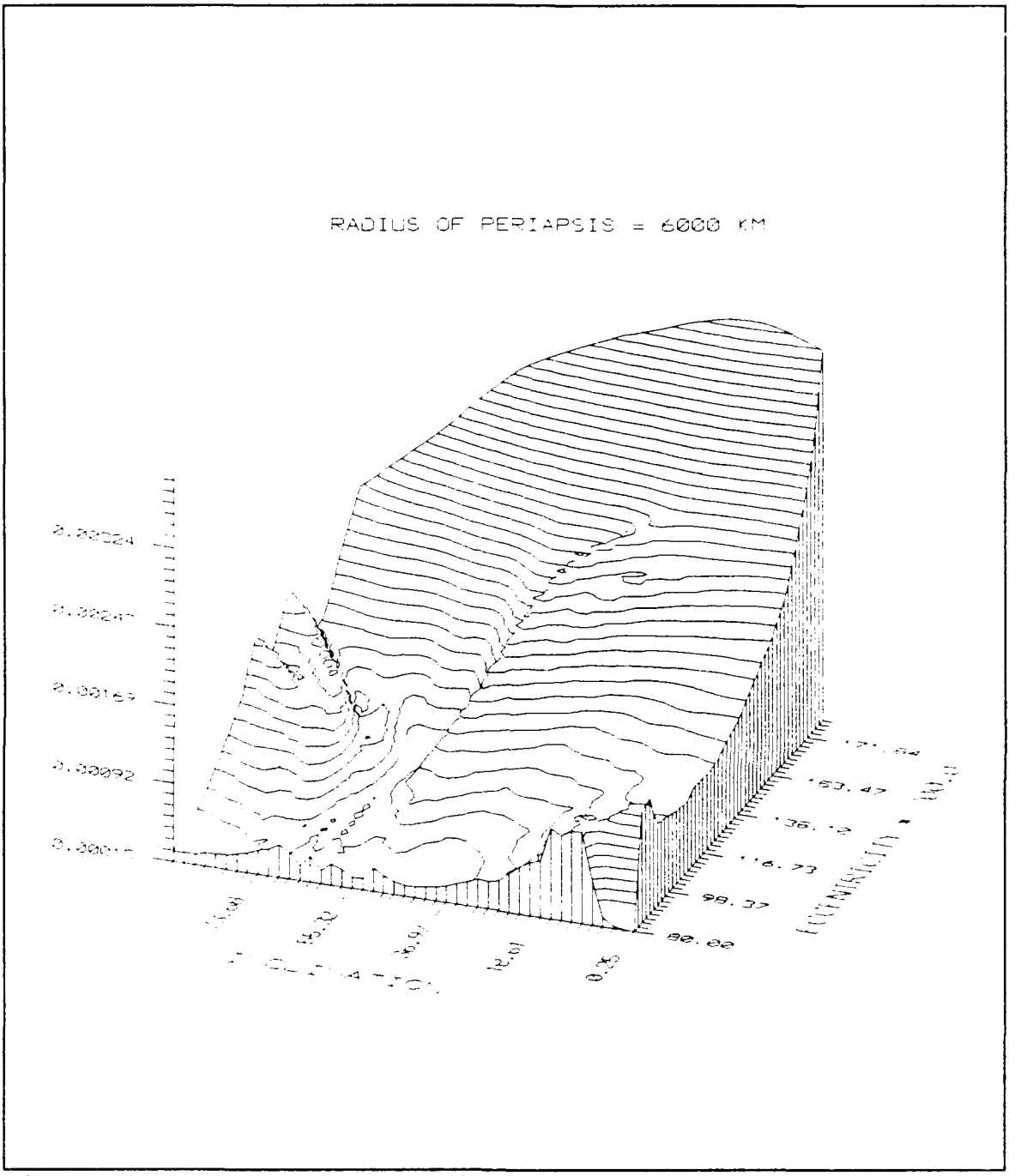

Figure 10. Standard Deviation in Eccentricity vs Inclination and Eccentricity: Periapse Radius = 6000 Km, Cubic Data Fit

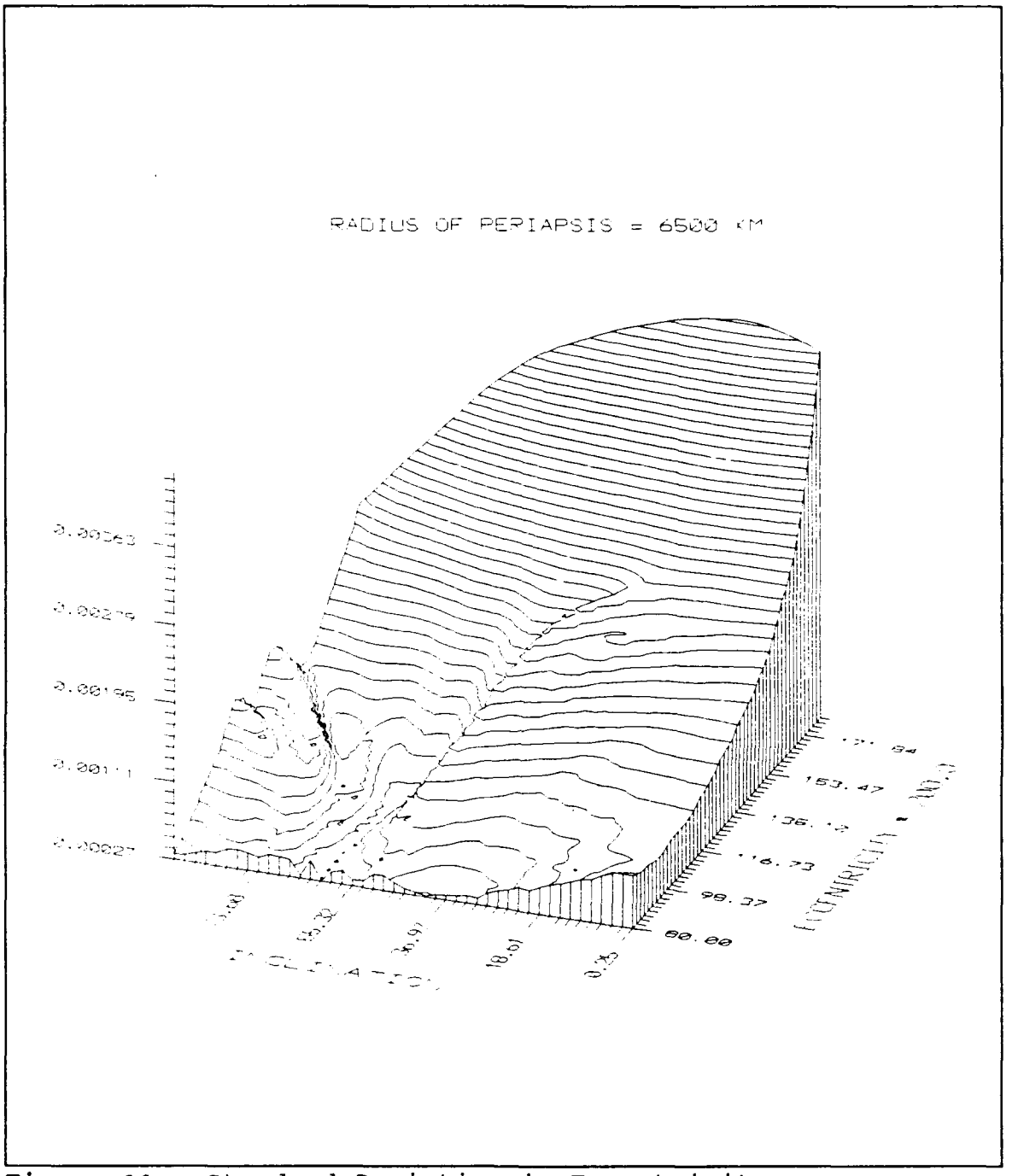

Figure 11. Standard Deviation in Eccentricity vs Inclination and Eccentricity: Periapse Radius = 6500 Km, Cubic Data Fit

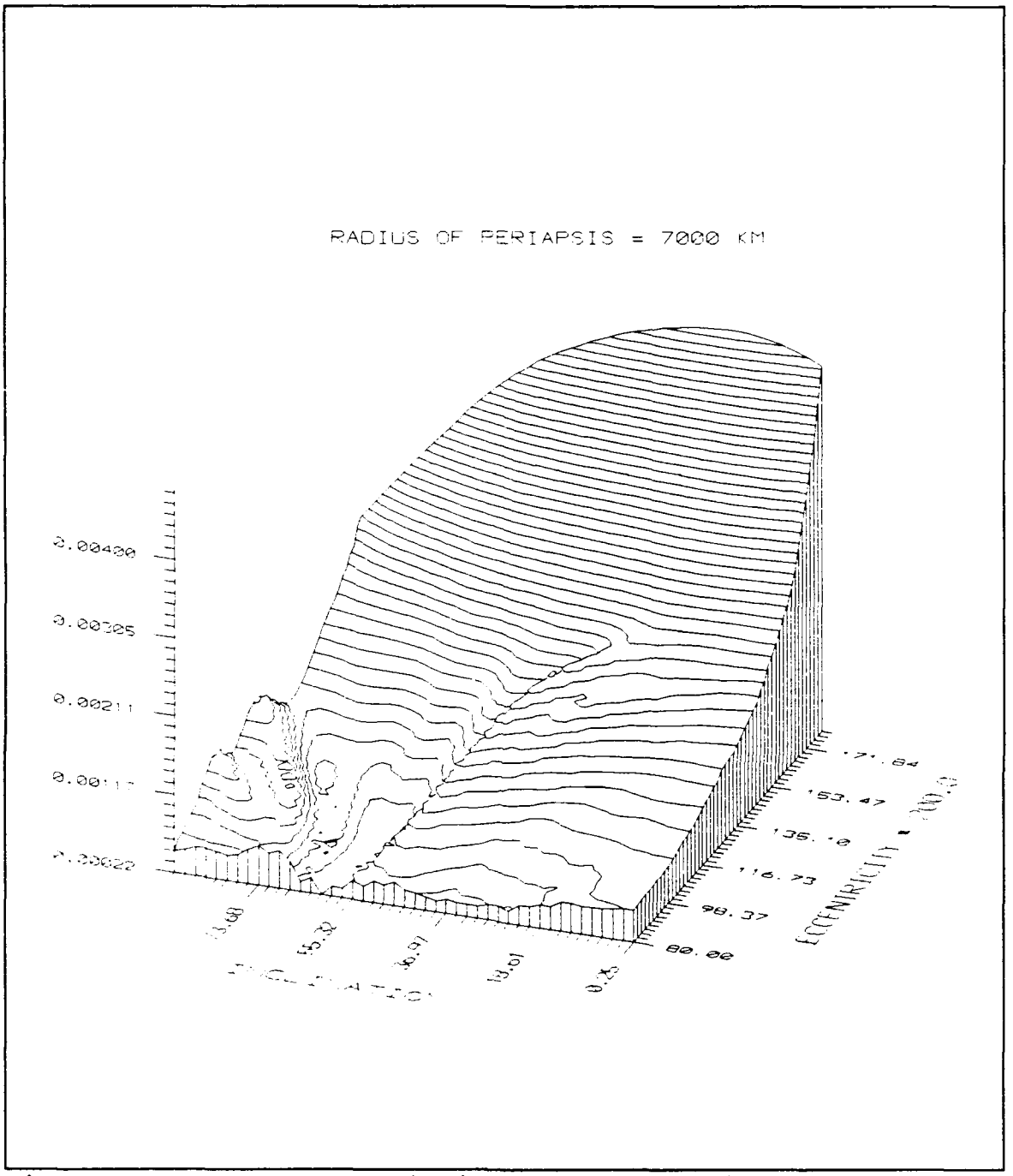

Figure 12. Standard Deviation in Eccentricity vs Inclination and Eccentricity: Periapse Radius = 7000 Km, Cubic Data Fit

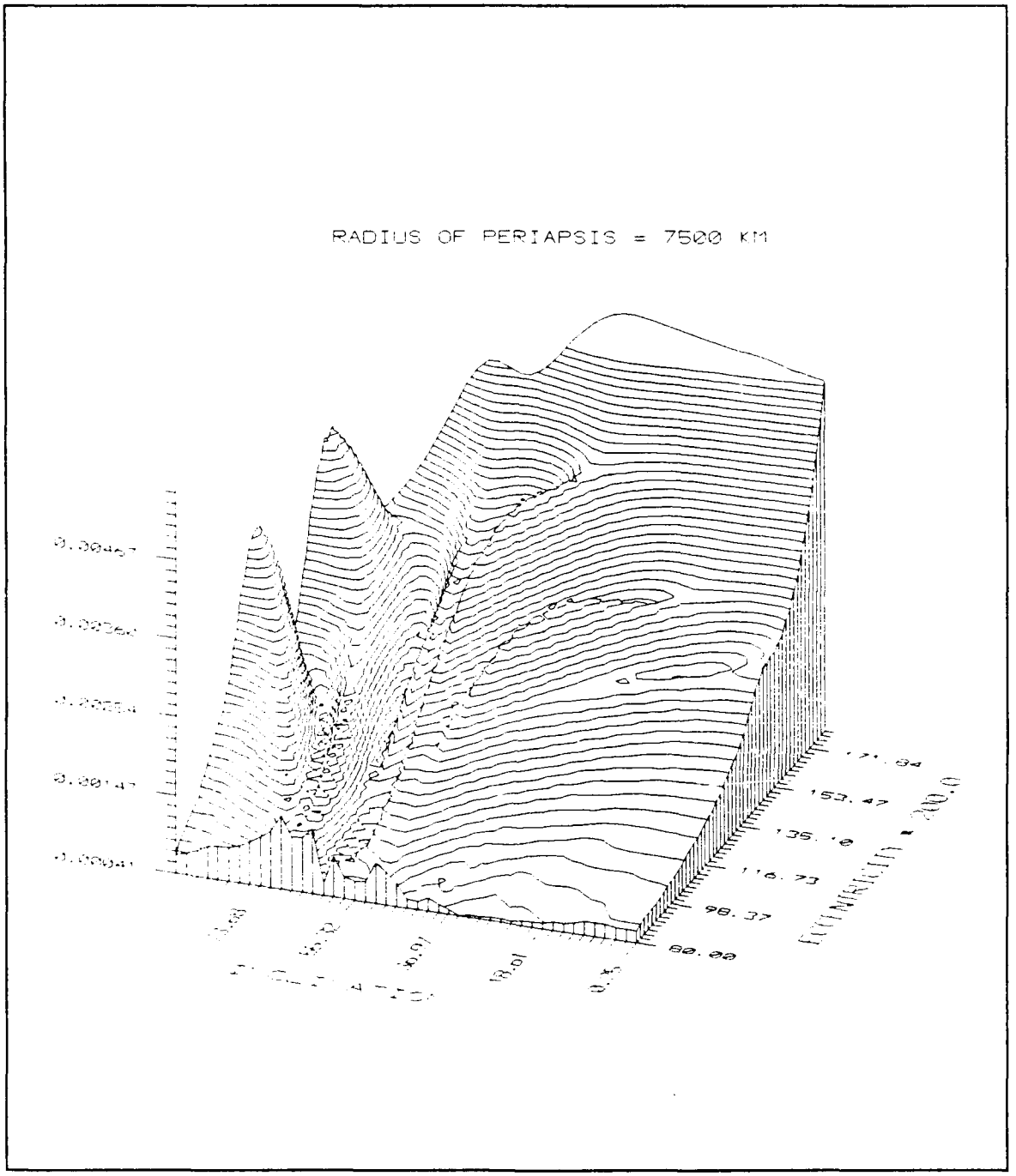

Figure 13. Standard Deviation in Eccentricity vs Inclination and Eccentricity: Periapse Radius = 7500 Km, Linear Data Fit

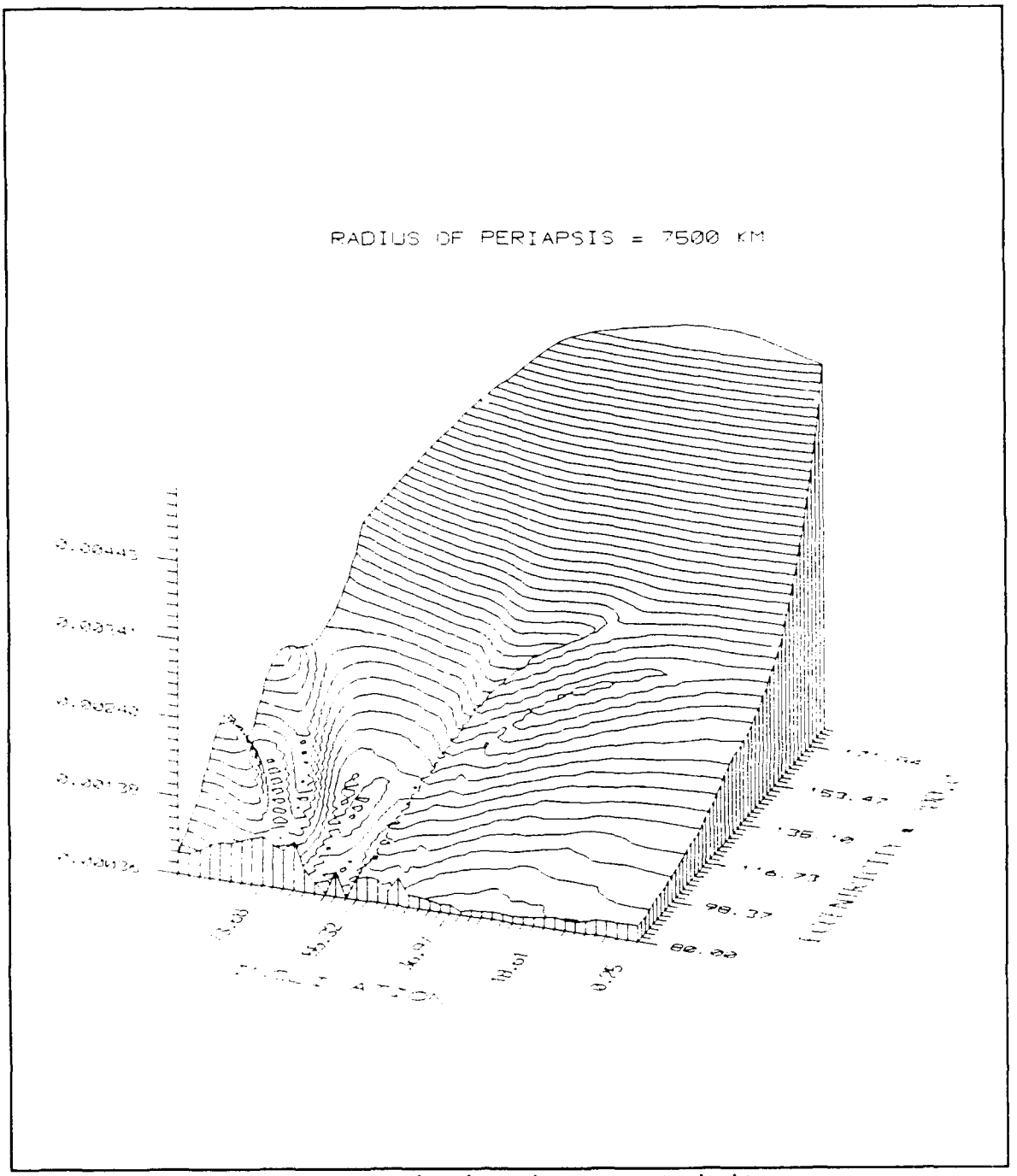

Figure 14. Standard Deviation in Eccentricity vs Inclination and Eccentricity: Periapse Radius = 7500 Km, Quadratic Data Fit

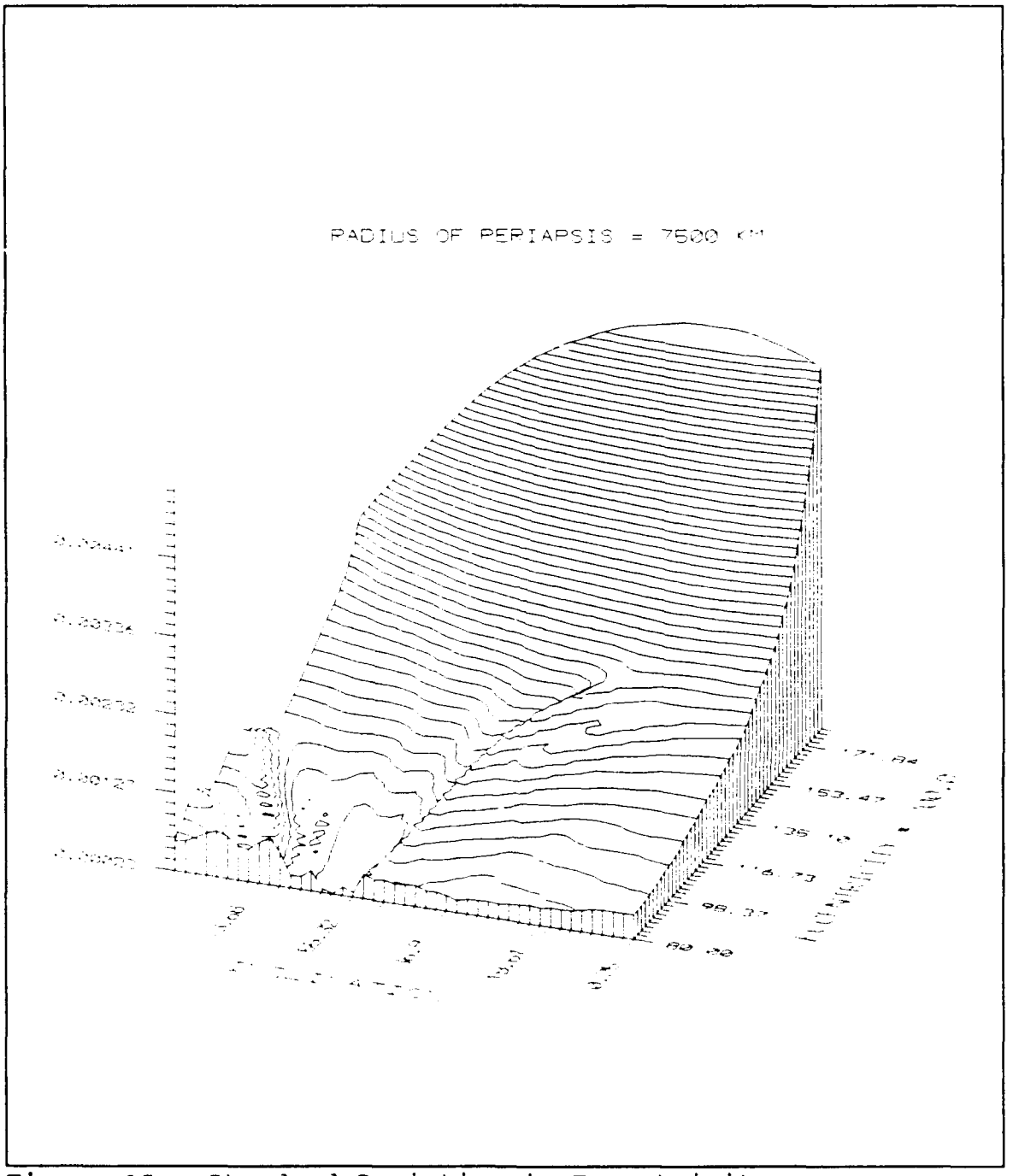

Figure 15. Standard Deviation in Eccentricity vs Inclination and Eccentricity: Periapse Radius = 7500 Km, Cubic Data Fit

Standard Deviation in Inclination (SDI) Surface Plots

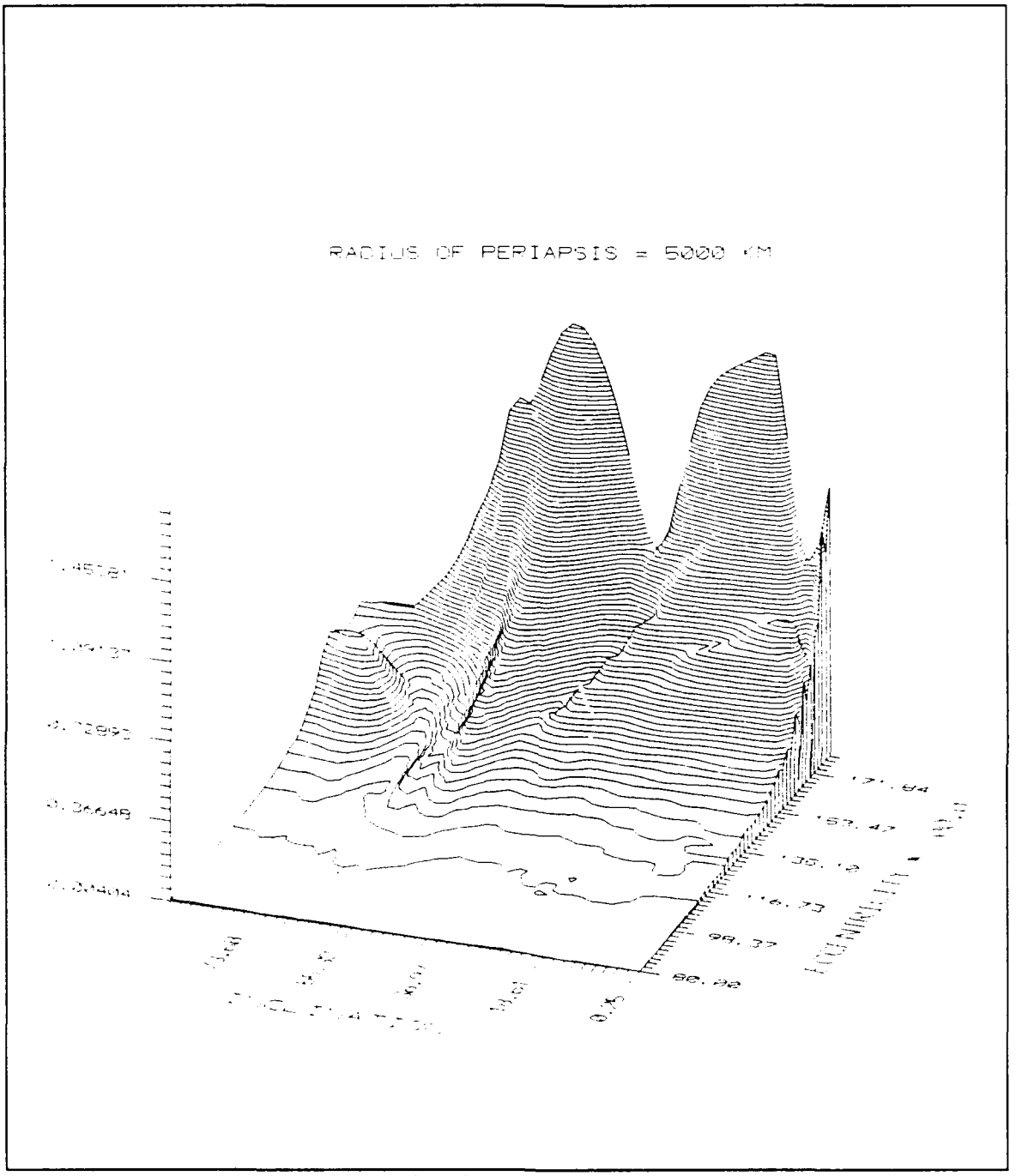

Figure 16. Standard Deviation in Inclination vs Inclination and Eccentricity: Periapse Radius = 5000 Km, Linear Data Fit

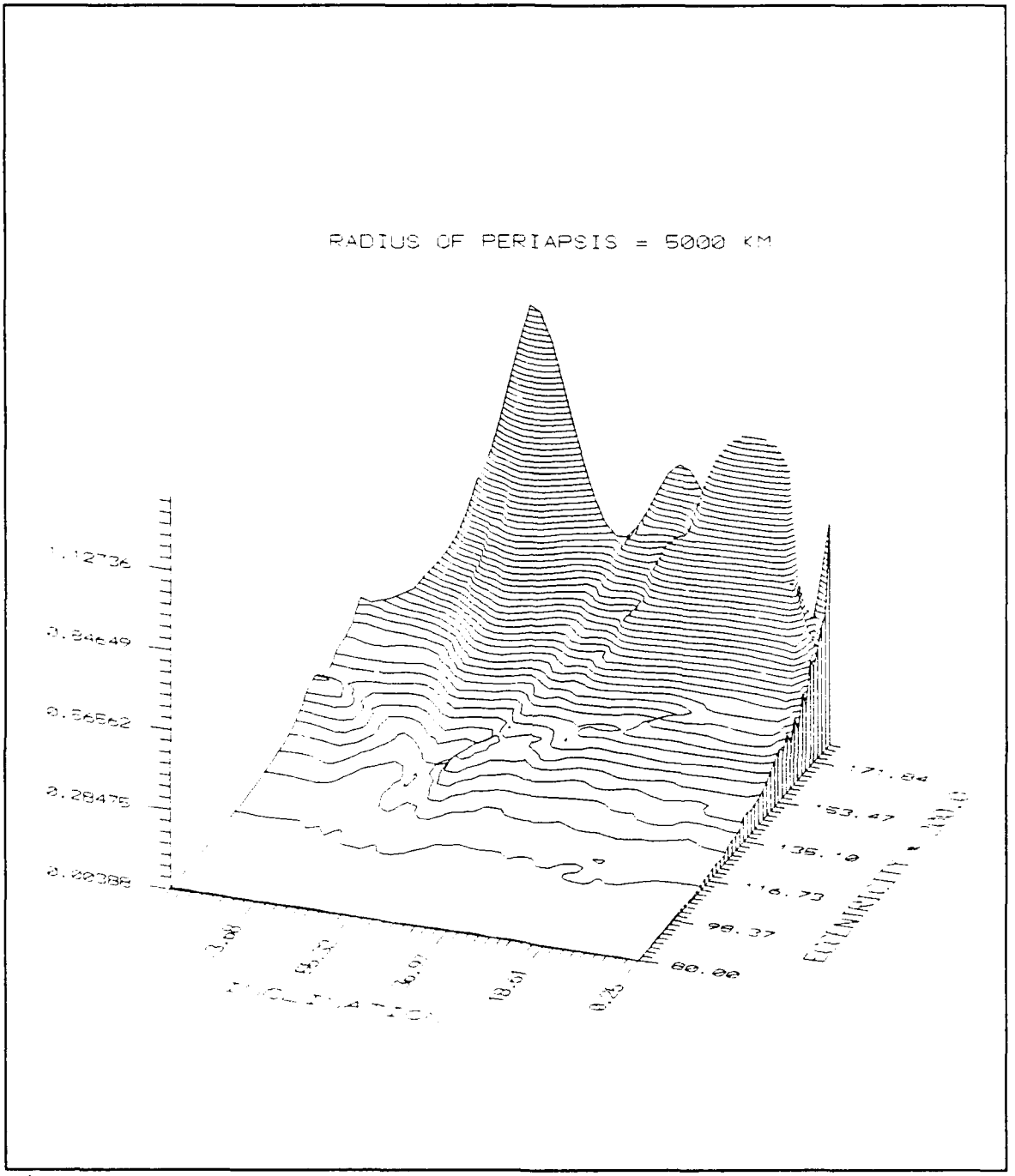

Figure 17. Standard Deviation in Inclination vs Inclination and Eccentricity: Periapse Radius = 5000 Km, Quadratic Data Fit

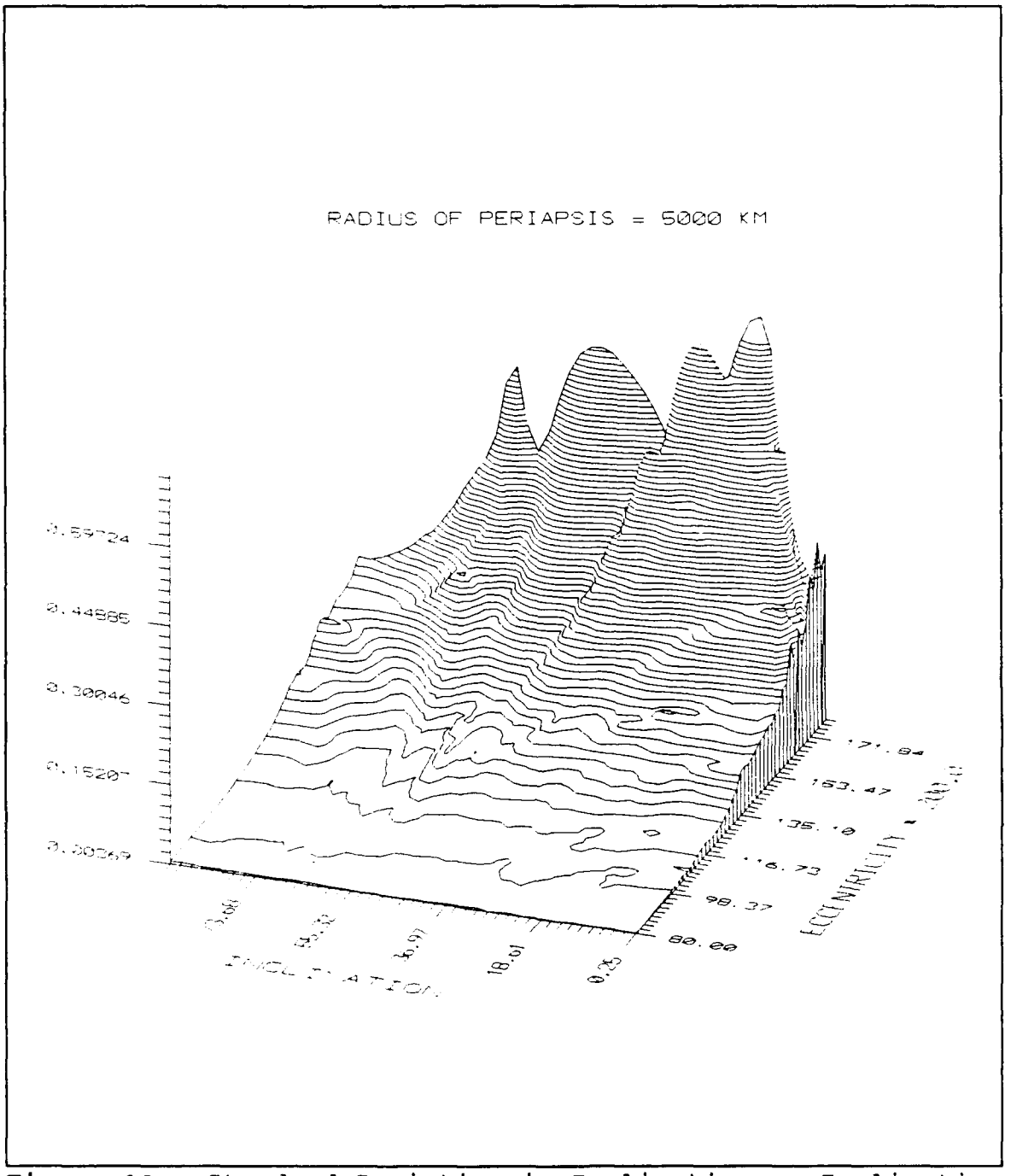

Figure 18. Standard Deviation in Inclination vs Inclination and Eccentricity: Periapse Radius = 5000 Km, Cubic Data Fit

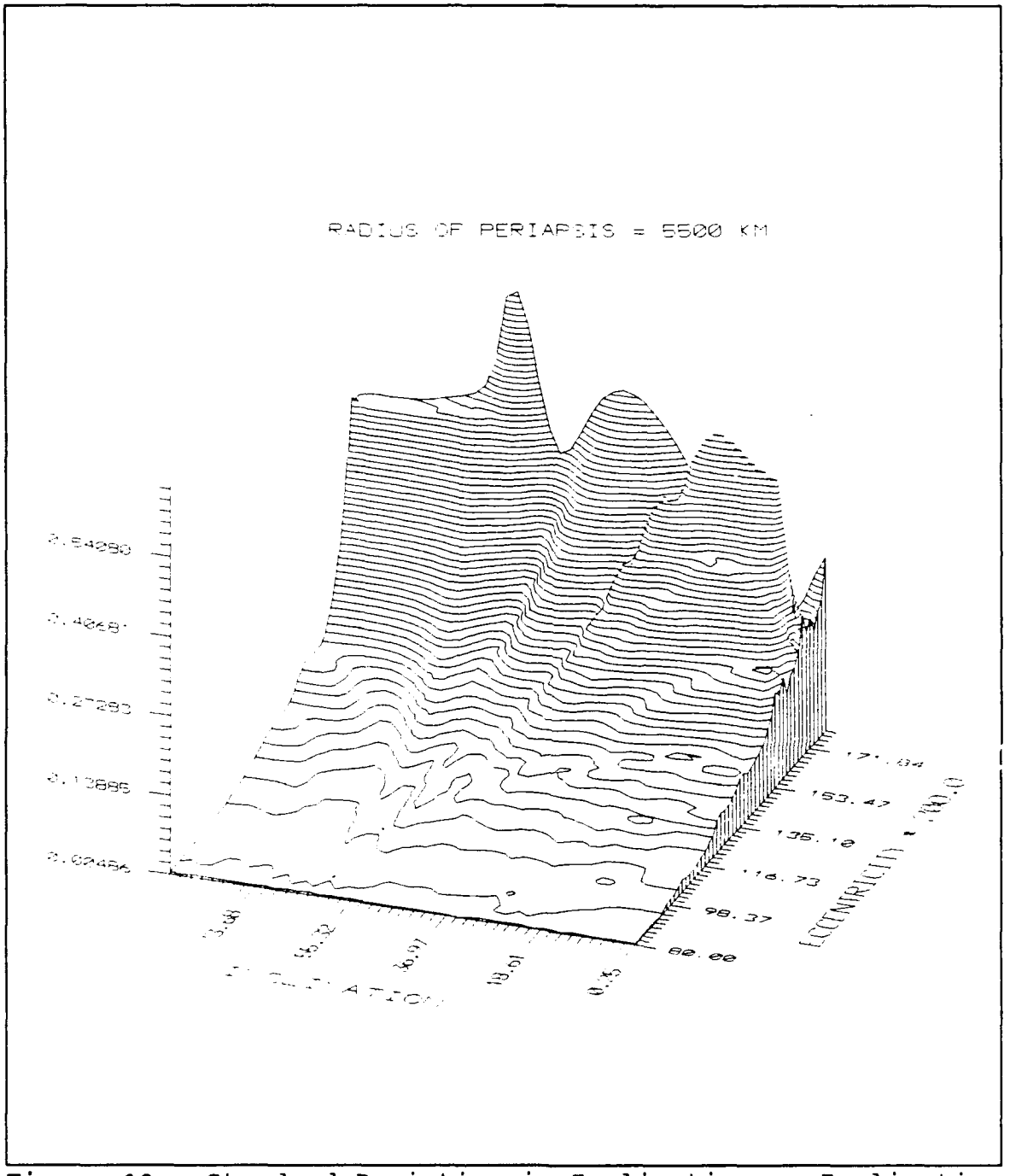

Figure 19. Standard Deviation in Inclination vs Inclination and Eccentricity: Periapse Radius = 5500 Km, Cubic Data Fit

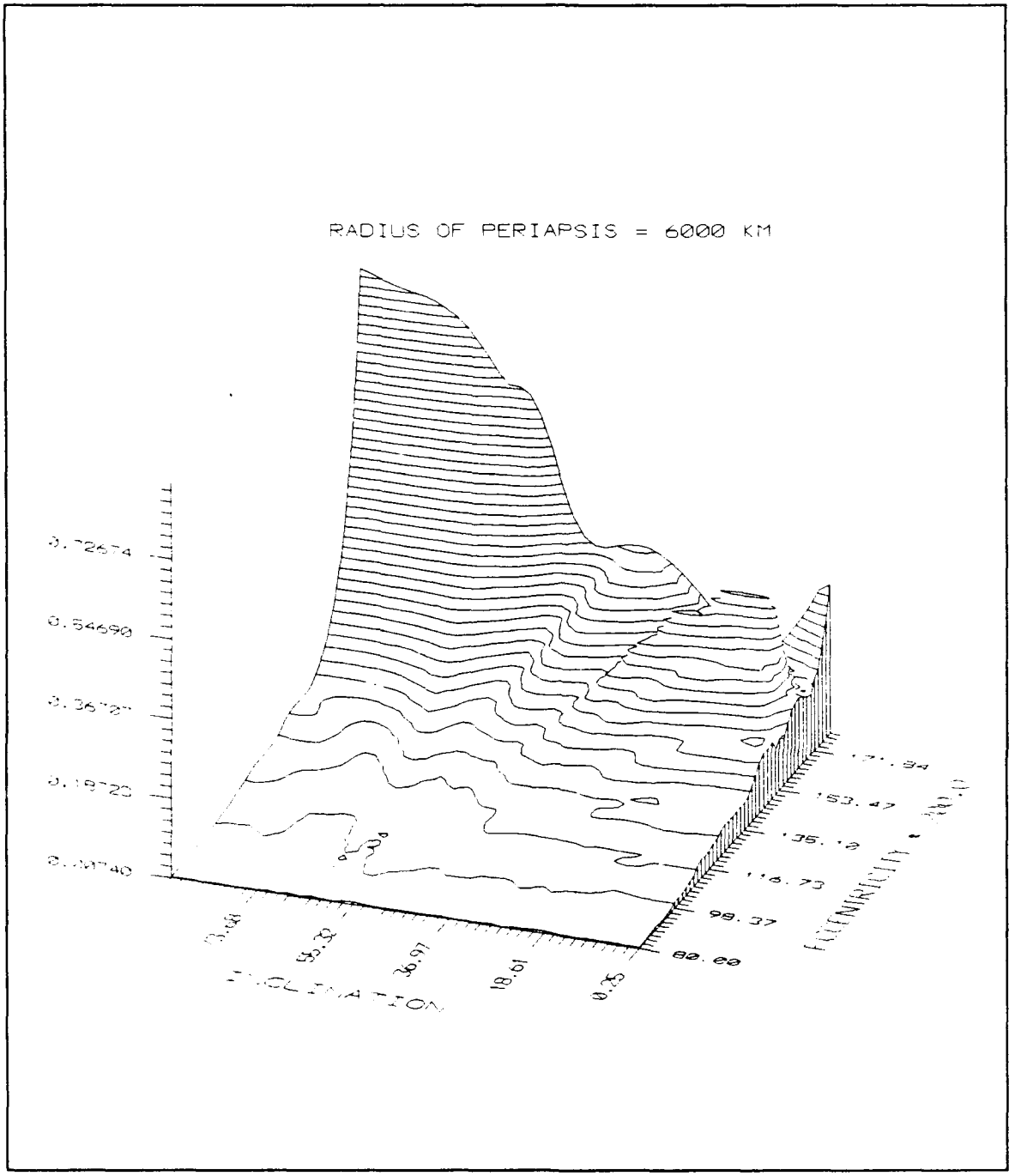

Figure 20. Standard Deviation in Inclination vs Inclination and Eccentricity: Periapse Radius = 6000 Km, Cubic Data Fit

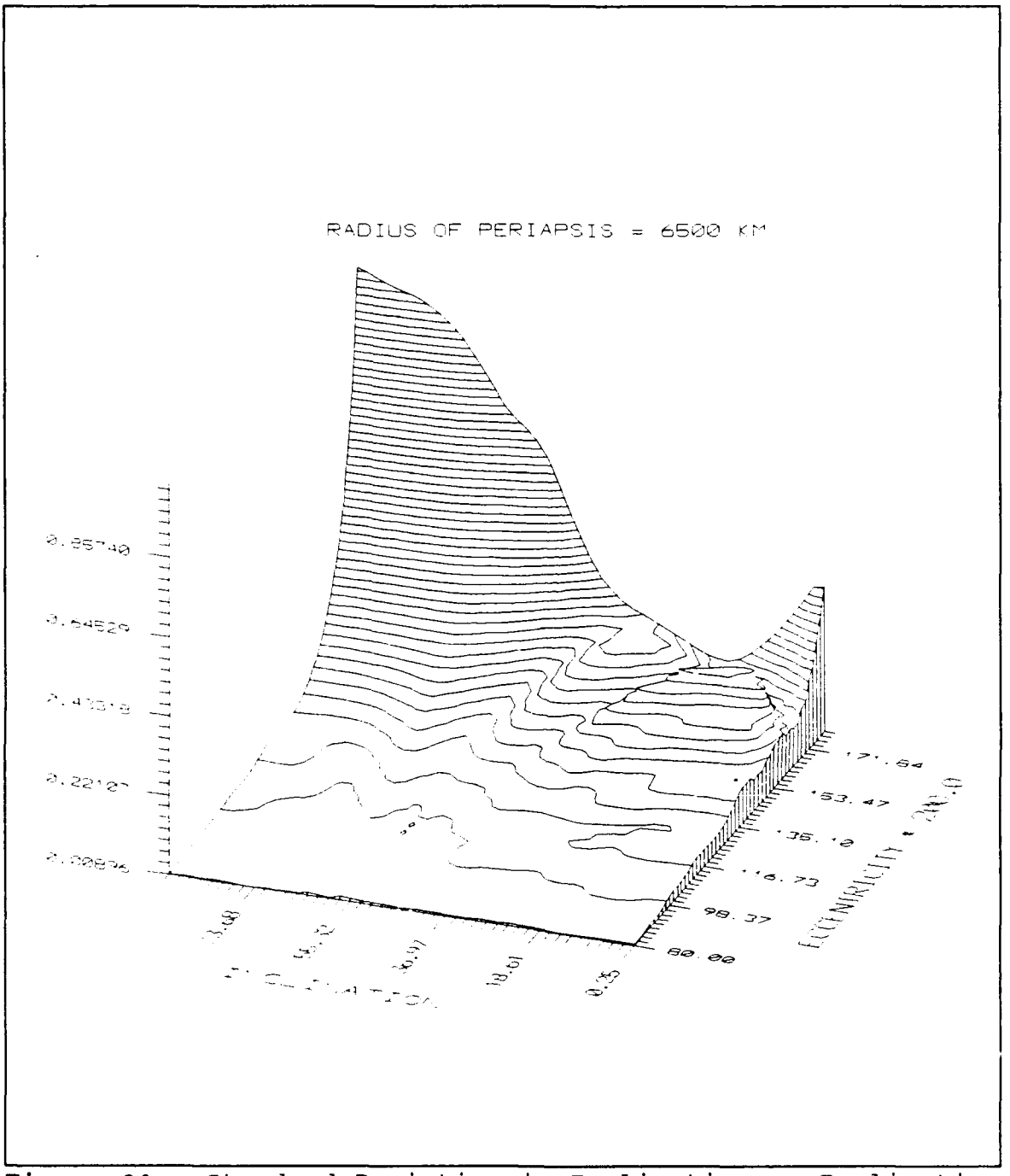

Figure 21. Standard Deviation in Inclination vs Inclination and Eccentricity: Periapse Radius = 6500 Km, Cubic Data Fit

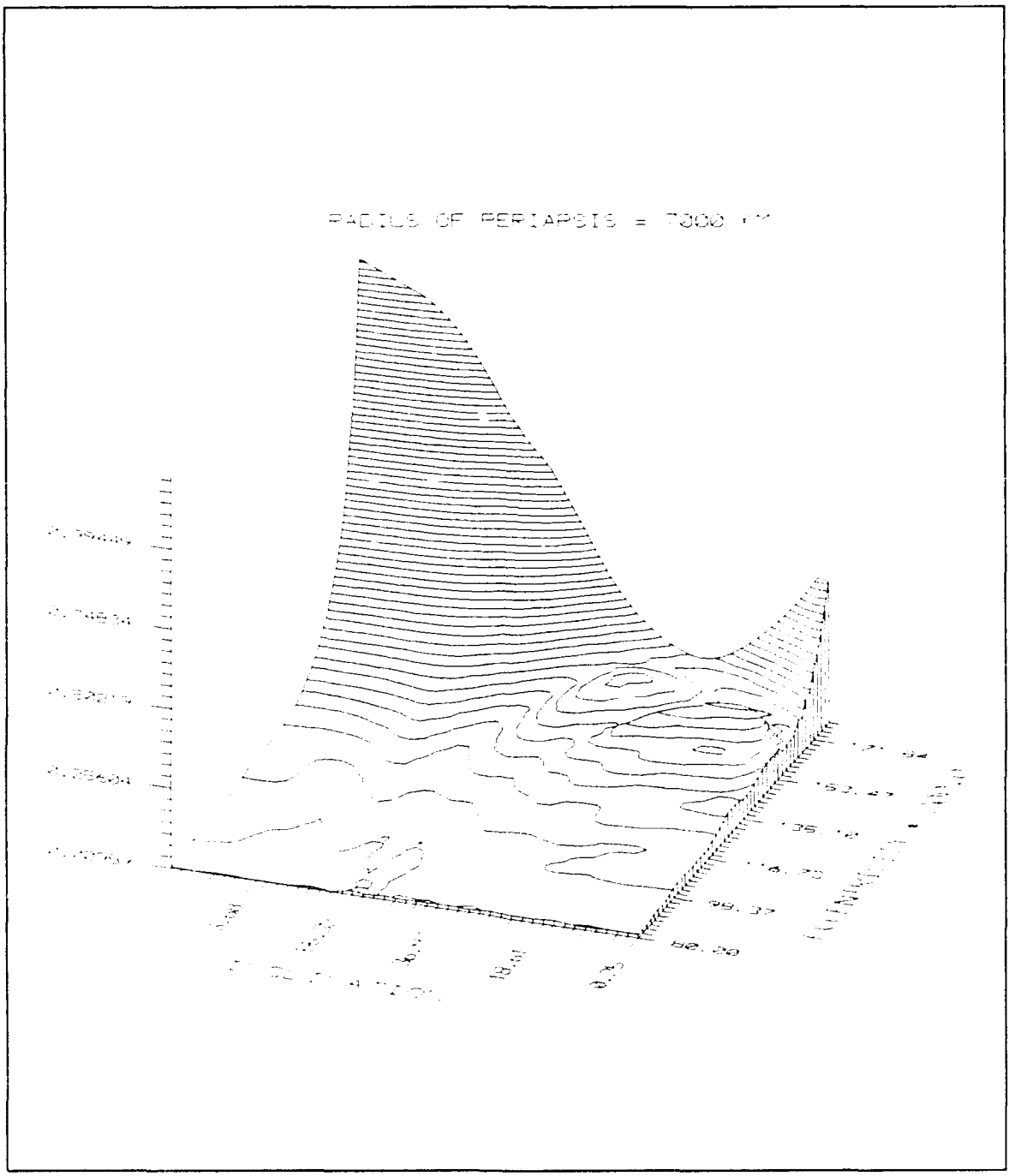

Figure 22. Standard Deviation in Inclination vs Inclination and Eccentricity: Periapse Radius = 7000 Km, Cubic Data Fit

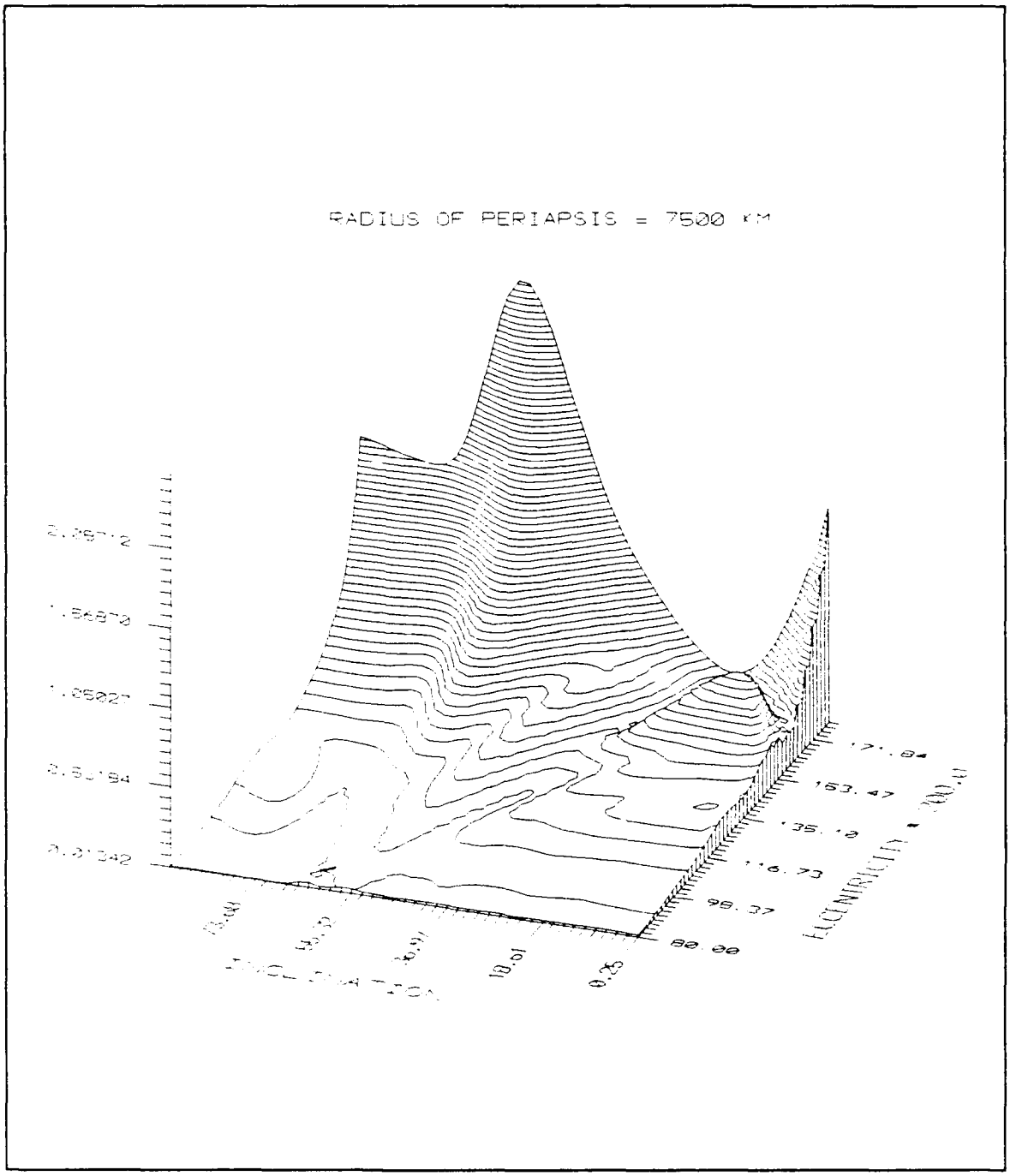

Figure 23. Standard Deviation in Inclination vs Inclination and Eccentricity: Periapse Radius = 7500 Km, Linear Data Fit

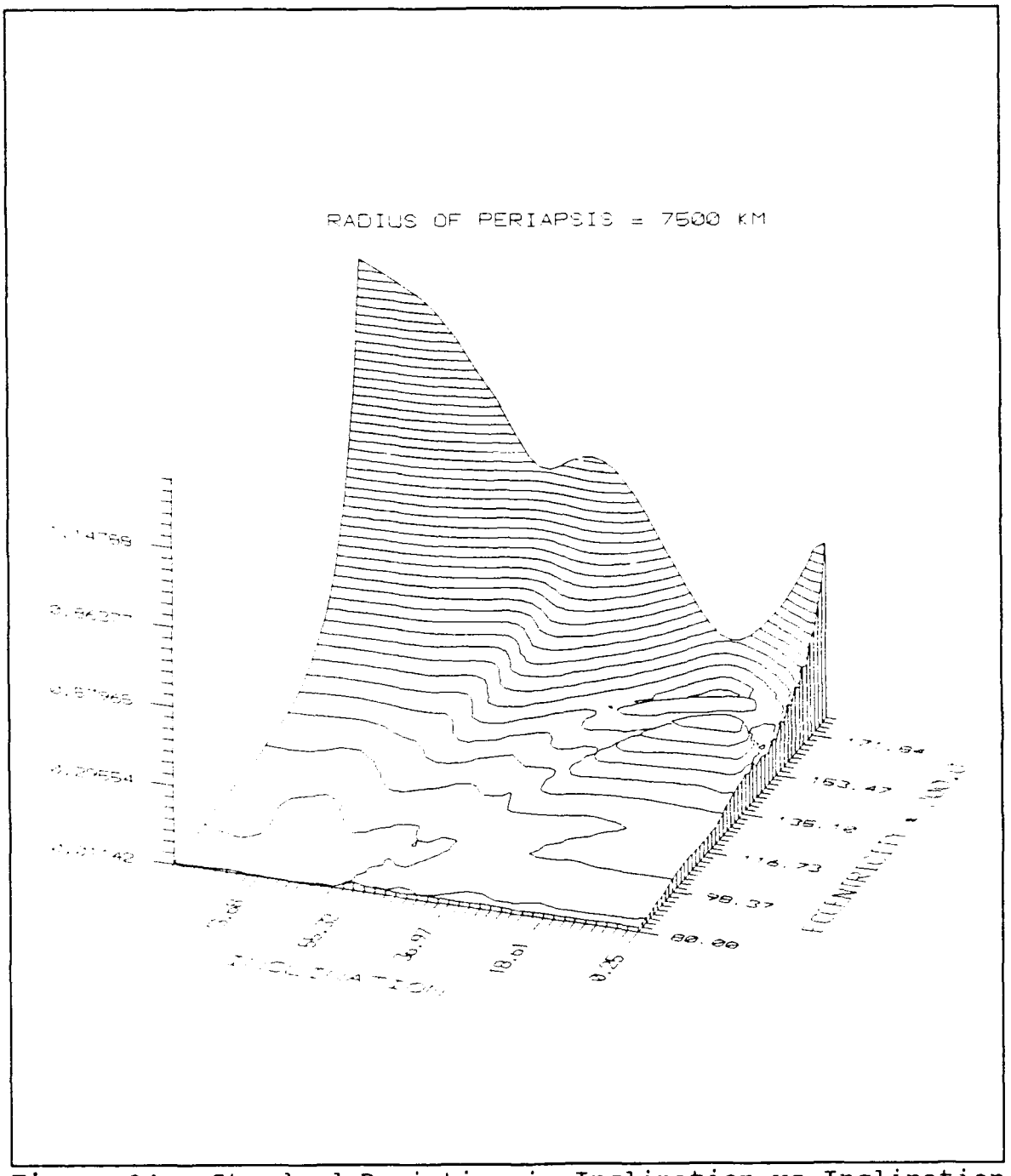

Figure 24. Standard Deviation in Inclination vs Inclination and Eccentricity: Periapse Radius = 7500 Km, Quadratic Data Fit

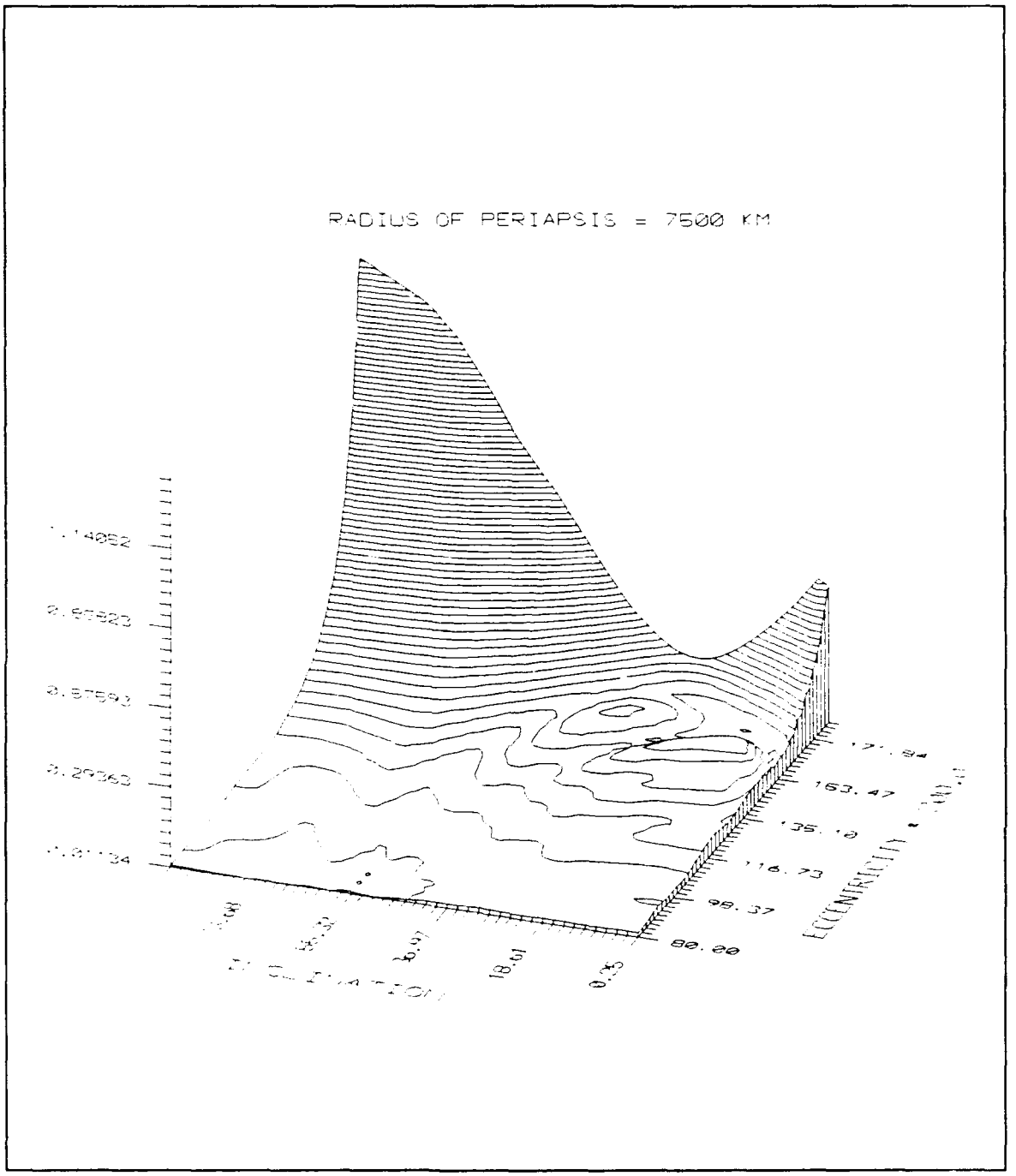

Figure 25. Standard Deviation in Inclination vs Inclination and Eccentricity: Periapse Radius = 7500 Km, Cubic Data Fit

2-D Critical Inclination Plots

For each of the SDE surface plots, a numerical procedure was used to sort the data and locate the predominate local maximums. These form the ridges in the surface plots and indicate the critical inclinations. Cubic polynomials were fitted to the local maximum data and then plotted on a two dimension graph of the initial eccentricity vs initial inclination (orbit insertion). These are the plots of critical inclination as a function of insertion eccentricity and inclination. Two-dimensional contour plots of the surfaces for a cubic data fit are also included. The linear and quadratic data fits not included here are in Appendix D. The features in the SDI surface plots were not predominate enough to locate accurately and were not plotted.

The curves for the linear, quadratic, and cubic data fits in calculating the standard deviations were roughly similar. As expected, some of the curves disappeared with the higher order fits due to the decreasing magnitudes of the standard deviations. However, the curves were also shifted in position. They exhibited a shift to lower eccentricities and a shift away from a dividing line of 53.3 degrees initial inclination.

Critical Inclination Curves for SDE

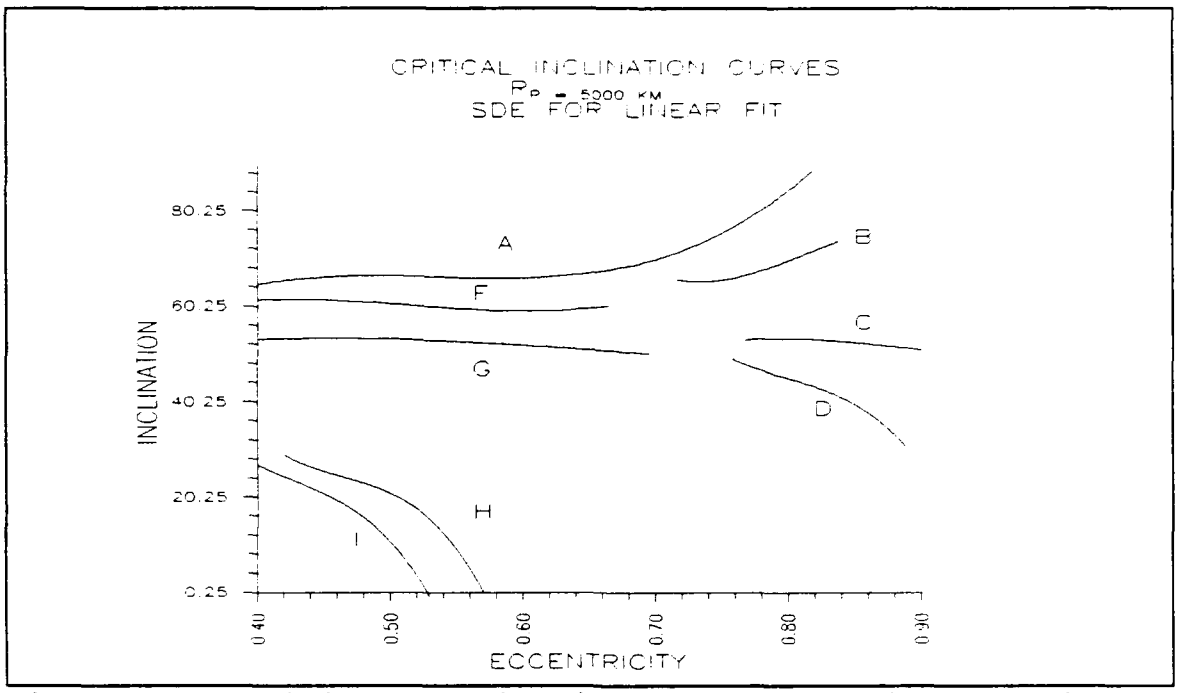

Figure 26. Critical Inclination Curves: Periapse Radius = 5000 Km, Linear Data Fit

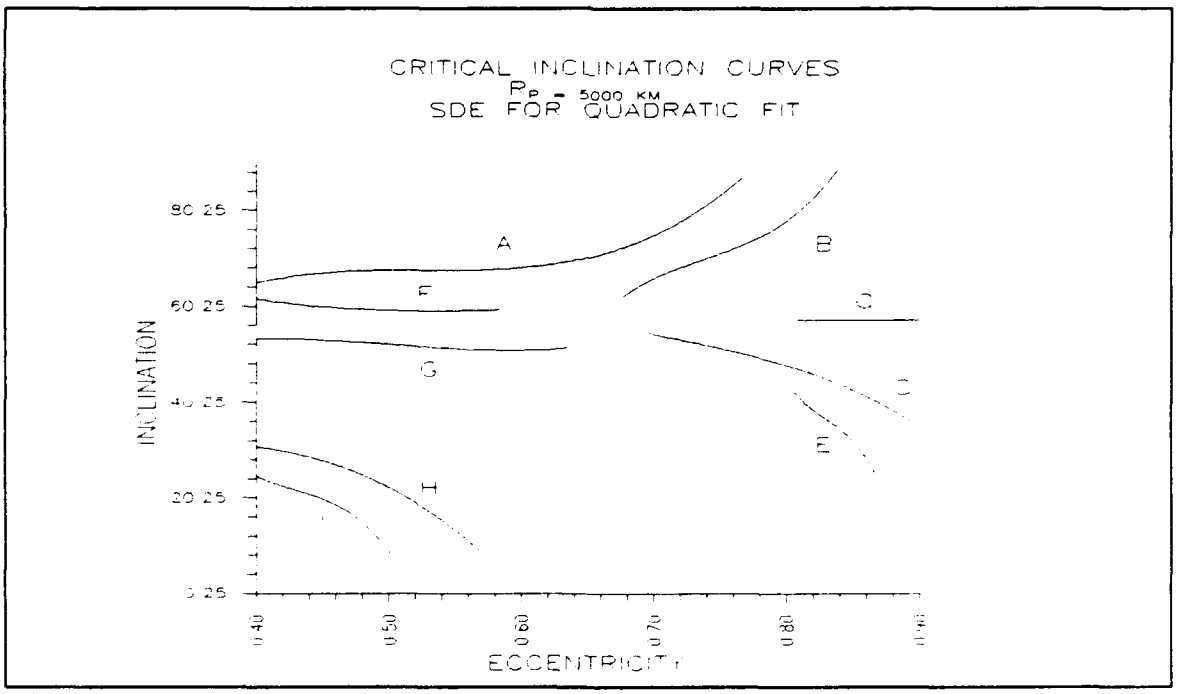

Figure 27. Critical Inclination Curves: Periapse Radius = 5000 Km, Quadratic Data Fit

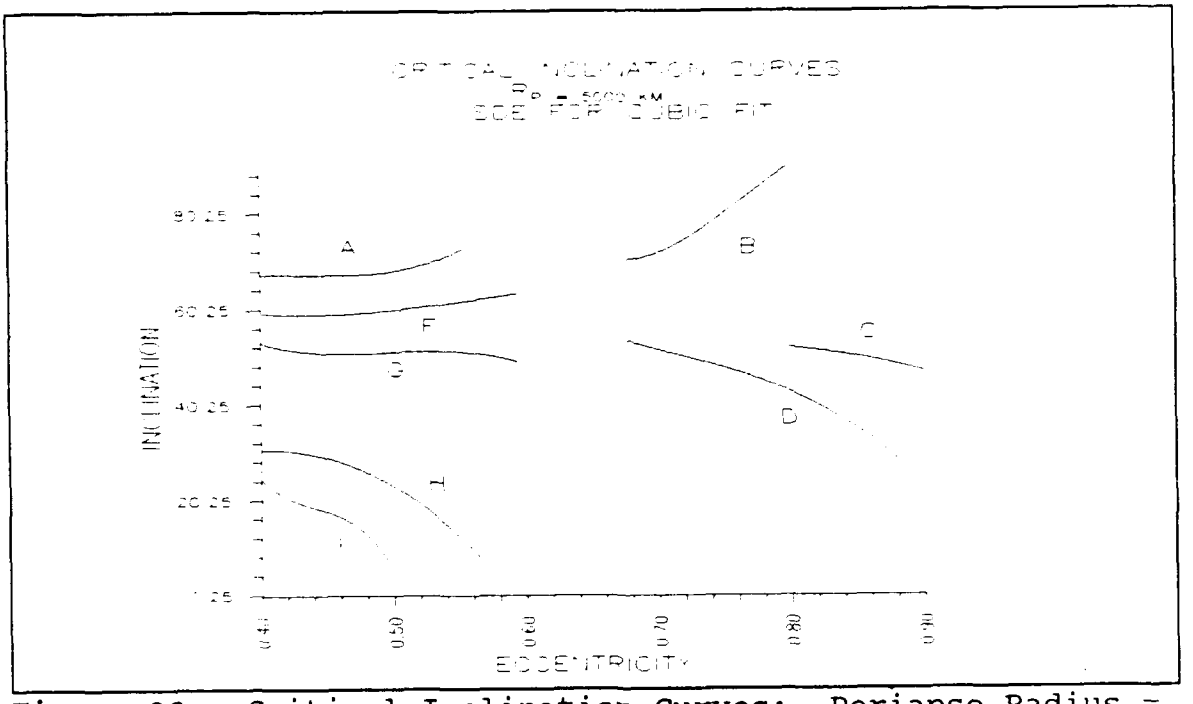

Figure 28. Critical Inclination Curves: Periapse Radius = 5000 Km, Cubic Data Fit

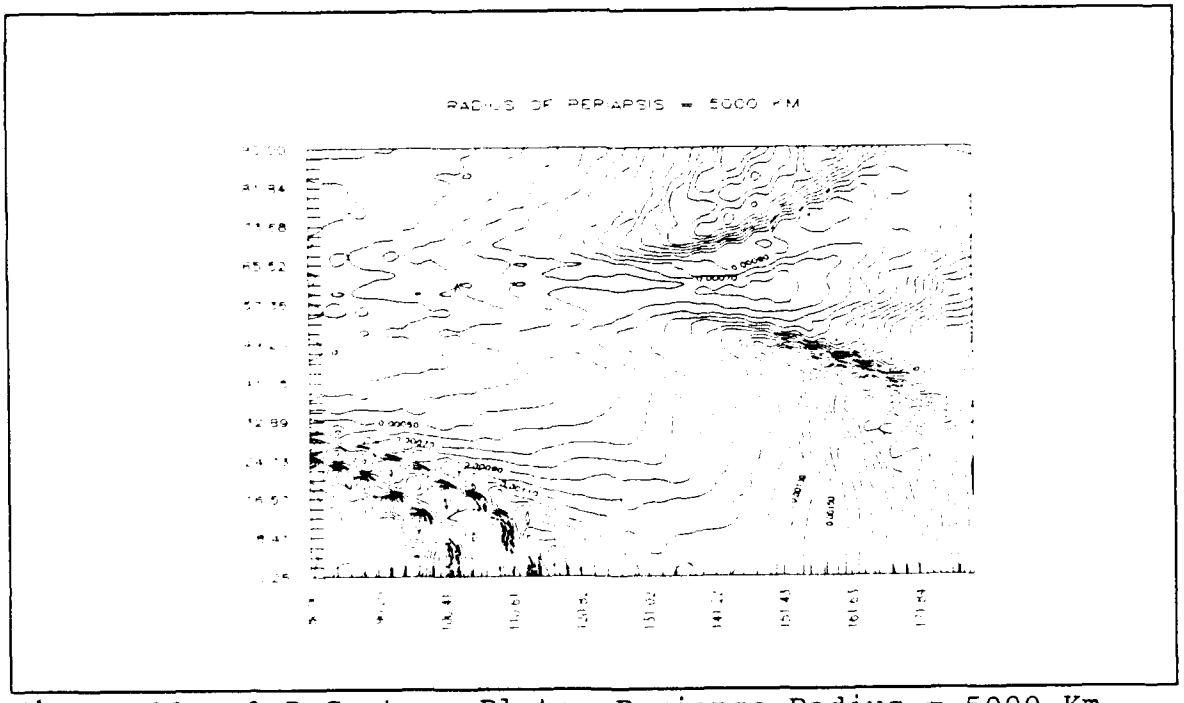

Figure 29. 2-D Contour Plot: Periapse Radius = 5000 Km, Cubic Data Fit

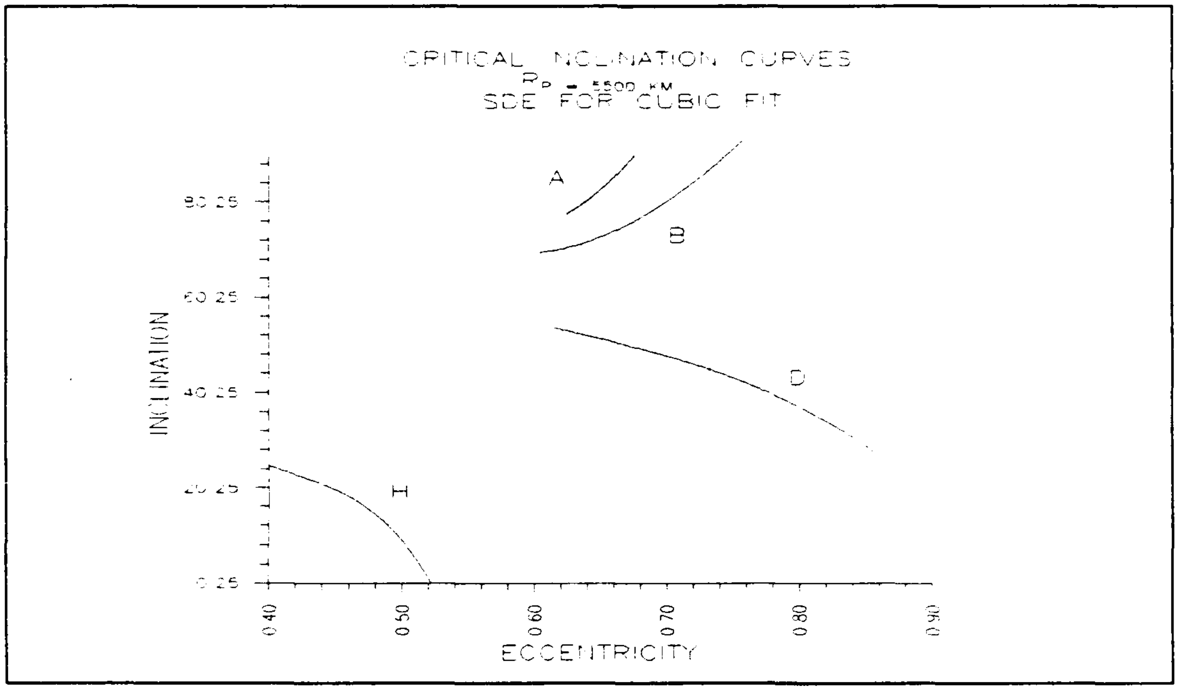

Figure 30. Critical Inclination Curves: Periapse Radius = 5500 Km, Cubic Data Fit

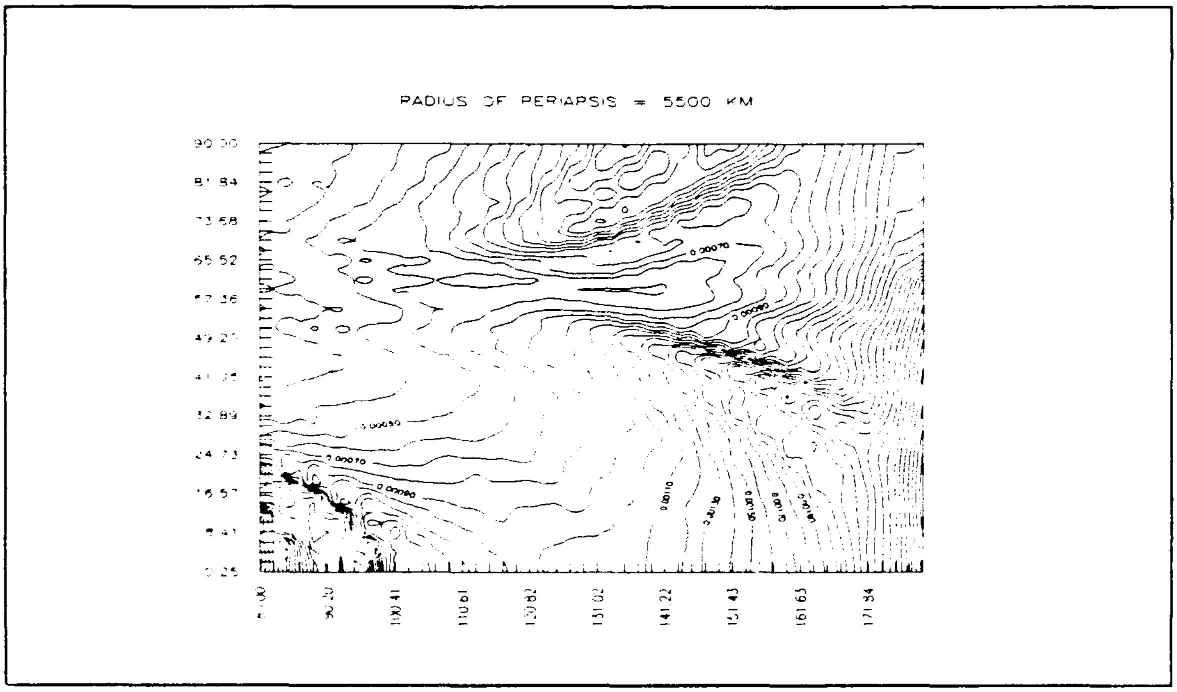

Figure 31. 2-D Contour Plot: Periapse Radius = 5500 Km, Cubic Data Fit

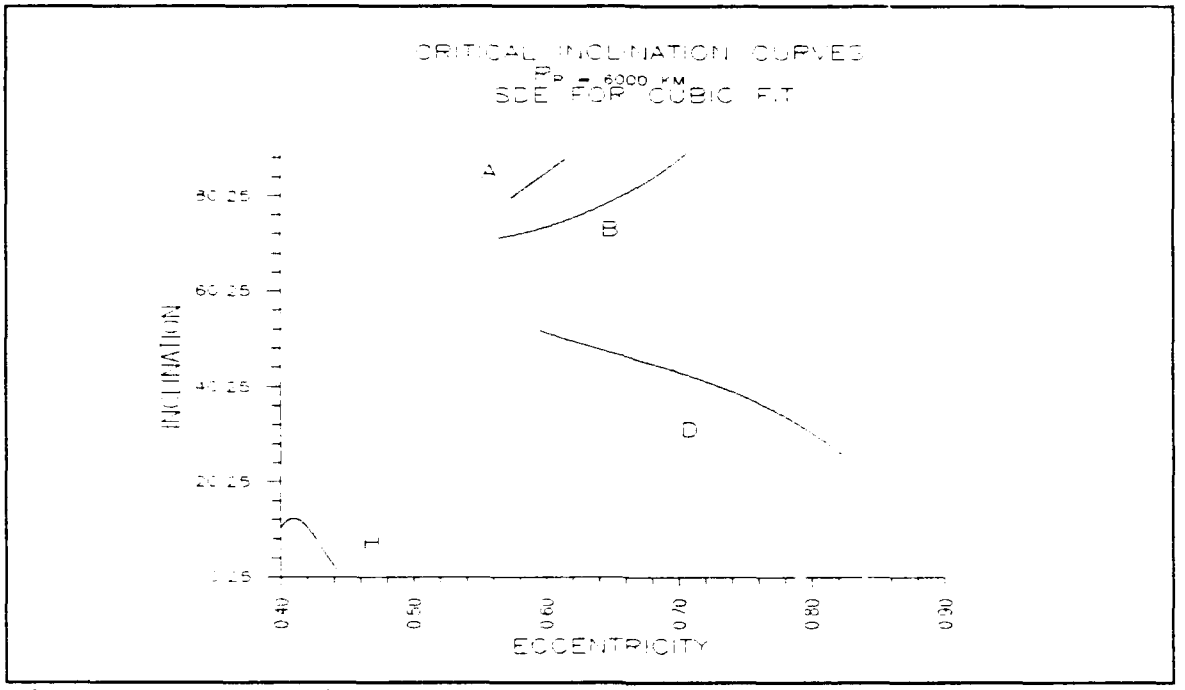

Figure 32. Critical Inclination Curves: Periapse Radius = 6000 Km, Cubic Data Fit

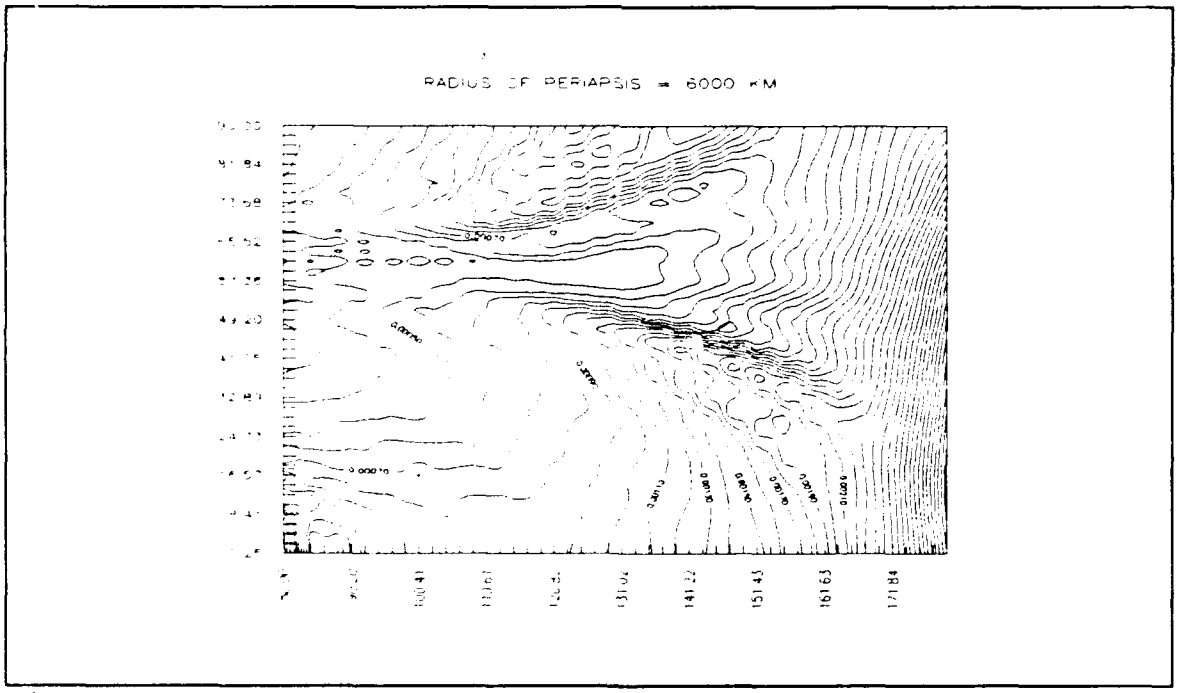

Figure 33. 2-D Contour Plot: Periapse Radius = 6000 Km, Cubic Data Fit

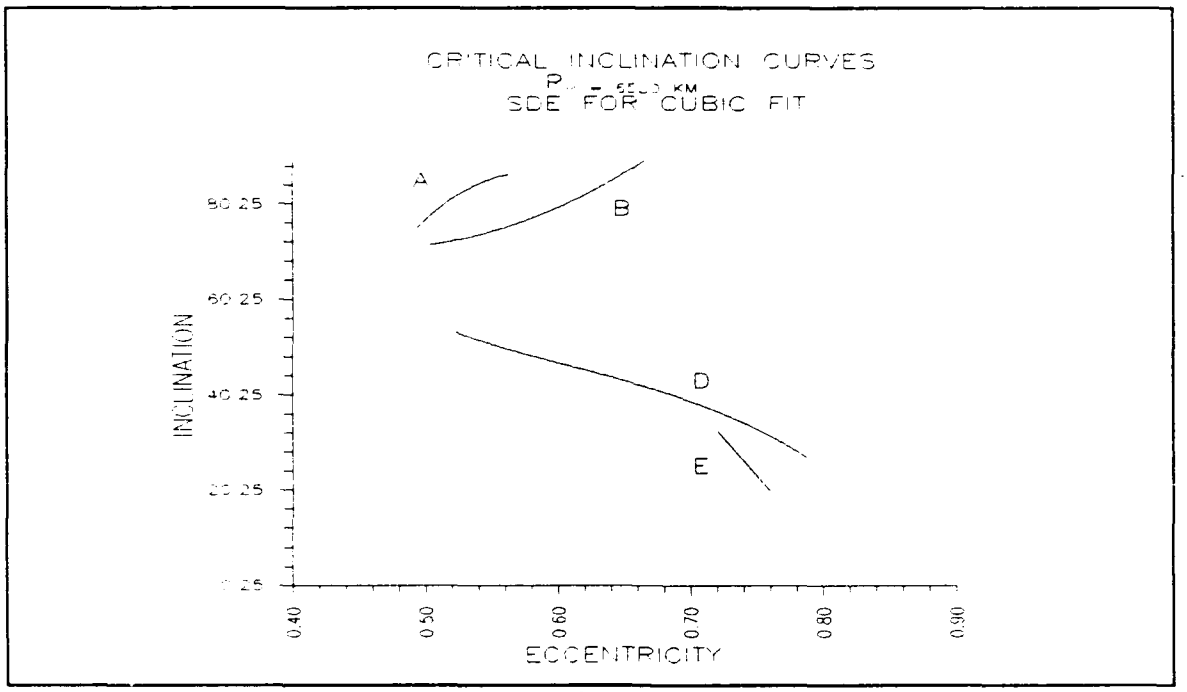

Figure 34. Critical Inclination Curves: Periapse Radius = 6500 Km, Cubic Data Fit

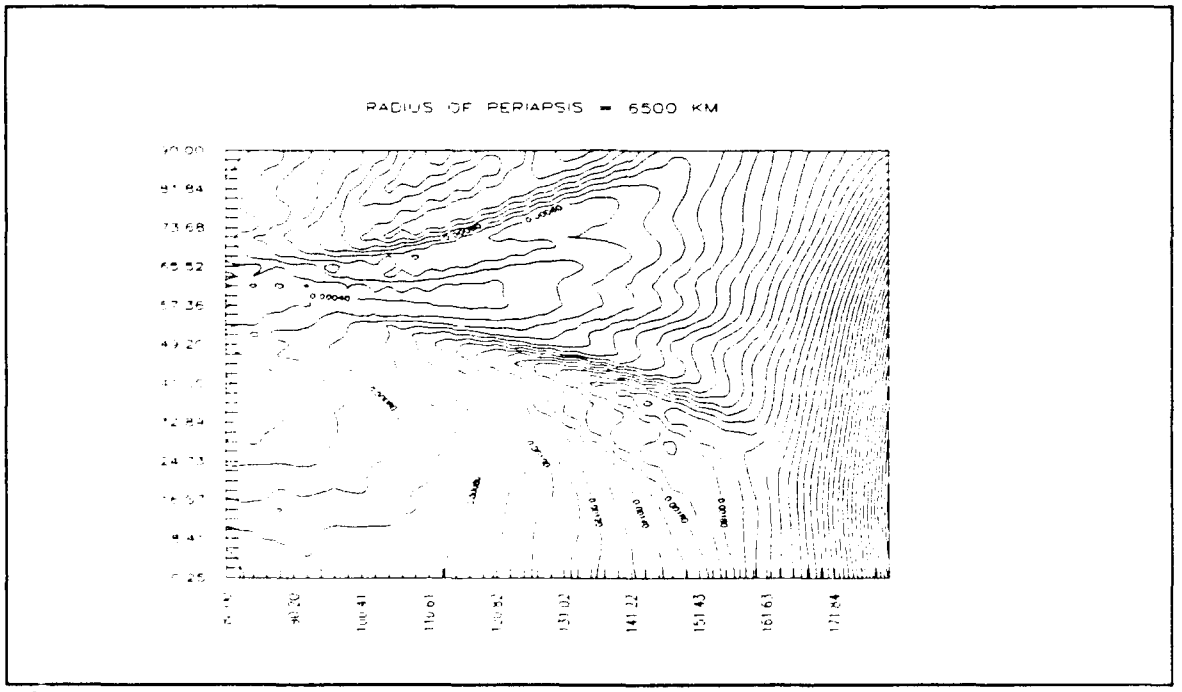

Figure 35. 2-D Contour Plot: Periapse Radius = 6500 Km, Cubic Data Fit

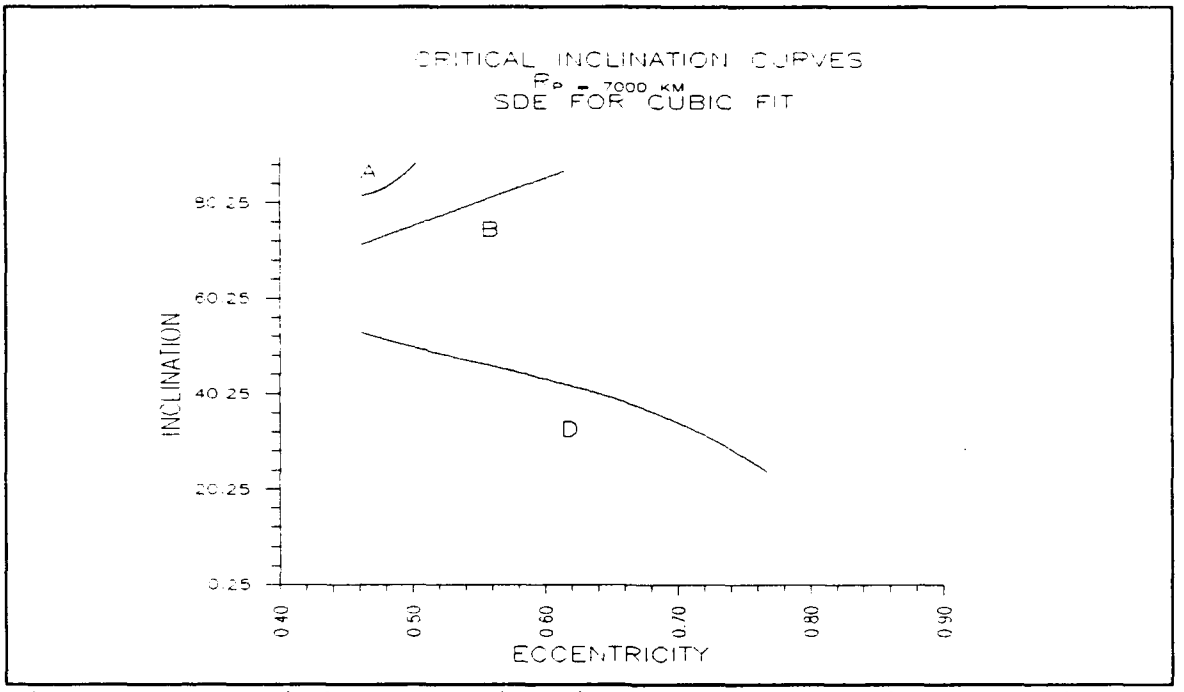

Figure 36. Critical Inclination Curves: Periapse Radius = 7000 Km, Cubic Data Fit

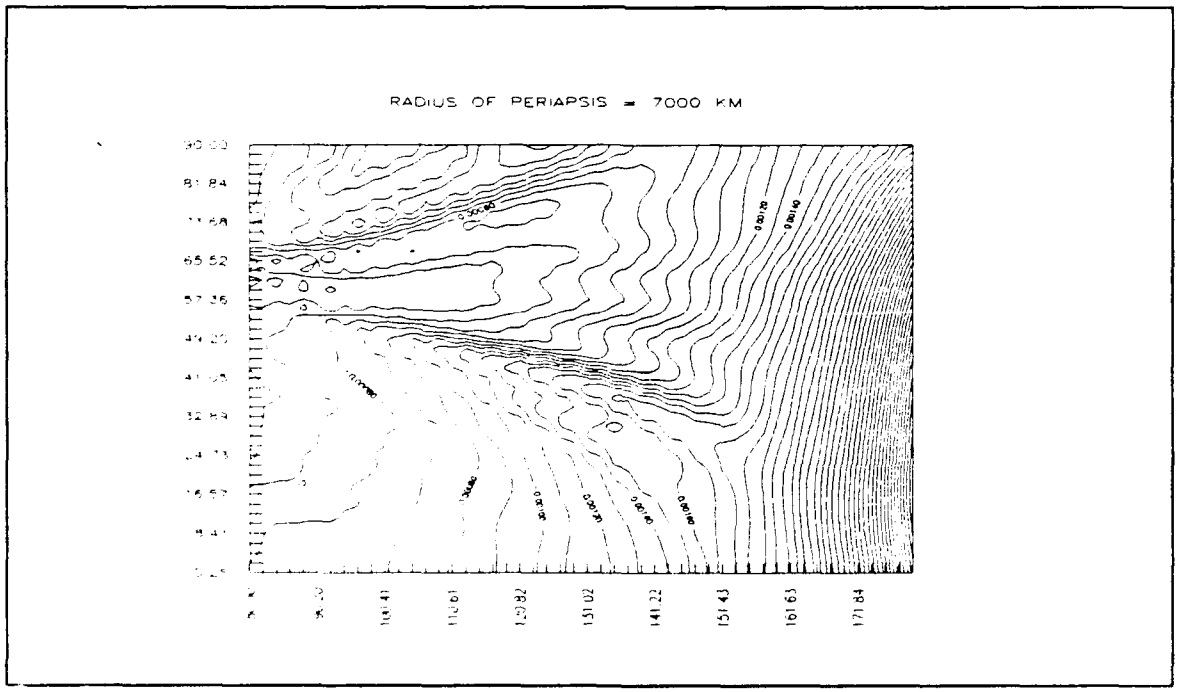

Figure 37. 2-D Contour Plot: Periapse Radius = 7000 Km, Cubic Data Fit

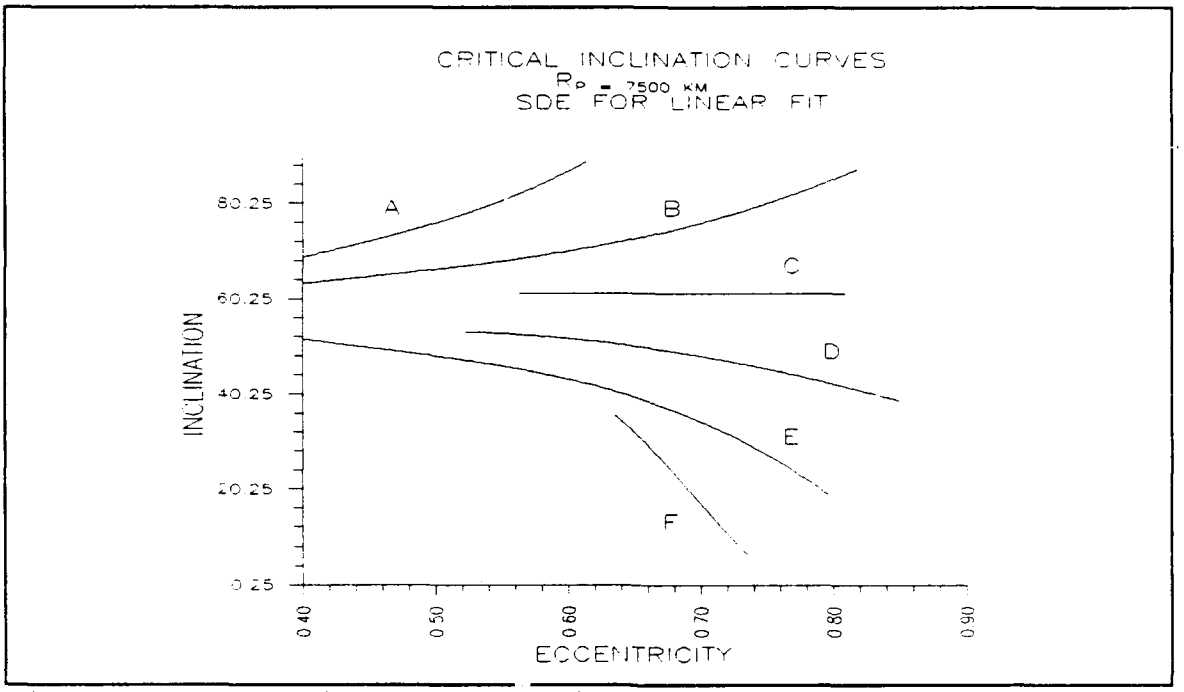

Figure 38. Critical Inclination Curves: Periapse Radius = 7500 Km, Linear Data Fit

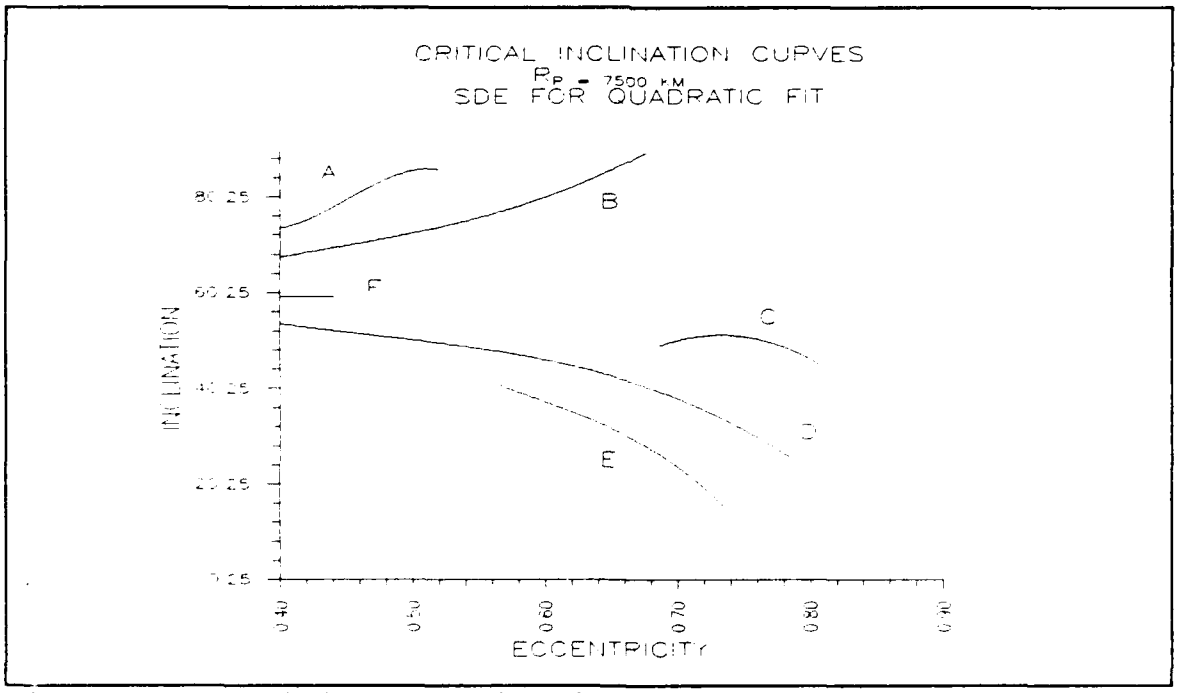

Figure 39. Critical Inclination Curves: Periapse Radius = 7500 Km, Quadratic Data Fit

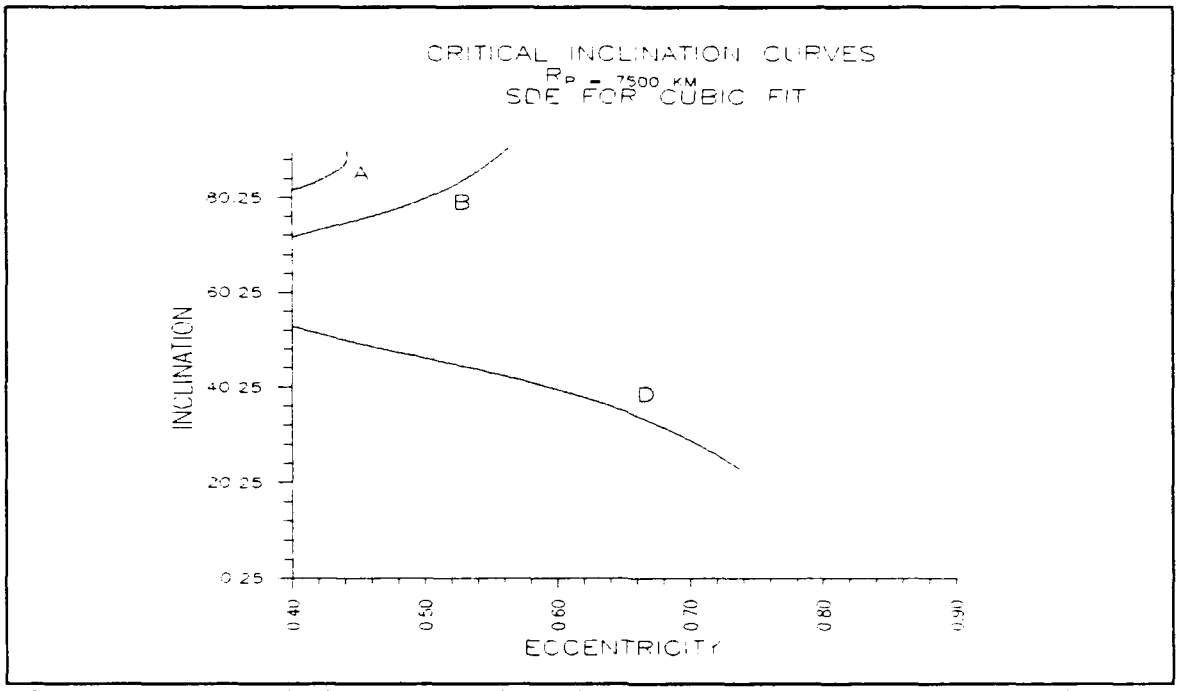

Figure 40. Critical Inclination Curves: Periapse Radius = 7500 km, Cubic Data Fit

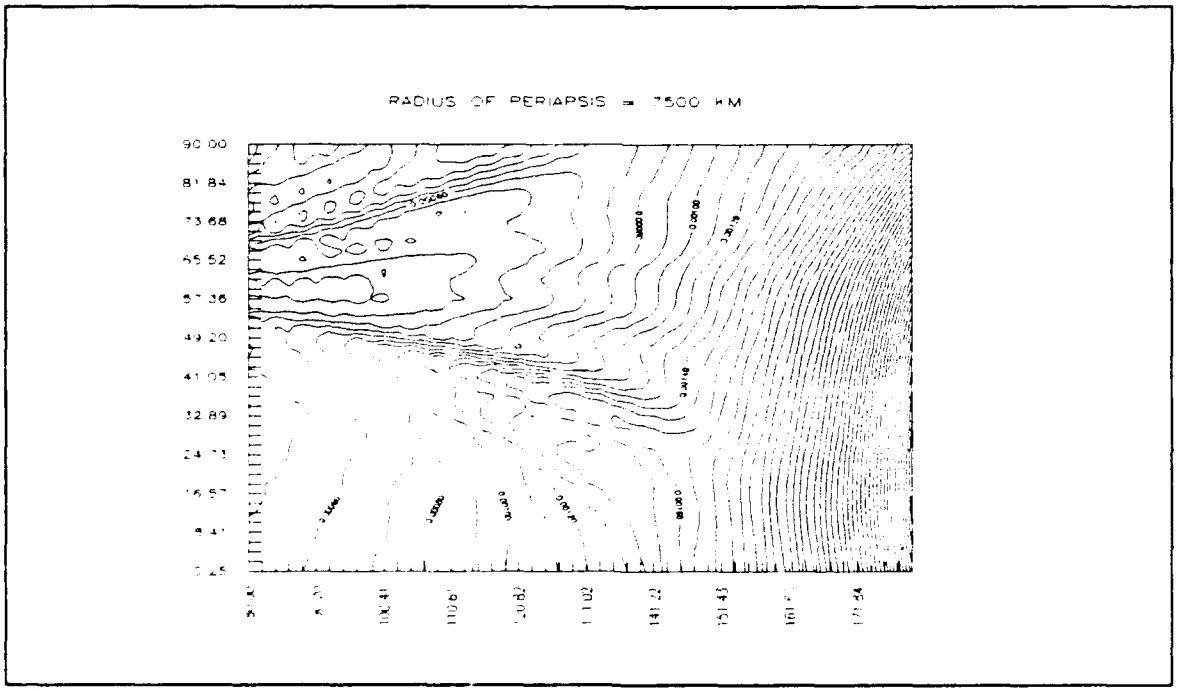

Figure 41. 2-D Contour Plot: Periapse Radius = 7500 Km, Cubic Data Fit

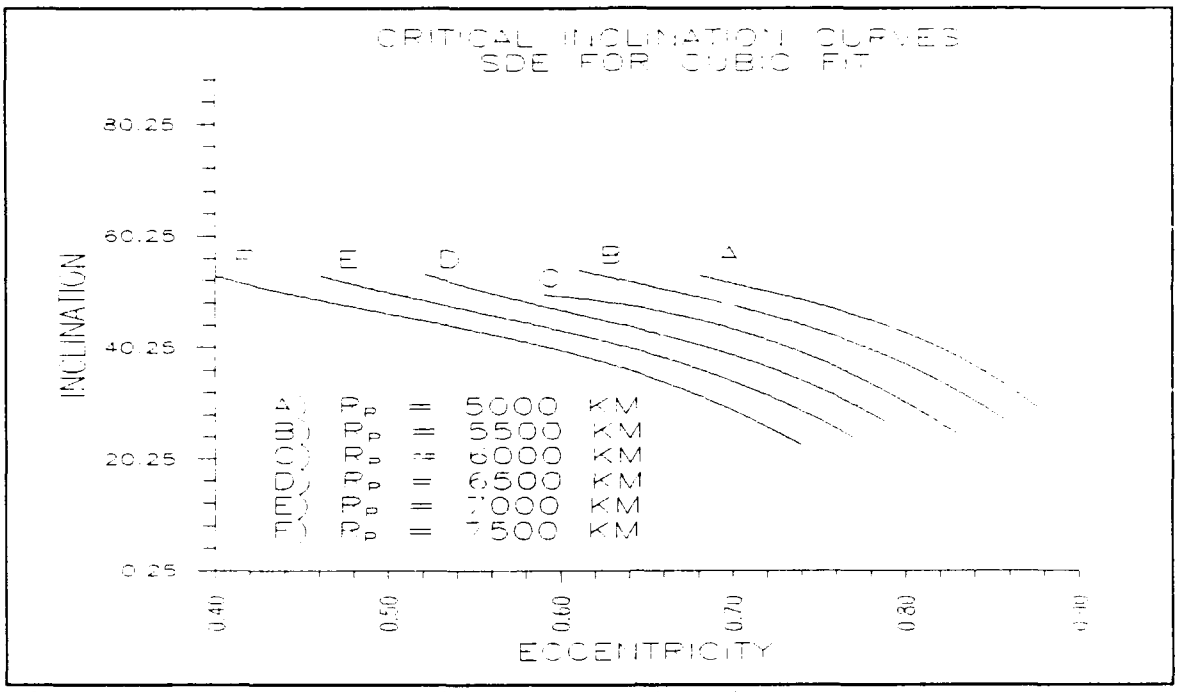

Figure 42. Primary Critical Inclination Curves for SDE (Cubic Data Fit)

Equations for curves of figure 42:

$$i_A = -1956.28e^3+4150.69e^2-3008.36e+794.74$$

$$For \quad 0.68 \le e_A \le 0.88$$

$$i_B = -1019.10e^3+1968.60e^2-1336.05e+367.94$$

$$For \quad 0.61 \le e_B \le= 0.86$$

$$i_C = -445.74e^3+570.55e^2-233.95e+80.66$$

$$For \quad 0.59 \le e_C \le 0.83$$

$$i_D = -1121.95e^3+2053.21e^2-1324.73e+344.94 \qquad (64)$$

$$For \quad 0.52 \le e_D \le 0.79$$

$$i_E = -751.01e^3+1235.47e^2-743.30e+206.72$$

$$For \quad 0.46 \le e_E \le 0.77$$

$$i_F = -731.68e^3+1108.97e^2-619.54e+170.27$$

$$For \quad 0.40 \le e_F \le 0.74$$

IV. Conclusions and Recommendations

Critical inclinations were defined as those initial inclinations which result in a large variation in either eccentricity or inclination. The location of these inclinations through numerical means was the desired goal.

To provide a bound on the problem, an analytic method was outlined (e.g., see Breakwell ref. 5). This resulted in eleven critical inclinations based on the simplifications of averaging out the mean anomaly terms and averaging the affects of the Sun.

Table 3. Critical Inclinations

63.4 deg	116.6 deg
46.4 deg	106.8 deg
73.2 deg	133.6 deg
56.1 deg	111.0 deg
69.0 deg	123.9 deg
90.0 deg	

However, this method didn't bring out the dependence of the critical inclination on initial eccentricity and periapsis height.

The numerical approach involved the integration of orbits over a range of initial eccentricities and

inclinations. The standard deviations in eccentricity (SDE) and inclination (SDI), based upon a polynomial curve fit to the data, were employed as the search parameters. The local maximums in the surface plots of SDE and SDI vs initial conditions indicated the resonances and thus the critical inclinations (e.g., see figures 6-25).

The SDI plots proved to be relatively smooth and no predominate features were discerned. Therefore, critical inclinations for large variations in inclination were not determined.

However, the SDE plots demonstrated numerous resonant conditions. The curves for critical inclinations were identified and roughly corresponded to the analytic results (e.g., see table 1).

Experimenting with higher order polynomial curve fits, in calculating the standard deviations, resulted in a smoothing of the surface plots as expected. The more accurate curve fits reduced the magnitude of the deviations and brought out the predominate resonance effects (e.g., see figure 42). The equations for these curves indicated the critical inclinations were a function of the initial conditions.

A second effect of the higher degree polynomial data fits was a shifting of the critical inclination curves. Increasing the degree of the polynomial shifted the critical

curves toward decreasing eccentricity and away from a dividing line of 53.3 degrees initial inclination. This dividing line also corresponded to the approximate inclination of the predominate resonance effects (e.g., see figure 42) and the analytic critical inclination of 56.1 degrees.

Based on these results, the numeric approach utilizing the standard deviation as a search parameter provided a means of identifying the critical inclinations for large variations in eccentricity. Furthermore, the use of higher degree polynomial data fits in determining standard deviations assisted in isolating the predominate resonance effects.

A further study could explore the shifting of the critical inclination curves for higher degree polynomial data fits. Non-polynomial data fits may also be explored.

Appendix A. Hansen's Coefficients

The following is a more detailed explanation of the steps used in deriving the disturbing functions using Hansen's Coefficients. A complete explanation of Hansen's Coefficients is in reference (2).

Let

$$x = \exp(jf), \quad y = \exp(jE), \quad z = \exp(jM), \quad j = \sqrt{-1} \tag{65}$$

where f is the true anomaly, M is the Mean anomaly, and E is the eccentric anomaly. Hansen's coefficients are then defined

$$X_p^{n,m} = \frac{1}{2\pi} \int_0^{2\pi} \left(\frac{r}{a}\right)^n x^m z^{-p} \, dM \tag{66}$$

For p=0:

$$X_0^{n,M} = \left(-\frac{e}{2}\right)^{|m|} \binom{n+|m|+1}{|m|} F\left(\frac{|m|-n-1}{2}, \frac{|m|-n}{2}; |m|+1; e^2\right) \tag{67}$$

where F is the hypergeometric function [1:272-277] defined

$$F = (a,b;c;y) = \sum_{n=0}^{\infty} \frac{(a)_n (b)_n}{(c)_n} \frac{y^n}{n!}, \quad |y| < 1 \tag{68}$$

One property of Hansen's Coefficients is

$$X_0^{m,n} = X_0^{m,-n} \tag{69}$$

The Pochhammer symbol $(a)_n$ has the following properties:

$$\begin{aligned} (a)_0 &= 1 \\ (1)_n &= n! \\ (a)_n &= a(a+1)(a+2)\cdots(a+n-1) \qquad n = 1,2,3,\ldots \end{aligned} \tag{70}$$

The Pochhammer symbol and the binomial coefficient are related by

$$(a)_n = (-1)^n n! \binom{-a}{n} \tag{71}$$

Derivation of Integral Terms in the Disturbing Functions

Derivation of Eqn. (11):

$$\frac{1}{2\pi}\int_0^{2\pi}\left(\frac{r}{a}\right)^{-3} dM = X_0^{-3,0}$$

$$= \left(-\frac{e}{2}\right)^0 \binom{-2}{0} F\left(1, \frac{3}{2}; 1; e^2\right)$$

$$= (1)\,(1) \sum_{n=0}^{\infty} \frac{(1)_n \left(\frac{3}{2}\right)_n}{(1)_n} \frac{e^{2n}}{n!} \qquad (72)$$

$$= \sum_{n=0}^{\infty} n! \binom{-3/2}{n} (-1)^n \frac{e^{2n}}{n!}$$

$$= \sum_{n=0}^{\infty} \binom{-3/2}{n} (-e^2)^n$$

Recognizing this as a binomial expansion

$$X_0^{-3,0} = (1 - e^2)^{-\frac{3}{2}} \qquad (73)$$

Derivation of Eqn. (11):

Using the identity

$$\sin 2f = \frac{1}{2j}\left[\exp(j2f) - \exp(-j2f)\right] \qquad (74)$$

$$\frac{1}{2\pi}\int_0^{2\pi}\left(\frac{r}{a}\right)^{-3}\sin 2f\,dM =$$

$$= \frac{1}{2\pi}\int_0^{2\pi}\left(\frac{r}{a}\right)^{-3}\frac{1}{2j}\left[\exp(j2f) - \exp(-j2f)\right]dM$$

$$= \frac{1}{2j}\left[\frac{1}{2\pi}\int_0^{2\pi}\left(\frac{r}{a}\right)^{-3}\exp(j2f)\,dM - \frac{1}{2\pi}\int_0^{2\pi}\left(\frac{r}{a}\right)^{-3}\exp(-j2f)\,dM\right]$$

$$= \frac{1}{2j}\left(X_0^{-3,2} - X_0^{-3,-2}\right) = 0$$

(75)

Derivation of Eqn. (11):

Using the identity

$$\cos 2f = \frac{1}{2}\left[\exp(j2f) + \exp(-j2f)\right] \qquad \textbf{(76)}$$

then

$$\frac{1}{2\pi}\int_0^{2\pi}\left(\frac{r}{a}\right)^{-3}\cos 2f\,dM =$$

$$= \frac{1}{2\pi}\int_0^{2\pi}\left(\frac{r}{a}\right)^{-3}\frac{1}{2}\left[\exp(j2f) + \exp(-j2f)\right]dM$$

$$= \frac{1}{2}\left[\frac{1}{2\pi}\int_0^{2\pi}\left(\frac{r}{a}\right)^{-3}\exp(j2f)\,dM + \frac{1}{2\pi}\int_0^{2\pi}\left(\frac{r}{a}\right)^{-3}\exp(-j2f)\,dM\right]$$

$$= \frac{1}{2}\left(X_0^{-3,2} + X_0^{-3,2}\right) = X_0^{-3,2}$$

(77)

$$X_0^{-3,2} = \left(-\frac{e}{2}\right)^2\binom{0}{2}F\left(2,\tfrac{5}{2};3;e^2\right) = 0 \qquad \textbf{(78)}$$

Derivation of Eqn. (41):

$$\frac{1}{2\pi}\int_0^{2\pi}\left(\frac{r}{a}\right)^2 \cos 2f\, dM =$$

$$= \frac{1}{2\pi}\int_0^{2\pi}\left(\frac{r}{a}\right)^2 \frac{1}{2}\left[\exp(j2f) + \exp(-j2f)\right] dM$$

$$= \frac{1}{2}\left[\frac{1}{2\pi}\int_0^{2\pi}\left(\frac{r}{a}\right)^2 \exp(j2f)\, dM + \frac{1}{2\pi}\int_0^{2\pi}\left(\frac{r}{a}\right)^2 \exp(-j2f)\, dM\right]$$

$$= \frac{1}{2}\left(X_0^{2,2} + X_0^{2,2}\right) = X_0^{2,2}$$

(79)

$$X_0^{2,2} = \left(-\frac{e}{2}\right)^2 \binom{5}{2} F\left(-\tfrac{1}{2}, 0; 3; e^2\right)$$

$$= \left(\frac{e^2}{4}\right)(10)\,(1) \qquad \textbf{(80)}$$

$$= \frac{5e^2}{2}$$

Derivation of Eqn. (41):

$$\frac{1}{2\pi}\int_0^{2\pi}\left(\frac{r}{a}\right)^2 \sin 2f\, dM =$$

$$= \frac{1}{2\pi}\int_0^{2\pi}\left(\frac{r}{a}\right)^2 \frac{1}{2j}\left[\exp(j2f) - \exp(-j2f)\right] dM$$

$$= \frac{1}{2}\left[\frac{1}{2\pi}\int_0^{2\pi}\left(\frac{r}{a}\right)^2 \exp(j2f)\, dM - \frac{1}{2\pi}\int_0^{2\pi}\left(\frac{r}{a}\right)^2 \exp(-j2f)\, dM\right]$$

$$= \frac{1}{2j}\left(X_0^{2,2} - X_0^{2,-2}\right) = 0$$

(81)

Derivation of Eqn. (41):

$$\frac{1}{2\pi}\int_0^{2\pi}\left(\frac{r}{a}\right)^2 dM = X_0^{2,0}$$

$$= \left(-\frac{e}{2}\right)^0 \binom{3}{0} F\left(-\tfrac{3}{2};-1;1;e^2\right)$$

$$= (1)(1)\sum_{n=0}^{\infty} \frac{\left(-\frac{3}{2}\right)_n (-1)_n}{(1)_n}\,\frac{e^{2n}}{n!} \qquad (82)$$

$$= 1 + \frac{3}{2}e^2$$

Appendix B. SDE Surface Plots

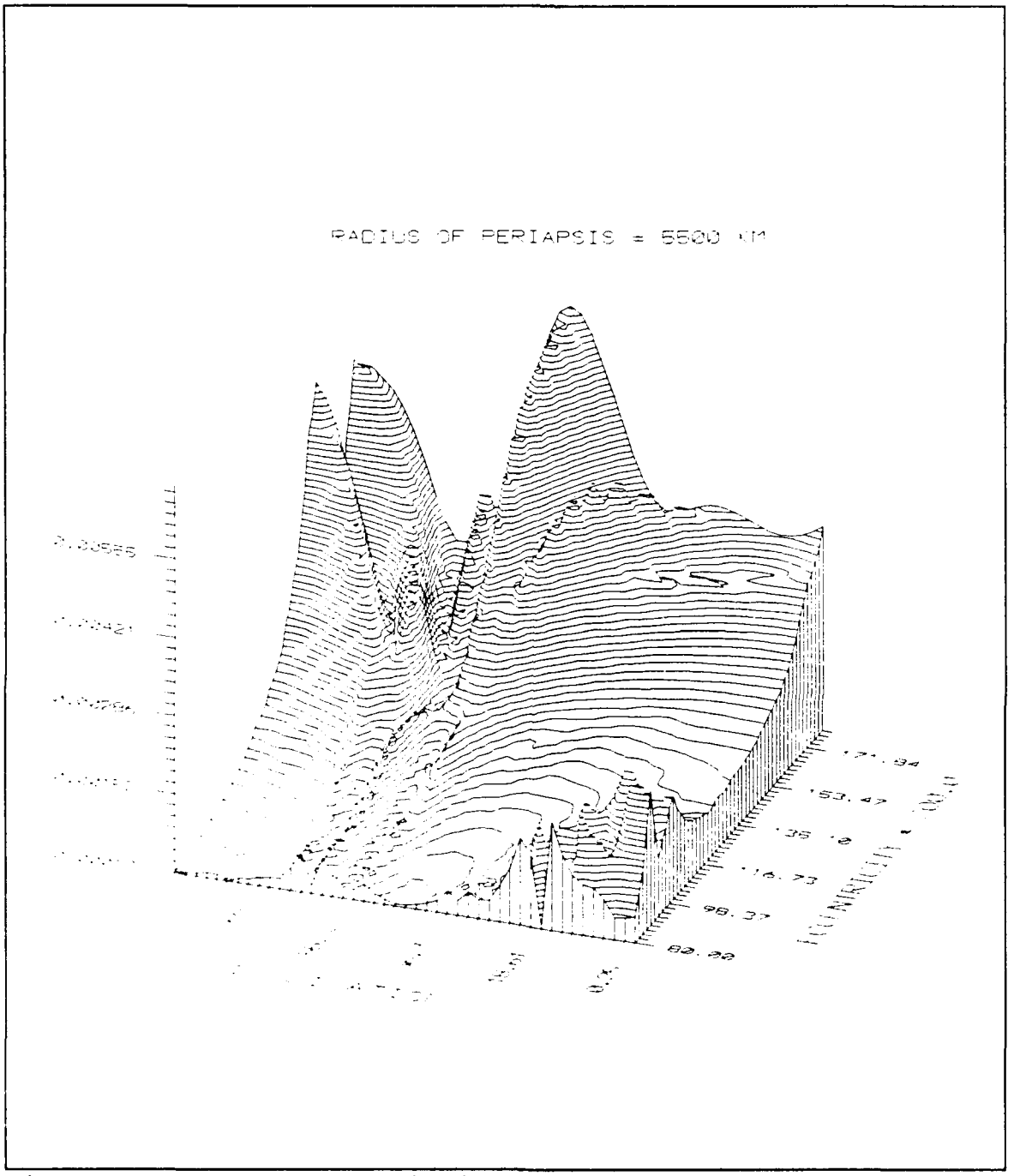

Figure 43. Standard Deviation in Eccentricity vs Inclination and Eccentricity: Periapse Radius = 5500 Km, Linear Data Fit

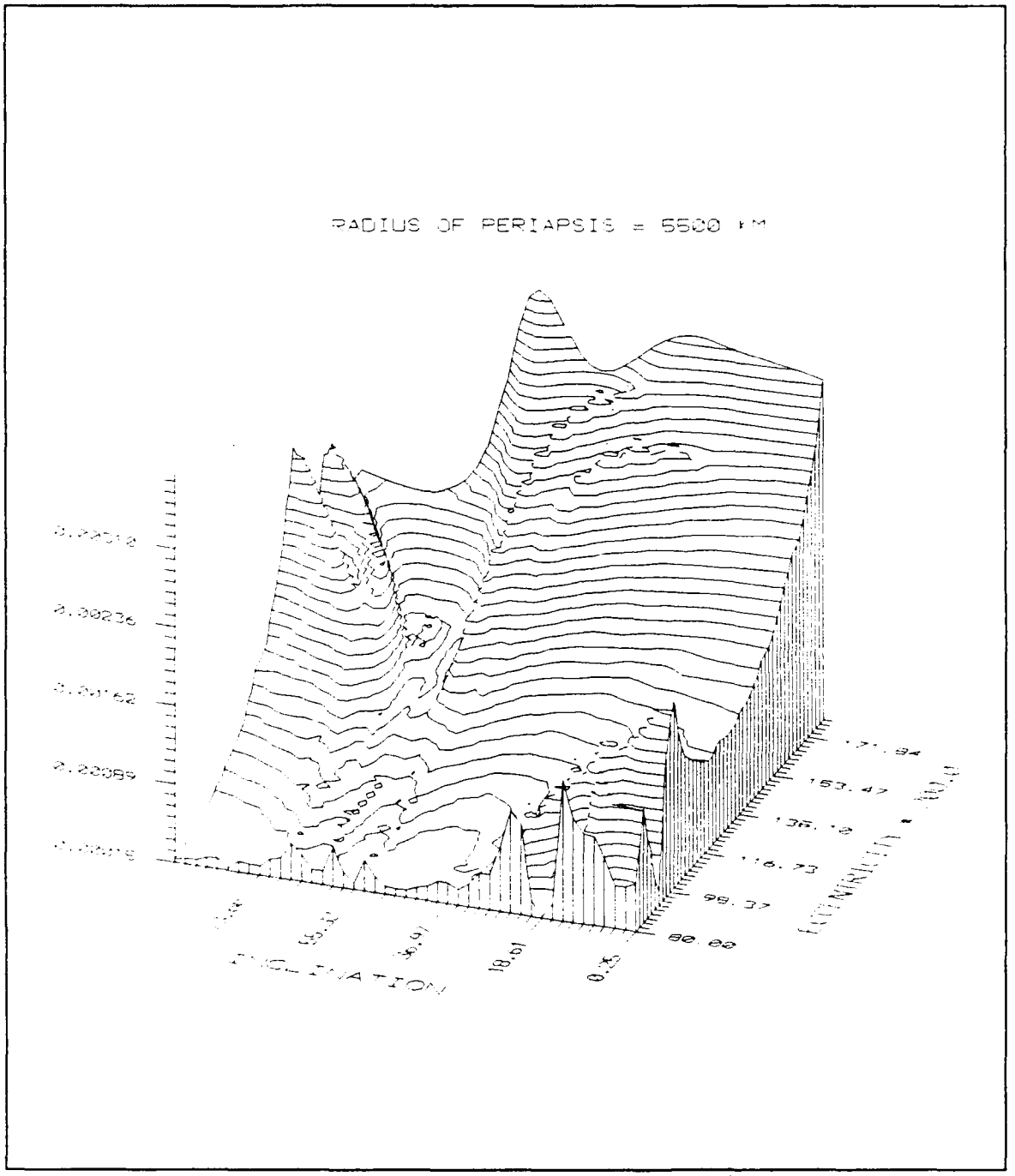

Figure 44. Standard Deviation in Eccentricity vs Inclination and Eccentricity: Periapse Radius = 5500 Km, Quadratic Data Fit

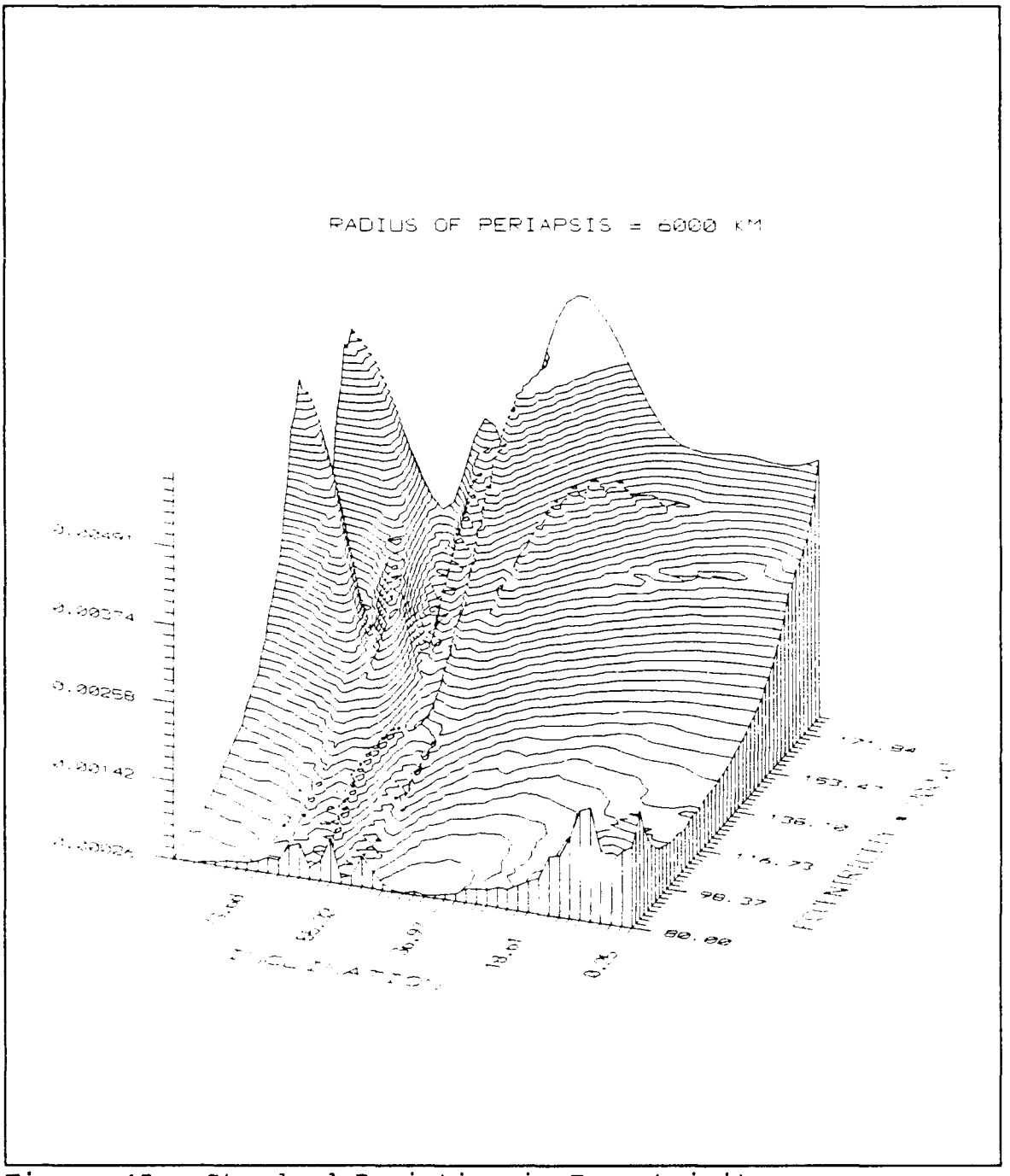

Figure 45. Standard Deviation in Eccentricity vs Inclination and Eccentricity: Periapse Radius = 6000 Km, Linear Data Fit

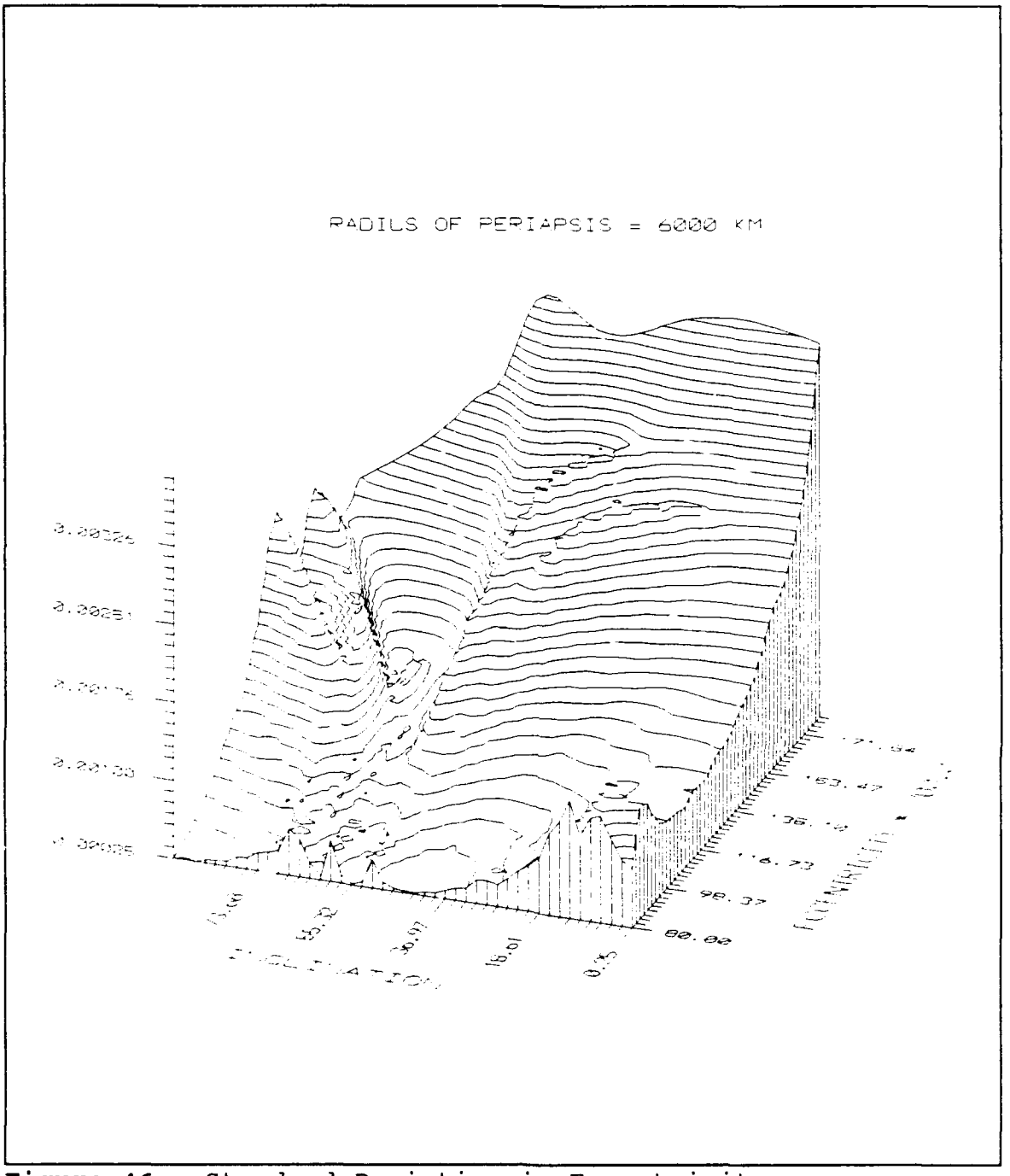

Figure 46. Standard Deviation in Eccentricity vs Inclination and Eccentricity: Periapse Radius = 6000 Km,

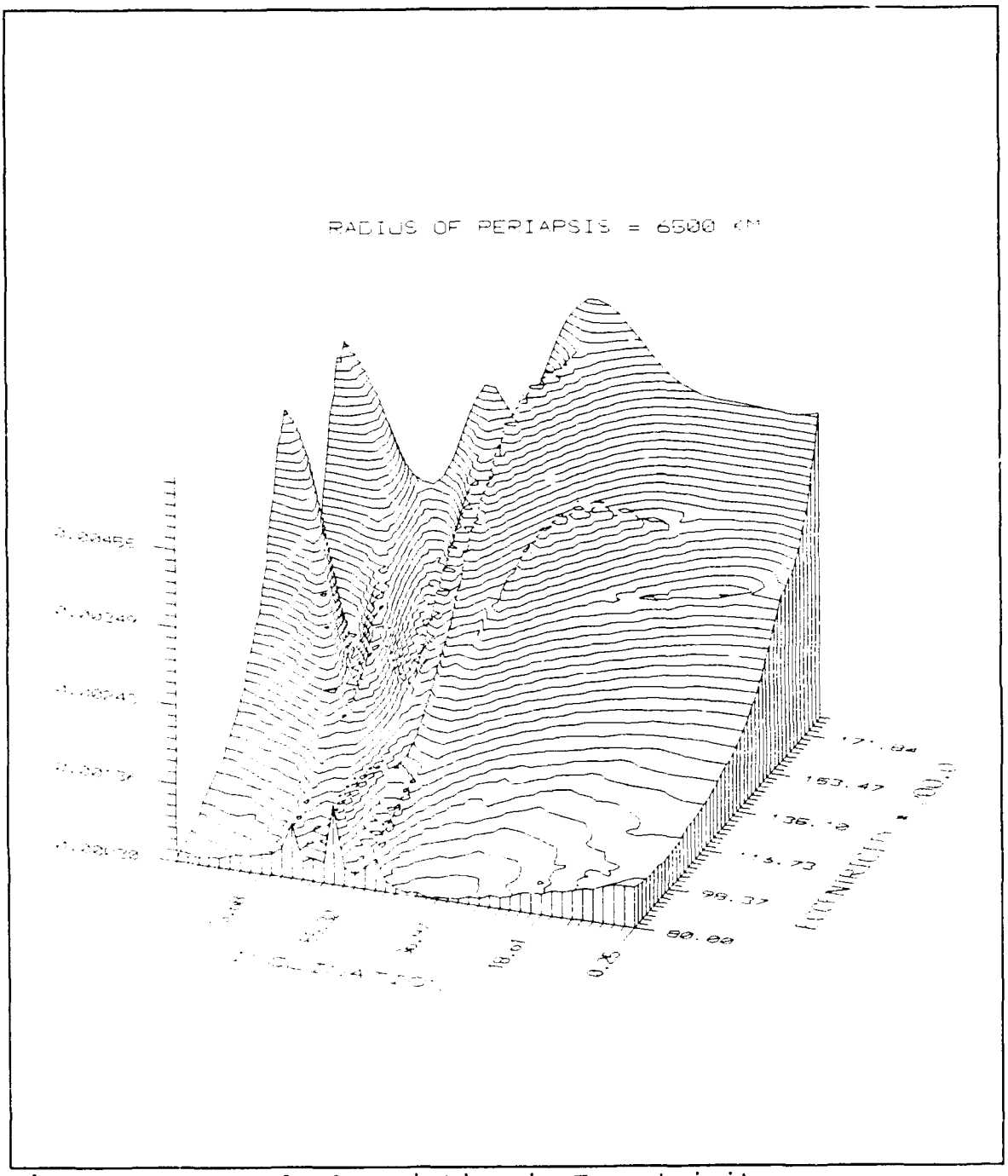

Figure 47. Standard Deviation in Eccentricity vs Inclination and Eccentricity: Periapse Radius = 6500 Km, Linear Data Fit

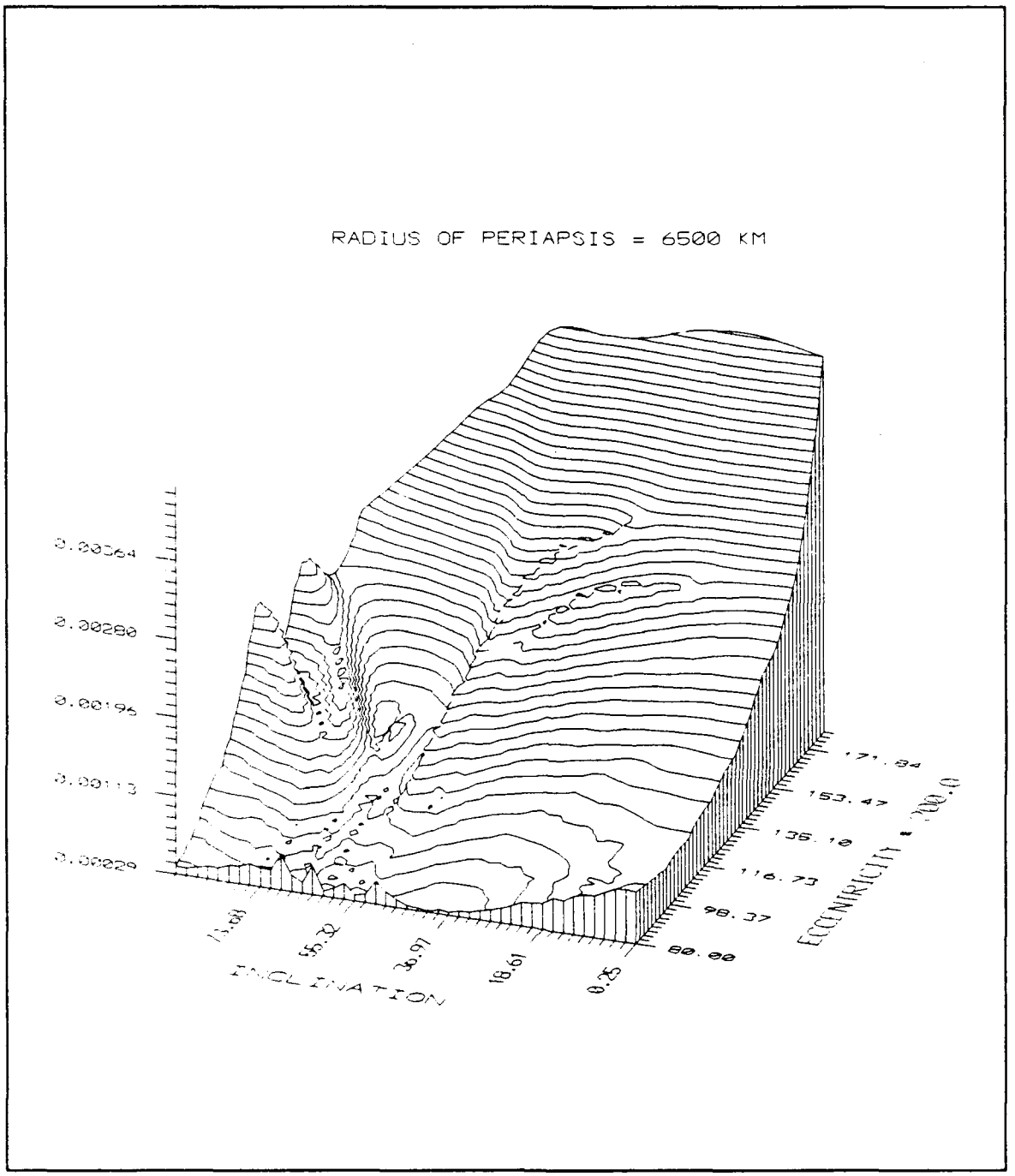

Figure 48. Standard Deviation in Eccentricity vs Inclination and Eccentricity: Periapse Radius = 6500 Km, Quadratic Data Fit

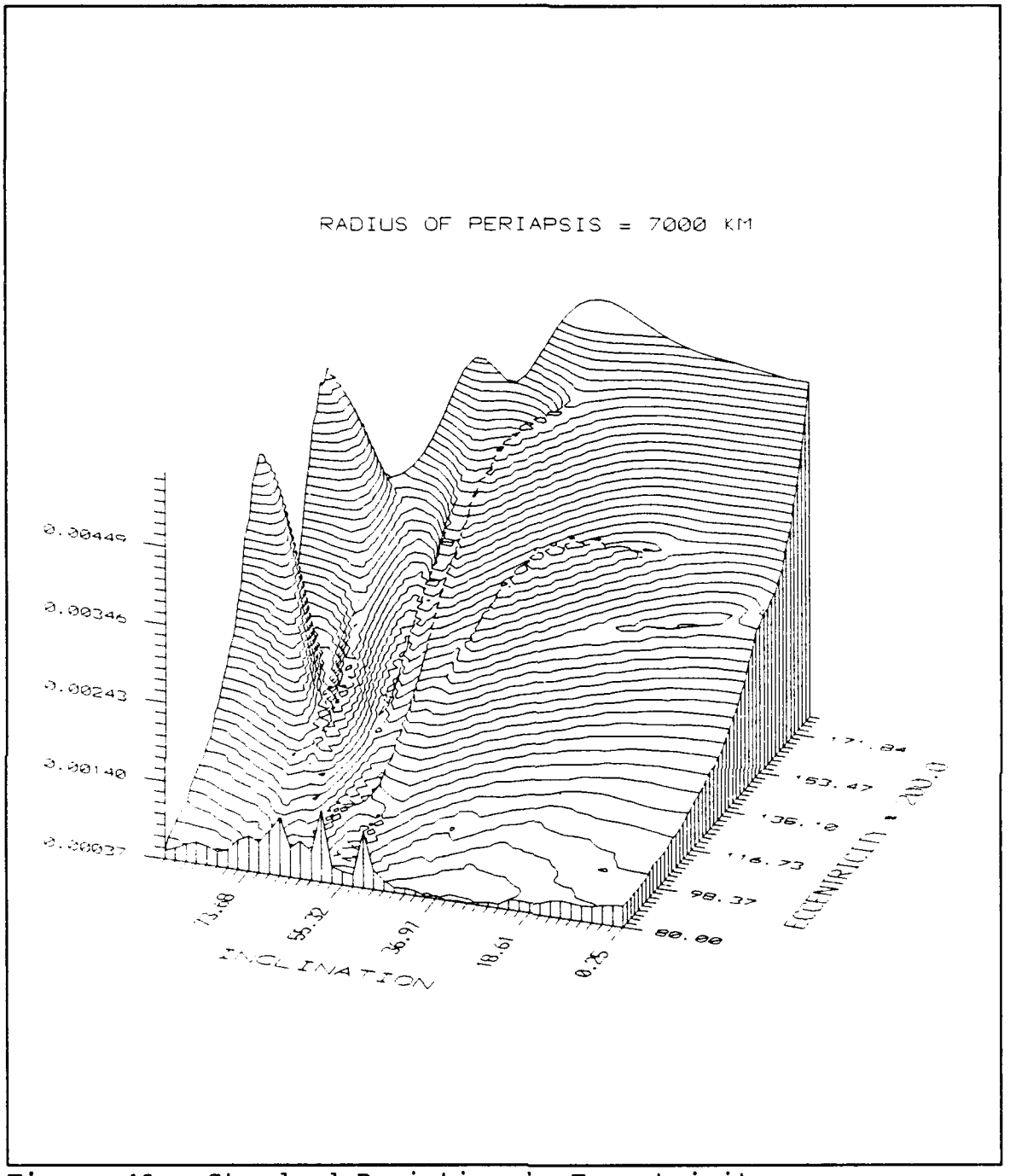

Figure 49. Standard Deviation in Eccentricity vs Inclination and Eccentricity: Periapse Radius = 7000 Km, Linear Data Fit

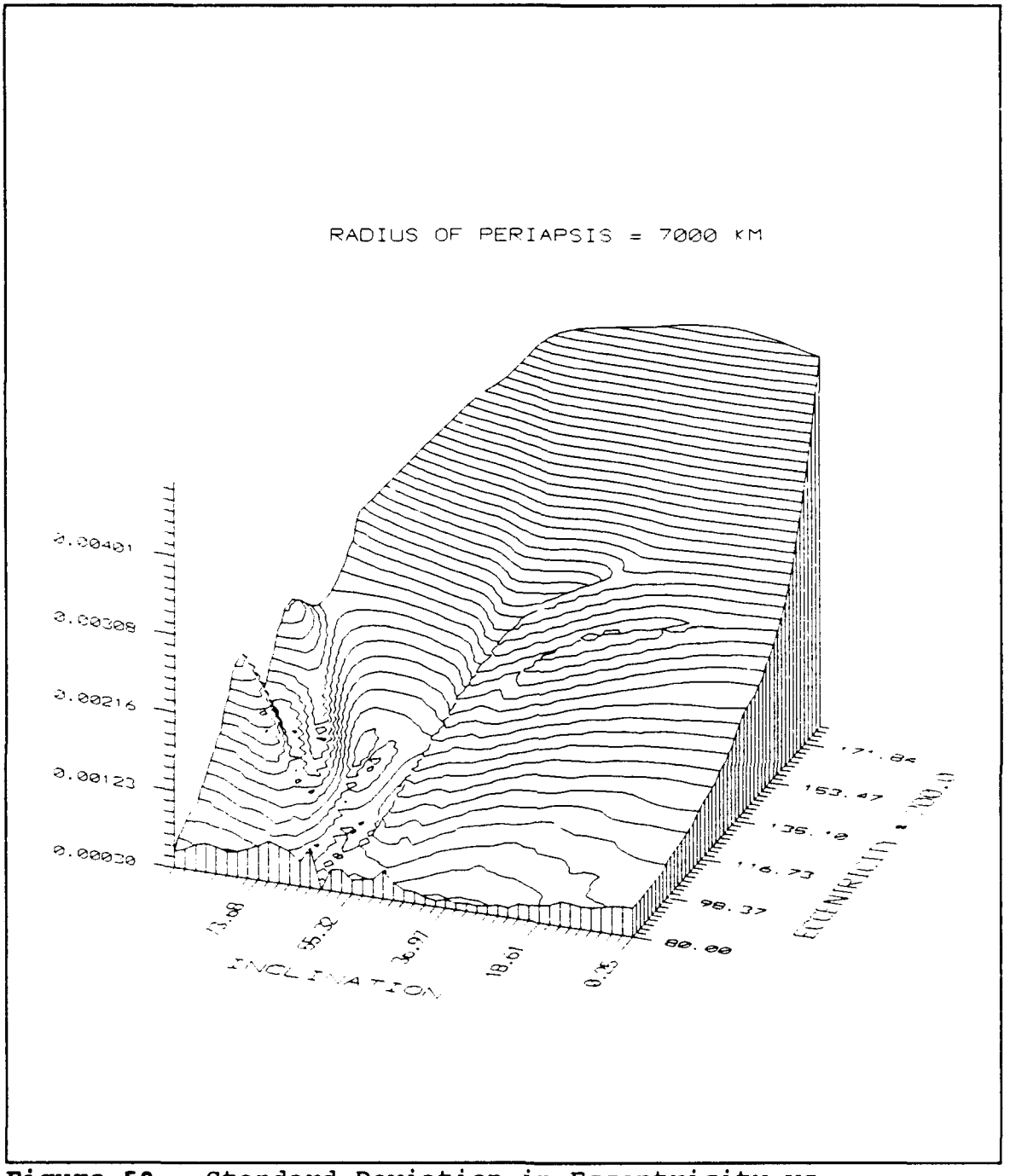

Figure 50. Standard Deviation in Eccentricity vs Inclination and Eccentricity: Periapse Radius = 7000 Km, Quadratic Data Fit

Appendix C. SDI Surface Plots

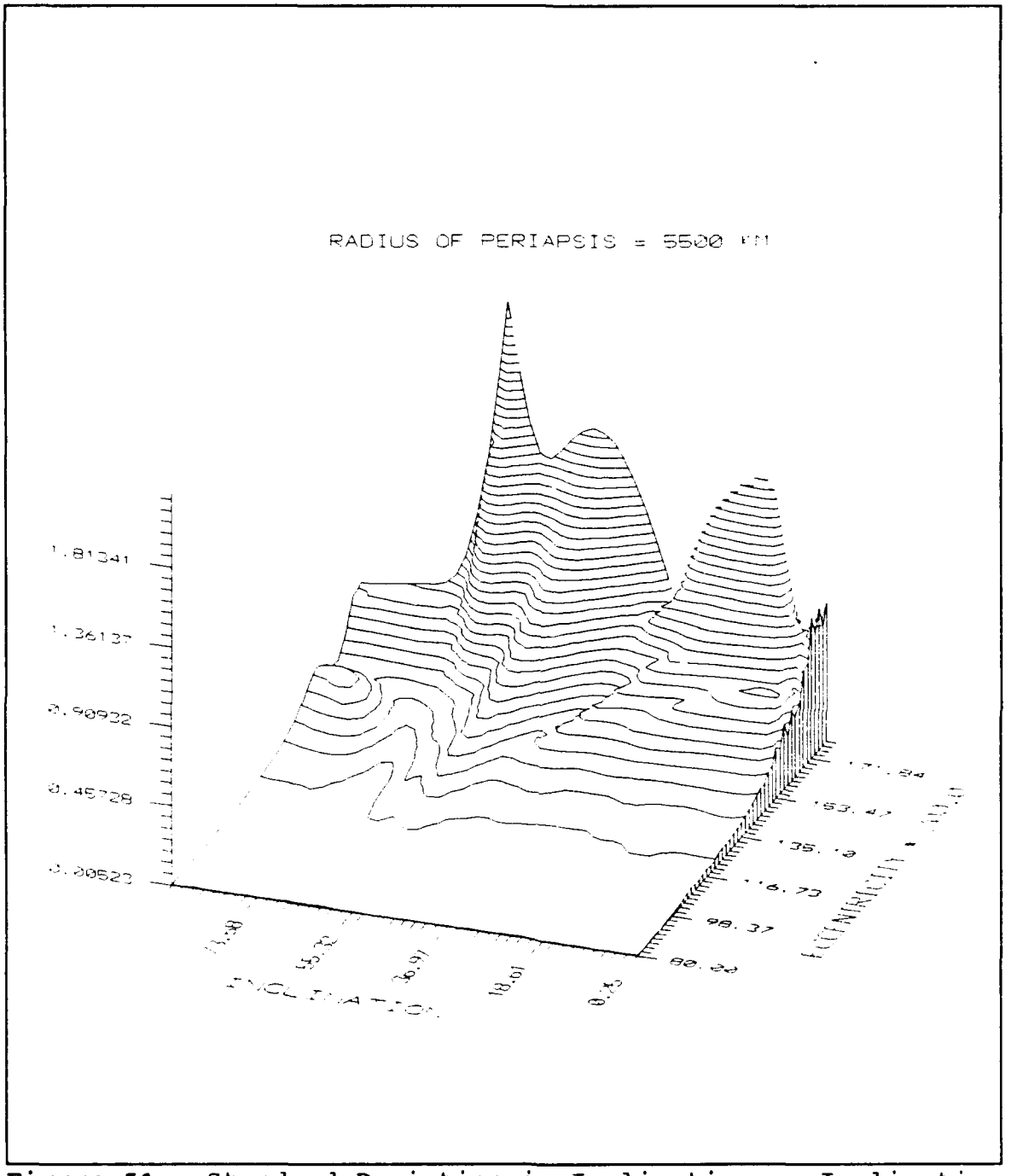

Figure 51. Standard Deviation in Inclination vs Inclination and Eccentricity: Periapse Radius = 5500 Km, Linear Data Fit

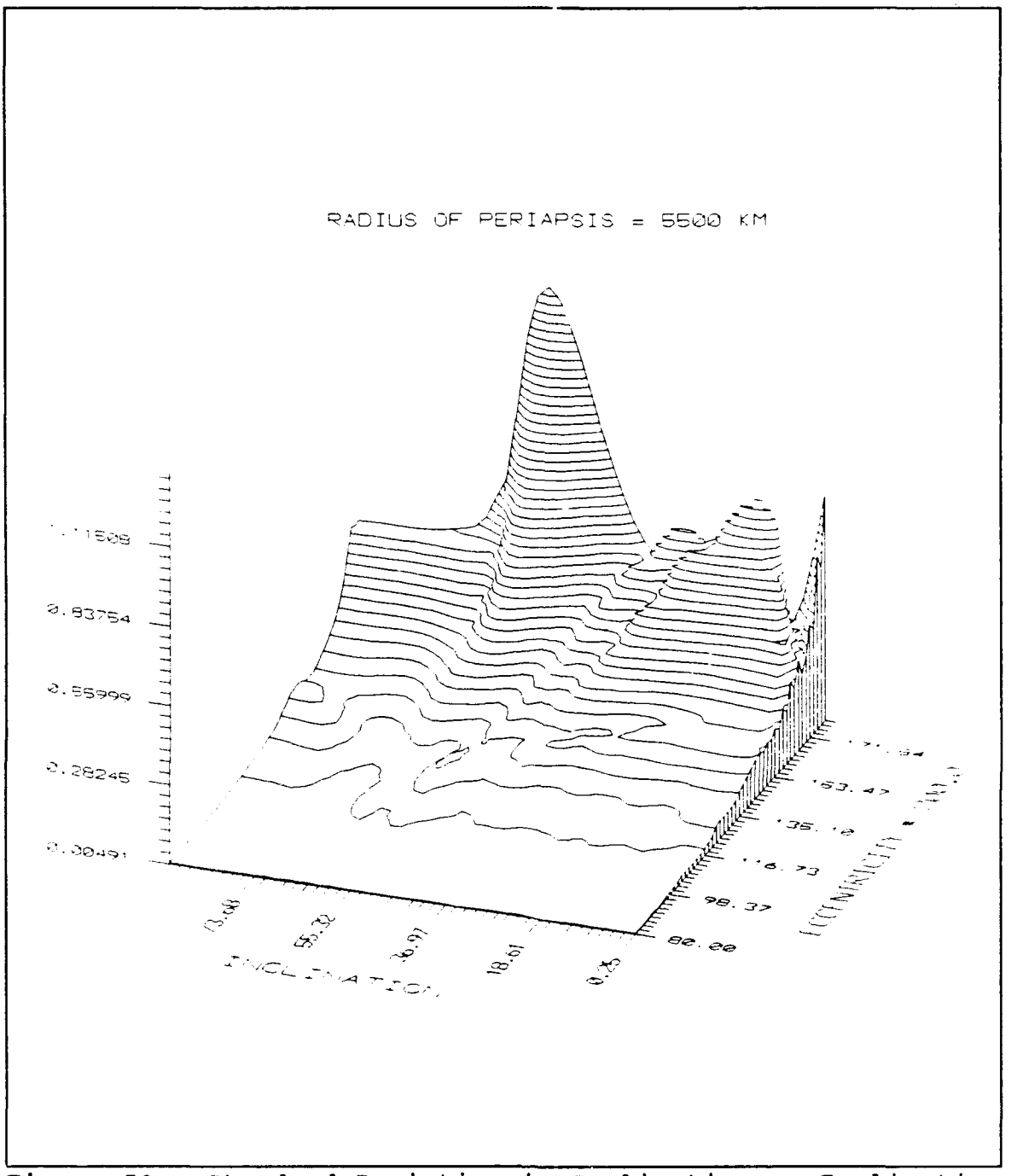

Figure 52. Standard Deviation in Inclination vs Inclination and Eccentricity: Periapse Radius = 5500 Km, Quadratic Data Fit

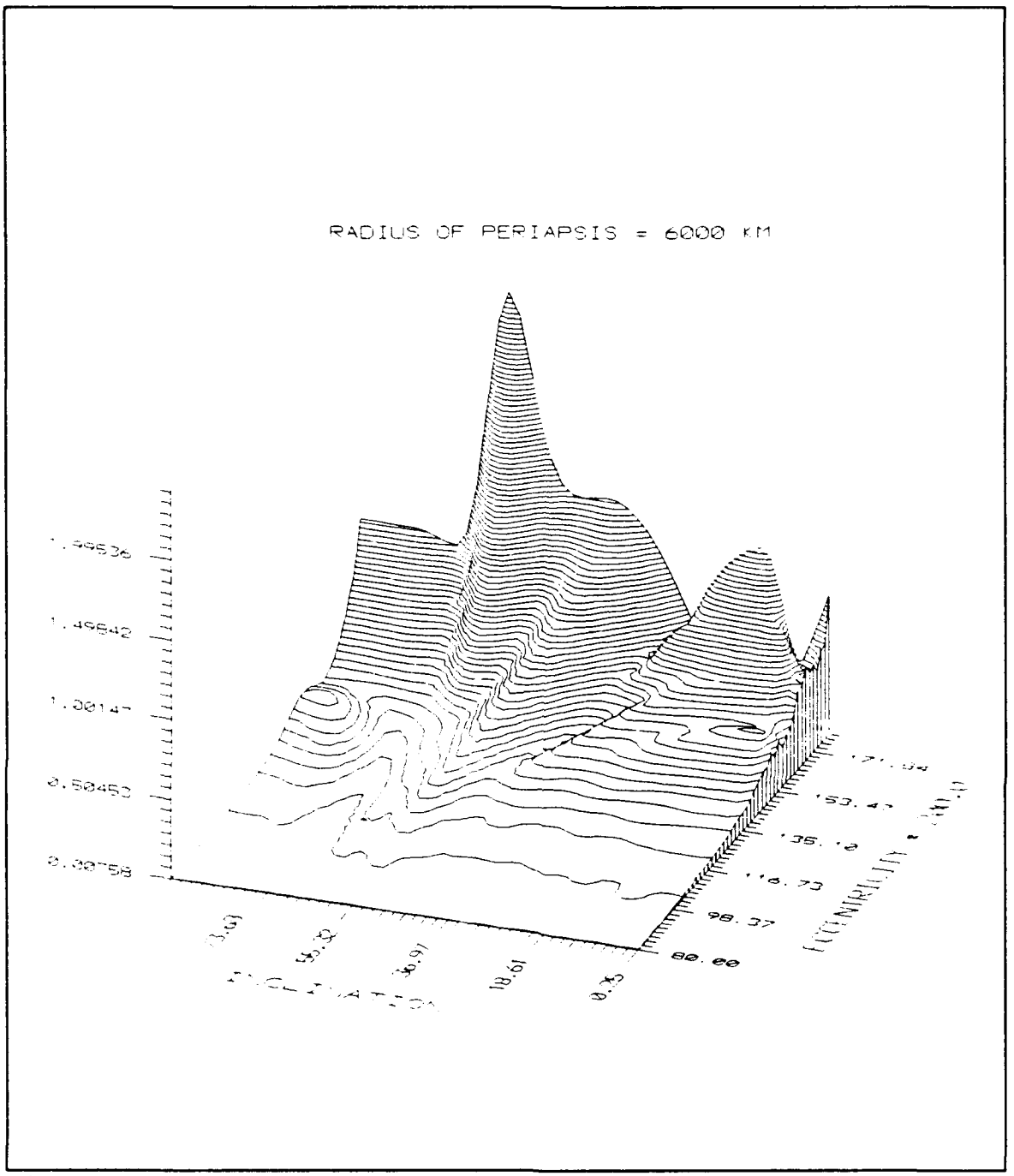

Figure 53. Standard Deviation in Inclination vs Inclination and Eccentricity: Periapse Radius = 6000 Km, Linear Data Fit

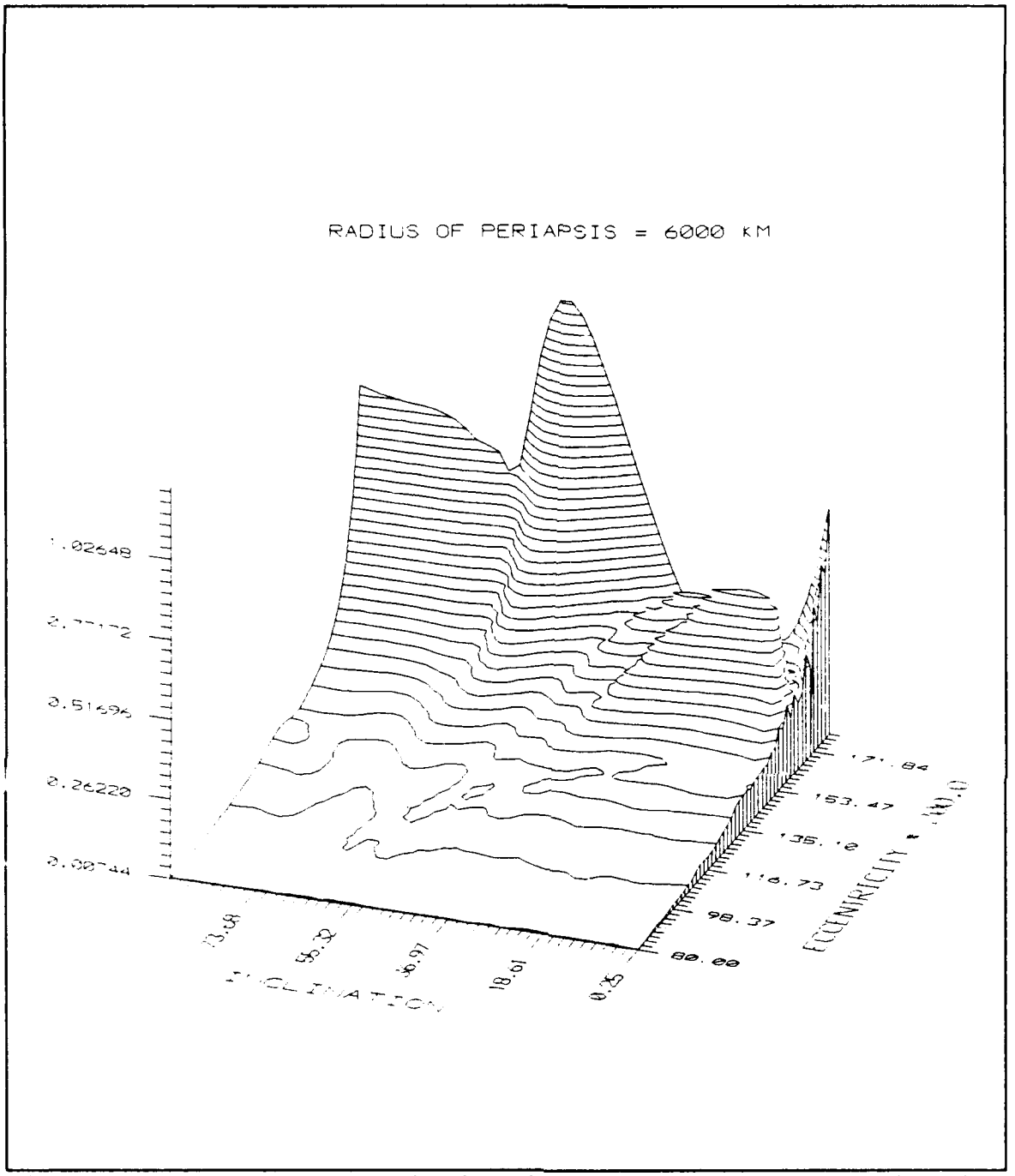

Figure 54. Standard Deviation in Inclination vs Inclination and Eccentricity: Periapse Radius = 6000 Km, Quadratic Data Fit

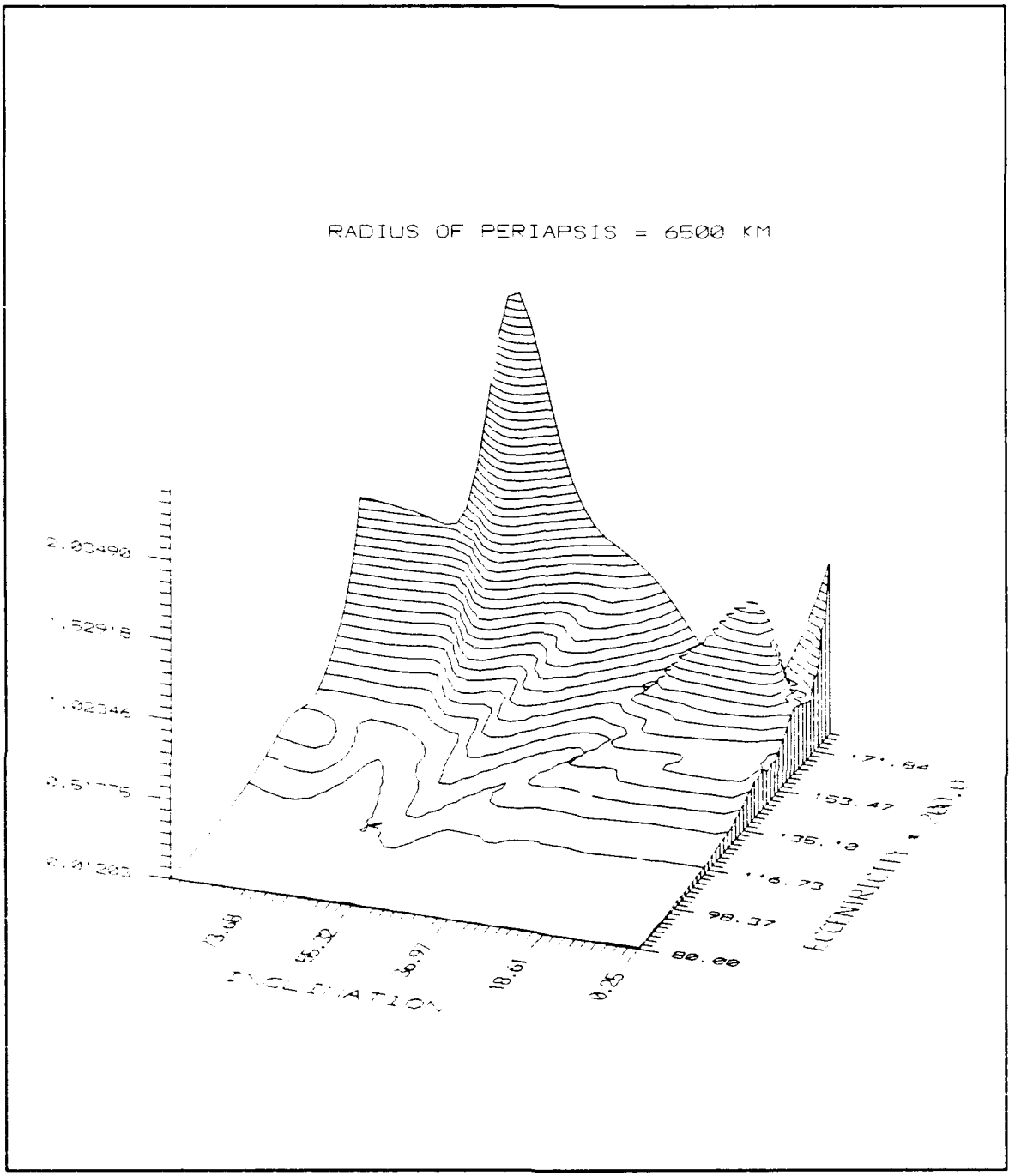

Figure 55. Standard Deviation in Inclination vs Inclination and Eccentricity: Periapse Radius = 6500 Km, Linear Data Fit

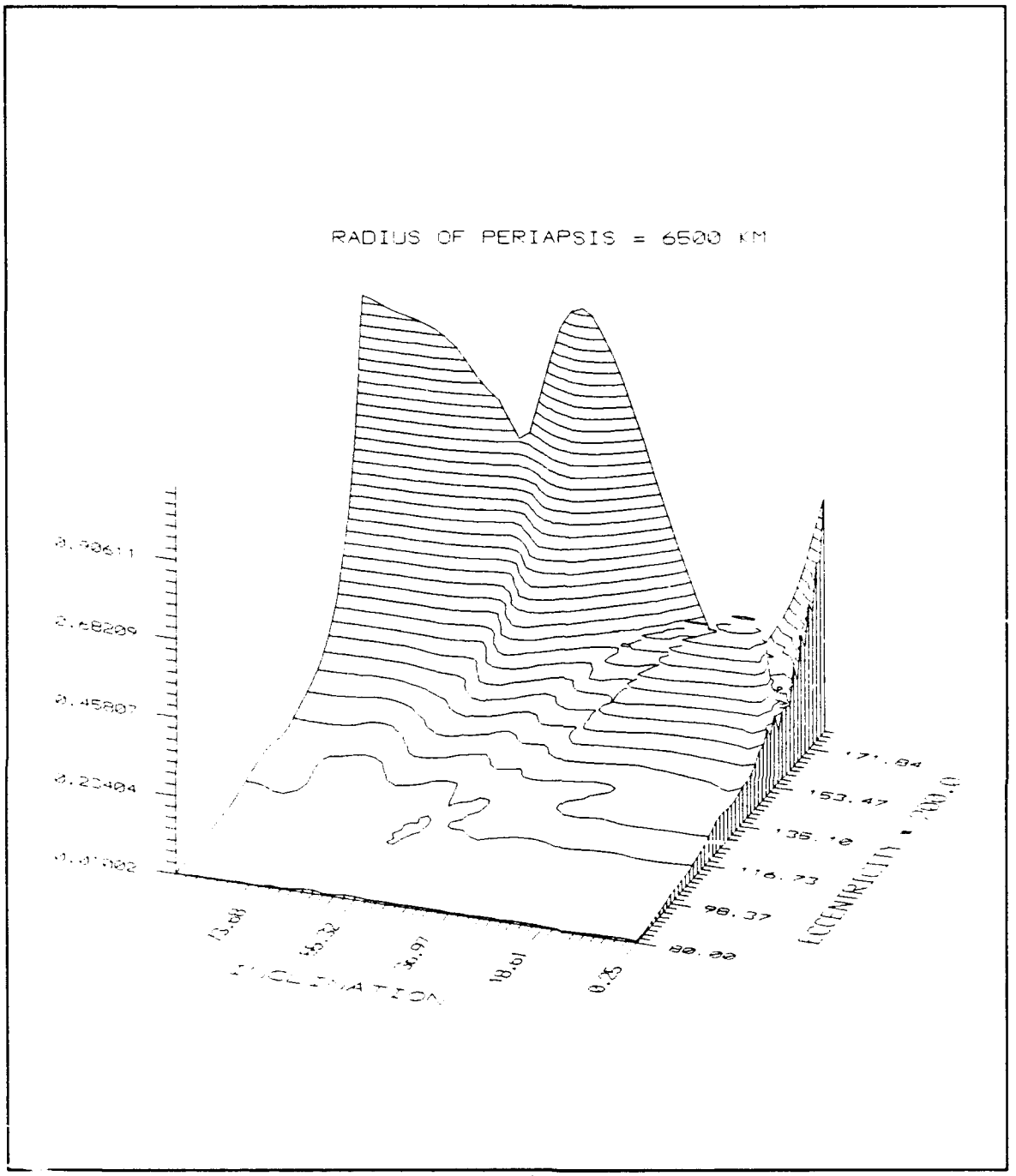

Figure 56. Standard Deviation in Inclination vs Inclination and Eccentricity: Periapse Radius = 6500 Km, Quadratic Data Fit

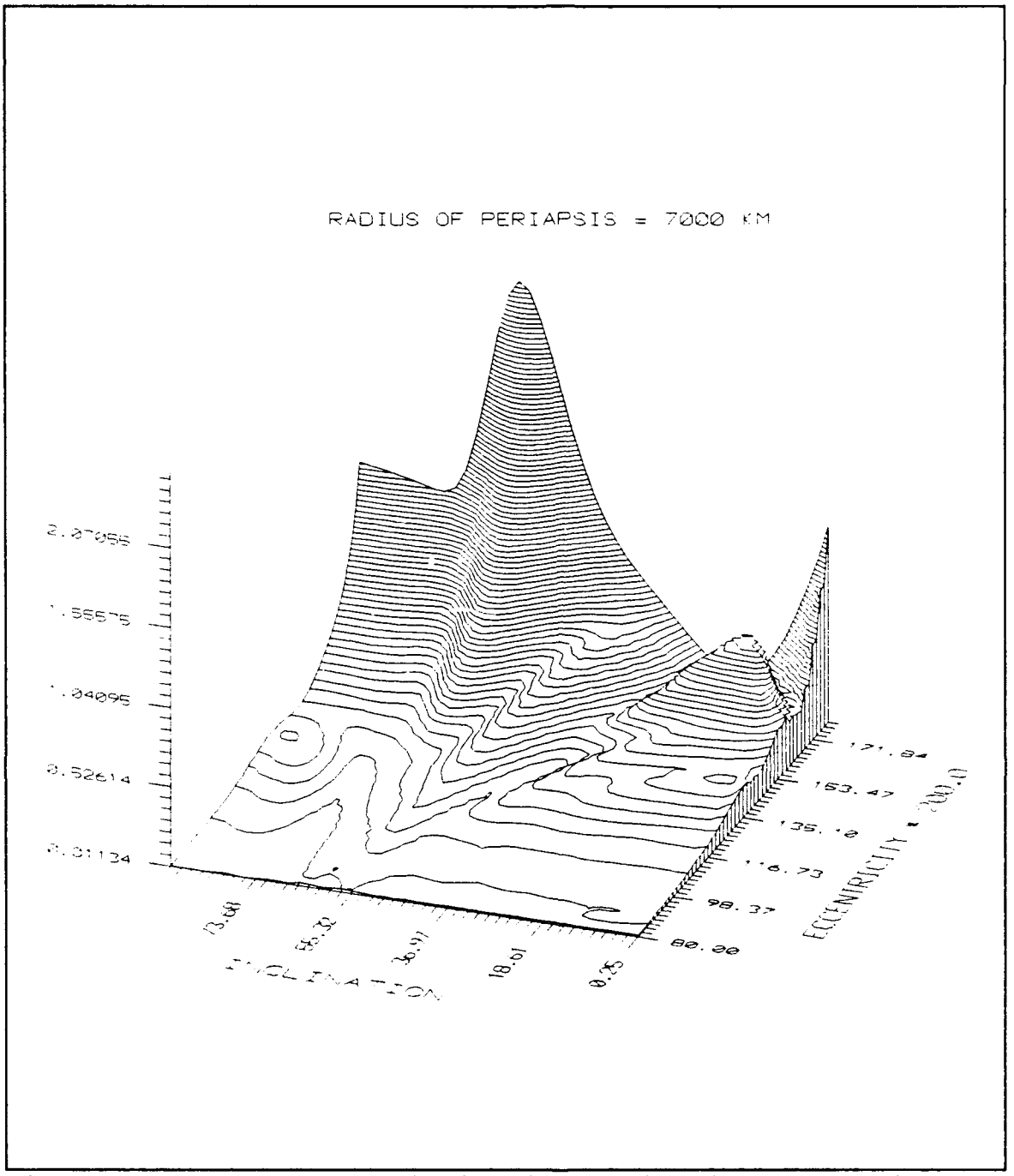

Figure 57. Standard Deviation in Inclination vs Inclination and Eccentricity: Periapse Radius = 7000 Km, Linear Data Fit

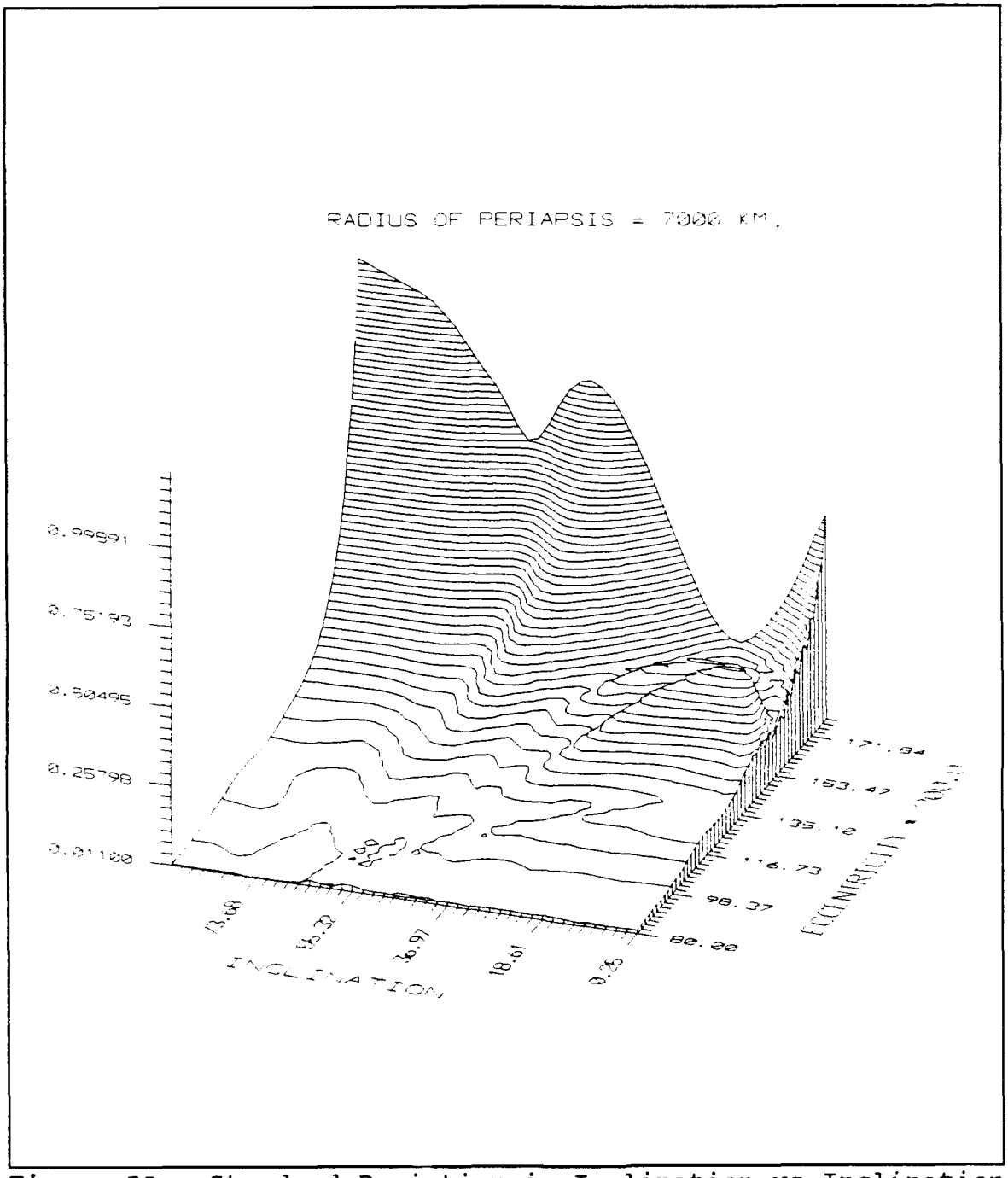

Figure 58. Standard Deviation in Inclination vs Inclination and Eccentricity: Periapse Radius = 7000 Km, Quadratic Data Fit

Appendix D. Critical Inclination Plots

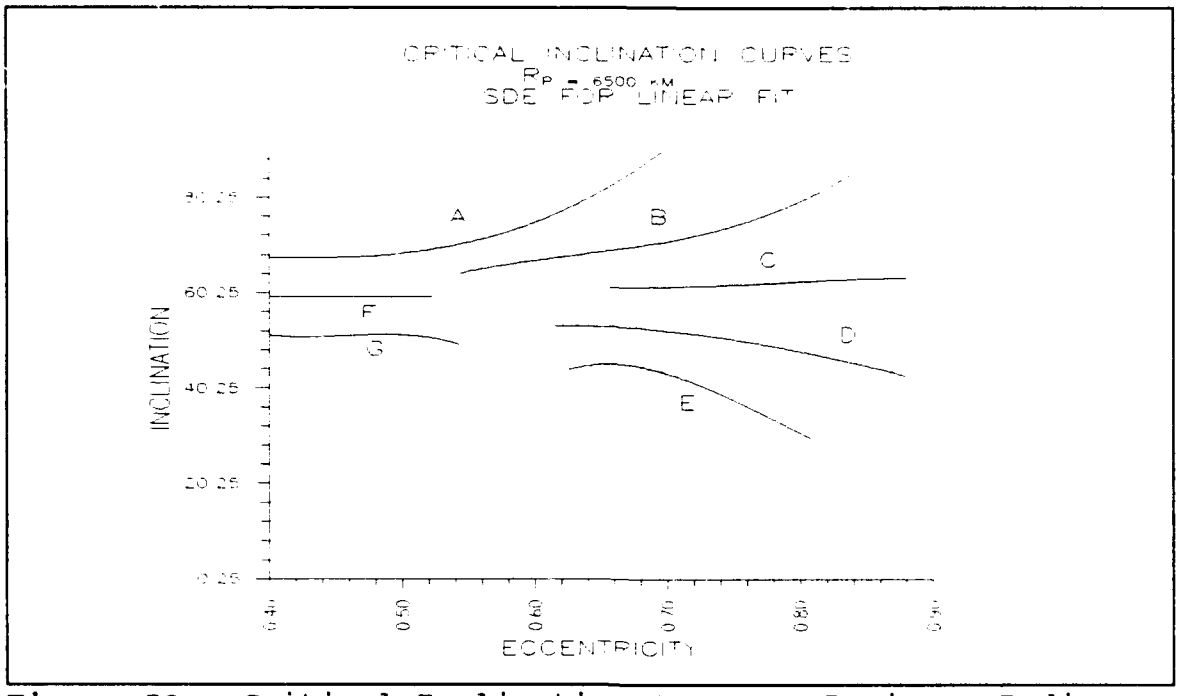

Figure 59. Critical Inclination Curves: Periapse Radius = 6500 km, Linear Data Fit

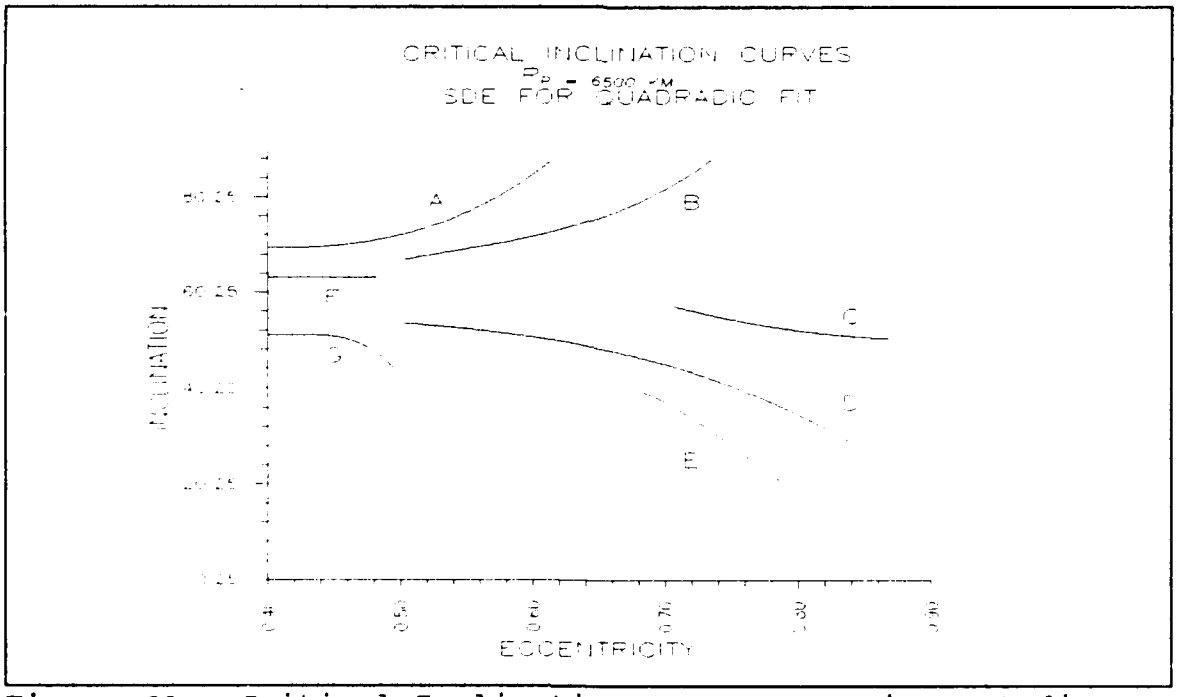

Figure 60. Critical Inclination Curves: Periapse Radius = 6500 km, Quadratic Data Fit

Bibliography

1. Andrews, Larry C. Special Functions for Engineers and Applied Mathematicians. New York: Macmillian Publishing Company, 1985.

2. Bain, Rodney D. Lecture material, Advanced Astrodynamics. School of Engineering, Air Force Institute of Technology (AU), Wright-Patterson AFB OH, April 1990.

3. Bate, R.R. and others. Fundamentals of Astrodynamics. New York: Dover Publications Inc., 1971.

4. Battin, Richard H. An Introduction to the Mathematics and Methods of Astrodynamics. New York: American Institute of Aeronautics and Astronautics, Inc., 1987.

5. Breakwell, J.V. and Hensley, R.D. "An Investigation of High Eccentricity Orbits About Mars," Trajectory Analysis and Guidance Theory, NASA Cambridge: Electronics Research Center, 1966.

6. Chobotov, V.A. and others. Lecture Notes, Orbital Mechanics. Norchrop University, Los Angeles CA, 1987.

7. Durand, D.F. Numerical Determination of the Location of Critical Inclinations for Long Term High Eccentricity Orbits About Mars. MS thesis, AFIT/GA/ENY/89J-2. School of Engineering, Air Force Institute of Technology (AU), Wright-Patterson AFB OH, June 1989.

8. Garfinkel, Boris. "Formal Solution in the Problem of Small Divisors," The Astromomical Journal, 71-8: 657-786 (Oct 1966).

9. -----. "On the Motion of a Satellite in the Vicinity of the Critical Inclination," The Astronomical Journal, 65-10: 624-627 (Dec 1960).

10. -----. "Tesseral Harmonic Perturbations of an Artificial Satellite," The Astronomical Journal, 70-10: 784 (Dec 1963).

11. -----. "The Disturbing Function for an Artificial Satellite," The Astronomical Journal, 70-9: 699 (Nov 1965).

12. Gedeon, G.S. Tesseral Resonance Effects on Satellite Orbits," Celestial Mechanics, 1:167-189 (1969).

13. Gerald, Gerald F. and Patrick O. Wheatley. Applied Numerical Analysis. Reading Massachusetts: Addison-Wesley Publishing Company, 1985.

14. Goldreich, P. "Inclination of Satellite Orbits about an Oblate Precessing Planet," The Astronomical Journal, 70-1: 5 (Feb 1963).

15. Hori, G. "The Motion of an Artificial Satellite in the Vicinity of the Critical Inclination," The Astronomical Journal, 63-5: 291 (Jun 1960).

16. Kaula, William M. "Development of the Lunar and Solar Disturbing Functions for a Close Satellite," The Astronomical Journal, 67-5: 300-303 (June 1962).

17. Kwok, J.H. "LOP," Jet Propulsion Laboratory, Technical Report No. 86-151, June 1986.

Vita

Captain Kenneth J. Hyatt [redacted] He graduated from Stafford Senior High School in 1982 and attended Virginia Polytechnic Institute and State University. He was awarded a Bachelor of Science in Aerospace and Ocean Engineering in June 1986 and was commissioned a 2Lt through the ROTC program. His first assignment was Long Range Planning (XR) at HQ Space Division, Los Angeles AFB. He entered the Air Force Institute of Technology program in June 1989. Expected follow-on assignment (Dec 90) is the Foreign Technology Division, Wright Patterson AFB, OH.

[redacted]

REPORT DOCUMENTATION PAGE

Form Approved
OMB No 0704-0188

1. AGENCY USE ONLY (Leave blank)	2. REPORT DATE	3. REPORT TYPE AND DATES COVERED
	20 Nov 90	Master's Thesis

4. TITLE AND SUBTITLE

NUMERICAL ANALYSIS OF CRITICAL INCLINATIONS ABOUT THE PLANET MARS

5. FUNDING NUMBERS

6. AUTHOR(S)

Kenneth J. Hyatt, Captain, USAF

7. PERFORMING ORGANIZATION NAME(S) AND ADDRESS(ES)

Air Force Institute of Technology, WPAFB OH 45433-6583

8. PERFORMING ORGANIZATION REPORT NUMBER

AFIT/GA/ENY/90D-5

9. SPONSORING / MONITORING AGENCY NAME(S) AND ADDRESS(ES)

10. SPONSORING / MONITORING AGENCY REPORT NUMBER

11. SUPPLEMENTARY NOTES

12a. DISTRIBUTION / AVAILABILITY STATEMENT

Approved for public release; distribution unlimited

12b. DISTRIBUTION CODE

13. ABSTRACT *(Maximum 200 words)*

This study investigated critical inclinations about the planet Mars. Averaged equations of motion were numerically integrated over a time span of ten Earth years for various inclinations, eccentricities, and perigee heights. Each orbit (i.e. set of initial conditions) produced a standard deviation of the variations in eccentricity (SDE) and inclination (SDI). These were calculated using a polynomial approximation to the variations. Surface plots of SDI and SDE vs the initial conditions are then examined to ascertain the critical inclinations.

14. SUBJECT TERMS

Astronautics, Spacecraft Trajectories and Reentry, Artificial Satellite, Space Technology

15. NUMBER OF PAGES

111

16. PRICE CODE

17. SECURITY CLASSIFICATION OF REPORT	18. SECURITY CLASSIFICATION OF THIS PAGE	19. SECURITY CLASSIFICATION OF ABSTRACT	20. LIMITATION OF ABSTRACT
Unclassified	Unclassified	Unclassified	UL